Aus der Klinik für Strahlentherapie
Geschäftsführende Direktorin: Prof. Dr. Engenhart-Cabillic

des Fachbereichs Medizin der Philipps-Universität Marburg

Impact of tissue specific parameters on the prediction of the biological effectiveness for treatment planning in ion beam therapy

Inaugural-Dissertation

zur

Erlangung des Doktorgrades der Naturwissenschaften

(Dr. rer. nat.)

dem

Fachbereich Medizin der Philipps-Universität Marburg

vorgelegt von

Dipl.-Ing. (FH) Rebecca Antonia Grün

aus

Weilburg/Hessen

Marburg an der Lahn, 2014

Angenommen vom Fachbereich Medizin der Philipps-Universität Marburg am:
3. Juni 2014

Gedruckt mit Genehmigung des Fachbereichs.

Dekan: Prof. Dr. Helmut Schäfer
Referenten : Prof. Dr. Rita Engenhart-Cabillic und Prof. Dr. Klemens Zink
Korreferent: Prof. Dr. Gerhard Kraft

Die vorliegende kumulative Dissertation stellt eine Zusammenfassung der Forschungsergebnisse dar, welche wie folgt in Fachzeitschriften publiziert wurden:

[1] **Rebecca Grün**, Thomas Friedrich, Thilo Elsässer, Michael Krämer, Klemens Zink, Christian P. Karger, Marco Durante, Rita Engenhart-Cabillic and Michael Scholz. Impact of enhancements in the local effect model (LEM) on the predicted RBE-weighted target dose distribution in carbon ion therapy. *Physics in Medicine and Biology 2012;* 57:7261–74.

[2] Olaf Steinsträter, **Rebecca Grün**, Uwe Scholz, Thomas Friedrich, Marco Durante and Michael Scholz. Mapping of RBE-weighted doses between HIMAC- and LEM-based treatment planning systems for carbon ion therapy. *International Journal of Radiation Oncology, Biology, Physics* 2012; 84:854–60.

[3] Thomas Friedrich, **Rebecca Grün**, Uwe Scholz, Thilo Elsässer, Marco Durante and Michael Scholz. Sensitivity analysis of the relative biological effectiveness predicted by the local effect model. *Physics in Medicine and Biology 2013*; *58*:6827–49.

[4] **Rebecca Grün**, Thomas Friedrich, Michael Krämer, Klemens Zink, Marco Durante, Rita Engenhart-Cabillic and Michael Scholz. Physical and biological factors determining the effective proton range. Medical Physics 2013; 40:111716-1-10

Die aufgelisteten Publikationen wurden verfügbar gemacht mit einer Abdruckgenehmigung von Institute of Physics (IOP) Publishing [1,3], Elsevier [2] und American Association of Physicists in Medicine (AAPM) [4].

Anmerkung:
Die Publikationen werden im Text, entsprechend der oben definierten Reihenfolge, mit den Nummern 1-4 referenziert.

The publications are referenced in the text according to the order defined above with the numbers 1-4.

Die biologische Bestrahlungsplanung in der Partikeltherapie erfordert eine zuverlässige Abschätzung der relativen biologischen Wirksamkeit (RBW) im bestrahlten Gewebe. Für das Pilotprojekt an der GSI Helmholtzzentrum für Schwerionenforschung GmbH in Darmstadt und in den bisherigen europäischen Partikeltherapiezentren basiert die RBW-Vorhersage auf einem biophysikalischen Modell, dem Local Effect Model (LEM).

Die derzeit verwendete erste Version des Modells (LEM I) ist auf die Beschreibung der Wirkung von Kohlenstoffstrahlen im Zielvolumen optimiert. Es zeigt jedoch für den Eintrittsbereich der Kohlenstoffionen als auch generell für leichtere Ionen systematische Abweichungen der RBW. Aus diesem Grunde wurde das LEM kontinuierlich weiterentwickelt. Die aktuelle Version (LEM IV) zeigt eine bessere Übereinstimmung der Modellrechnung mit den Ergebnissen aus *in-vitro* Zellexperimenten. Für die Anwendung des LEM IV in der Bestrahlungsplanung ist daher die Untersuchung der möglichen Unterschiede zu LEM I unter klinisch relevanten Bestrahlungsbedingungen von Interesse.

Die in dieser Arbeit präsentierten Analysen haben das Ziel, die aus verschiedenen Verfahren und Modellvarianten resultierenden RBW-gewichteten Dosen für Protonen und Kohlenstoffionen zu vergleichen. Dadurch sollen mögliche Auswirkungen von Unterschieden auf die klinische Anwendung herausgestellt und die Interpretation von klinischen Ergebnissen verschiedener Institute ermöglicht werden.

In der vorliegenden Arbeit konnte gezeigt werden, dass sich für typische Bestrahlungssituationen mit Kohlenstoffstrahlen von Chordomen der Schädelbasis die aus Anwendung des LEM I und LEM IV resultierenden RBW-gewichteten Dosen im Mittel um weniger als 10 % unterscheiden und damit die Anwendung des LEM IV ebenfalls eine konsistente Interpretation der klinischen Daten erlaubt. In den japanischen Zentren wird die RBW aus der klinischen Erfahrung mit Neutronenstrahlung und *in-vitro* Zellexperimenten mit Kohlenstoffionen abgeschätzt (HIMAC Ansatz). Die in der Arbeit vorgestellten Methoden ermöglichen einen direkten Vergleich des HIMAC Ansatzes mit dem LEM und damit auch der erzielten klinischen Ergebnisse. Eine Sensitivitätsanalyse der RBW bezüglich der Modellparameter stellte die Charakterisierung der Photonen-Dosiseffektkurve als eine besonders relevante Kenngröße heraus. Die Anwendung des LEM IV für Protonenstrahlen gibt die experimentell beobachtete Erhöhung der RBW im Vergleich zu dem klinisch verwendeten Wert von 1.1 am distalen Ende des Bestrahlungsfeldes genauer wieder. Sie erlaubt darüber hinaus eine bessere systematische Charakterisierung der Erhöhung der effektiven Reichweite von Protonenstrahlen, die eine Folge der RBW-Erhöhung am distalen Ende des Bestrahlungsfeldes ist.

Die Ergebnisse dieser Arbeit unterstreichen damit den Stellenwert der RBW Modellierung für eine langfristige Verbesserung der Bestrahlungsplanung in der Partikeltherapie und die damit verbundene bessere Ausnutzung der Vorteile dieser Bestrahlungsmodalität.

SUMMARY

Treatment planning in ion beam therapy requires a reliable estimation of the relative biological effectiveness (RBE) of the irradiated tissue. For the pilot project at GSI Helmholtzzentrum für Schwerionenforschung GmbH and at other European ion beam therapy centers RBE prediction is based on a biophysical model, the Local Effect Model (LEM).

The model version in use, LEM I, is optimized to give a reliable estimation of RBE in the target volume for carbon ion irradiation. However, systematic deviations are observed for the entrance channel of carbon ions and in general for lighter ions. Thus, the LEM has been continuously developed to improve accuracy. The recent version LEM IV has proven to better describe *in-vitro* cell experiments. Thus, for the clinical application of LEM IV it is of interest to analyze potential differences compared to LEM I under treatment-like conditions.

The systematic analysis presented in this work is aiming at the comparison of RBE-weighted doses resulting from different approaches and model versions for protons and carbon ions. This will facilitate the assessment of consequences for clinical application and the interpretation of clinical results from different institutions.

In the course of this thesis it has been shown that the RBE-weighted doses predicted on the basis of LEM IV for typical situations representing chordoma treatments differ on average by less than 10 % to those based on LEM I and thus also allow a consistent interpretation of the clinical results. At Japanese ion beam therapy centers the RBE is estimated using their clinical experience from neutron therapy in combination with *in-vitro* measurements for carbon ions (HIMAC approach). The methods presented in this work allow direct comparison of the HIMAC approach and the LEM and thus of the clinical results obtained at Japanese and European ion beam therapy centers. Furthermore, the sensitivity of the RBE on the model parameters was evaluated. Among all parameters the characterization of the photon dose-response curve has been found to be of particular importance for the determination of RBE. The application of the LEM IV for proton beams more correctly represents the experimentally observed increase of RBE towards the distal end of the irradiation field compared to the clinically considered constant value of 1.1. It further allowed a better systematic characterization of the increased effective range of proton beams that is a consequence of the RBE enhancement at the distal edge of the treatment field.

The results of this work underline the importance of detailed RBE modeling for a long-term improvement of treatment planning in particle therapy and the better exploitation of advantages inherent to this radiation modality.

TABLE OF CONTENTS

I. INTRODUCTION 1

I.I. DEPTH DOSE DISTRIBUTION OF PHOTONS AND ION BEAMS 2
I.II. BIOLOGICAL EFFECTIVENESS OF IONIZING RADIATION 4
I.III. TREATMENT PLANNING IN RADIOTHERAPY 6

II. SUMMARY OF THE PUBLISHED RESULTS (CUMULATIVE) 11

II.I. PROOF OF CONSISTENCY AND COMPARISON WITH *IN-VIVO* EXPERIMENTS 11
II.II. CONVERSION OF INSTITUTIONAL DEPENDENT RBE-WEIGHTED DOSES 13
II.III. SENSITIVITY OF RBE ON THE LEM INPUT PARAMETERS 15
II.IV. PROTON RBE AND ASSESSMENT OF UNCERTAINTY 16

III. AIM AND CONTRIBUTION 19

III.I. ARTICLE 1 19
III.II. ARTICLE 2 19
III.III. ARTICLE 3 20
III.IV. ARTICLE 4 20

IV. DISCUSSION 21

IV.I. GENERAL ASPECTS OF MODELING DOSE RESPONSE IN RADIOTHERAPY 21
IV.II. MODELING BIOLOGICAL EFFECTIVENESS IN HYPOFRACTIONATED TREATMENT REGIMENS 23
IV.III. PROTON RBE IN TREATMENT PLANNING: GAIN IN CONFORMITY 24
IV.IV. IMPORTANCE OF RBE ROBUSTNESS FOR CLINICAL ROUTINE 25
IV.V. OTHER RBE MODELS 26
IV.VI. OUTLOOK 28

V. REFERENCES 30

VI. ARTICLES 42

VI.I. ARTICLE 1 42

VI.II. ARTICLE 2 42
VI.III. ARTICLE 3 42
VI.IV. ARTICLE 4 42

VII. APPENDIX I

VII.I. VERZEICHNIS DER AKADEMISCHEN LEHRER I
VII.II. DANKSAGUNG IV

CSC	Cancer stem cells
CNAO	Centro nazionale di adroterapia
CNS	Central nervous system
CT	Computed tomography
CTV	Clinical target volume
DKFZ	Deutsches Krebsforschungszentrum
DNA	Deoxyribonucleic acid
DSB	Double strand break
EUD	Equivalent uniform dose
GSI	GSI Helmholtzzentrum für Schwerionenforschung GmbH
GTV	Gross tumor volume
HCC	hepatocellular cancer
HIMAC	Heavy-Ion Medical Accelerator
HIT	Heidelberg Ion-Beam Therapy Centre
HSG	Human salivary gland
IMRT	Intensity modulated radiotherapy
LBL	Lawrence Berkeley Laboratory
LEM	Local effect model
LET	Linear energy transfer
LQ	Linear quadratic
MKM	Microdosimetric kinetic model
MRI	Magnetic resonance imaging
NIRS	National Institute of Radiological Science
NSCLC	Non-small cell lung cancer
NTCP	Normal tissue complication probability
PTV	Planning target volume
RBE	Relative biological effectiveness
SOBP	Spread out Bragg peak
OAR	Organ at risk
OER	Oxygen enhancement ratio
TCP	Tumor control probability
TRiP	TReatment planning for Particles
WHO	World Health Organization

I. Introduction

With 7.6 million deaths (around 13 %), cancer is one of the leading causes of death worldwide in 2008 (WHO 2013) and the second most frequent cause of death in Germany after diseases of the circulatory system in 2010 (DKFZ 2013). Cancer is most commonly treated with surgery, chemotherapy, radiotherapy or a combination of these treatment methods. The aim is a curative or palliative treatment of the patient, i.e., to cure the patient or improve quality of life. To cure the patient from cancer the tumor needs to be removed or at least hindered from growth and spread. In radiotherapy, mostly high energetic photon radiation is used to achieve this goal. Common methods of radiotherapy are brachytherapy and external radiotherapy. For the latter primarily accelerators are used to deliver the desired dose to the tumor volume.

External radiotherapy with conventional photon irradiation is steadily improved and nowadays offers advanced technologies to achieve highly conformal dose delivery to the tumor and a lower dose to surrounding tissue. A common method is intensity-modulated radiotherapy (IMRT); the intensity of the photon beam is varied in a large number of fields from different angles. However, for this radiation modality normal tissue is burdened with a high integral dose (Pirzkall et al. 2000).

Radiotherapy with ion beams is a promising alternative treatment method to conventionally used photons (Wilson 1946; Castro et al. 1982; Kraft 2000; Tsujii et al. 2007; Schardt et al. 2010). The advantage of ion beams is the inverse depth dose distribution with the Bragg peak at the end of their range, maximizing the dose to the cancer region and sparing normal tissue as much as possible. The dose to the surrounding tissue can be reduced by around 60 % comparing proton radiotherapy with IMRT (Roelofs et al. 2011; Loeffler & Durante 2013).

In addition to physical advantages, ion beams show an increased effectiveness particularly in the Bragg peak region. This includes the increased response of hypoxic cells or tissue, in terms of a decreased oxygen enhancement ratio (OER), and of cancer stem cells (CSC) mainly for heavier ions like carbon or oxygen (Pignalosa & Durante 2012; Scifoni et al. 2013). Recently, the diverse genetic response in terms of different gene expressions has gained interest regarding ion beam compared to photon irradiation (Fokas et al. 2009; Ding et al. 2013).

The treatment with ion beams has a long history and started in 1954 in Berkeley with the application of protons. Later during phase I-II clinical trials different ion species were used ranging from protons to argon ions (Castro et al. 1982). In 1994 the first patient was treated with carbon ions at the Heavy-Ion Medical Accelerator (HIMAC) at the National Institute of Radiological Science (NIRS) in Chiba (Japan; Tsujii et al. 2004).

A pilot study at the GSI Helmholtzzentrum für Schwerionenforschung GmbH (GSI) in Darmstadt has been performed in cooperation with the radiological hospital in Heidelberg, the research institute Rossendorf FZR in Dresden and the German Cancer Research Center DKFZ from 1997 to 2008. Within that project over 400 patients were treated successfully with carbon ions. The excellent clinical results motivated the installation of dedicated facilities for daily patient treatment like the Heidelberg Ion-Beam Therapy Center (HIT; Combs et al. 2010) and the Centro Nazionale di Adroterapia (CNAO) in Pavia (Italy) (Rossi 2011), a facility at the University Medical Center Marburg has been installed and in principle is ready to start patient treatments. Protons are more commonly used compared to heavier ions since they are favorable from an economic and logistic point of view. More than 100.000 patients have been treated with protons compared to around 10.000 treated with carbon ions and around 2.500 with other ions (PTCOG 2013). Nevertheless, a drawback of protons compared to heavier ions is their high lateral and range straggling, which is rather similar to that of IMRT methods. However, typically in IMRT a higher number of fields is needed making results not directly comparable (DeLaney & Kooy 2007).

Up to now patients at HIT are treated only with carbon ions and protons but the use of other ions like helium or oxygen is considered for the future. Because of the increasing interest in ion beam therapy the biological based treatment planning with heavy ions plays an important role to fully exploit the advantage of therapy relevant ions (Krämer & Durante 2010). For the biological treatment planning the relative biological effectiveness (RBE) of the ions in tissue needs to be considered. To predict the RBE for the irradiated tissue the local effect model (LEM) was developed and implemented in the pilot project (Scholz et al. 1997). Further, it is applied in treatment planning at HIT. The LEM derives the biological effectiveness of ions from the effectiveness of a reference irradiation, typically using conventional photon irradiation, taking advantage of the long experience with this radiation modality. The model has been continuously improved and is now capable of predicting the RBE for all therapy relevant ions from protons to carbon with similar accuracy, based on a unique, consistent set of input parameters (Elsässer et al. 2010). To introduce the recent model version LEM IV to clinical routine intensive analysis and comparison with measurements and clinical results are required. The following sections focus on relevant physical and biological aspects, contributing to the benefits and challenges of ion beam radiotherapy.

I.I. Depth dose distribution of photons and ion beams

The interaction of ionizing irradiation with atoms and molecules is used in radiotherapy to treat cancer cells. Photons and ions show different mechanisms of interaction with

matter that lead to substantial different dose distributions. The relevant photon interactions are the photoelectric absorption and the Compton scattering transferring the total or partial energy of the photon to the electrons of the atom. On the contrary ion beams give continuously small fractions of energy to the target atoms via coloumb interaction (ionization and excitation) and can also undergo nuclear reactions leading to projectile or target fragmentation. A detailed description of the processes can be found in Podgorsak (2005).

In radiotherapy and biology often the measure linear energy transfer (LET) is used to describe the average energy deposited per unit length (in keV/µm) in an absorber material like a cell or tissue. The energy deposition of ions as a function of the depth in matter is characterized by the Bragg curve (fig. 1). The LET is increasing when particles slow down in the absorber material up to a maximum at the end of their path with the highest energy loss at the so called Bragg peak. The position of the Bragg peak depends on ion type and initial energy. This can be exploited in ion beam therapy since the Bragg peak can be shifted in depth by means of energy variation. Figure 1 illustrates the advantage of ion beams compared to photons regarding the depth dose distributions.

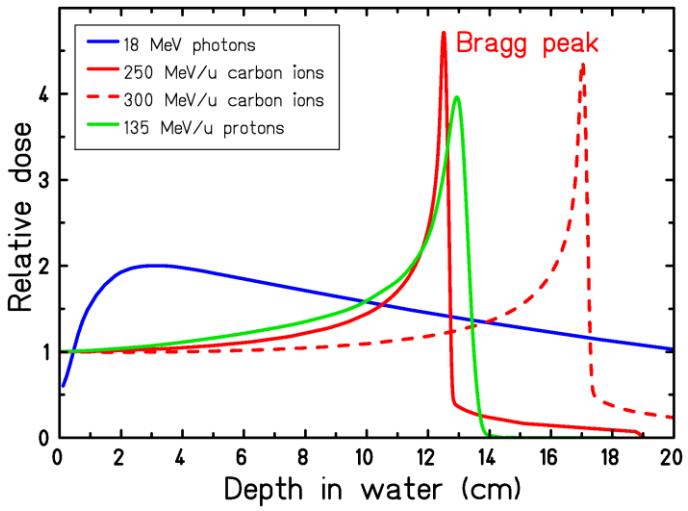

Figure 1: Relative depth dose distribution of photons, protons and ^{12}C-ions with different initial energies in water. The Bragg peak position can be shifted in depth by varying the initial energy of the ions. (Courtesy of Wilma Kraft-Weyrather, GSI Darmstadt, Germany)

After an initial build-up region that is caused by the range of the secondary electrons, photons show an exponential decrease of the dose with depth. In contrast, ion beams show an inverse depth dose distribution compared to photons with the maximum dose deposition at the end of their range. The depth dose distribution of ^{12}C-ions shows a sharp decrease beyond the Bragg Peak but exhibits a tail, which consists of fragments lighter than ^{12}C, thus having a higher penetration depth. Protons do not show a

fragment tail, but compared to ^{12}C-ions show a broader Bragg Peak since they are lighter and thus scattering effects are more pronounced when they interact with matter.

I.II. Biological effectiveness of ionizing radiation

So far, most of the knowledge about the response of cells or tissues to ionizing irradiation is based on the experience with photon irradiation, i.e., low-LET irradiation. Thus, most of the radio-oncological principles and radiobiological models invented were developed to describe the dose response of photon irradiation rather than the response to ion beam irradiation. The following section deals with biological effectiveness of ionizing radiation and a remedy to transfer the knowledge about the effectiveness of photon irradiation to ion beams.

Ionizing radiation causes damage to cells and tissues primarily as a consequence of damage to the DNA. The ability to repair damage strongly depends on the cell type and is reflected in the sensitivity to irradiation. In general, the radiosensitivity of a cell type is related to its proliferation capacity. For example, cells with a high mitotic activity, i.e., a high division rate, tend to be more sensitive to irradiation, whereas slow or non-proliferating cells are more radioresistant. Regarding *in-vivo* systems this can explain why for example cells of the hematopoietic system which are replaced continuously belong to the most radiosensitive cells whereas neurons which are highly differentiated and do not reproduce are very resistant to irradiation (Rubin & Casarett 1968).

Description of cell- and tissue sensitivity with the linear-quadratic (LQ)-model

From the response of cell or tissue types to irradiation dose-effect relationships can be established. The shouldered form of the dose-response curve observed for *in-vitro* cell survival experiments can be described by the linear-quadratic (LQ)-model

$$S(D) = \mathrm{e}^{-(\alpha \cdot D + \beta \cdot D^2)}$$

with the cell survival S as the function of the dose D described by the parameters α and β (Sinclair 1966; Kellerer & Rossi 1971; Douglas & Fowler 1976). The interpretation often used for the parameters α and β is the relation of hits to the induced lethal events. The parameter α characterizes a linear relationship, resulting from a single hit mechanism, and the parameter β a quadratic relationship, which is caused by lethal events resulting from multiple hits. The α/β-ratio describes the dose where the linear and quadratic components are equally contributing to the cell survival. For conventional irradiation with photons a high α/β-ratio (>6 Gy) is common in radiosensitive cells and early responding tissues including many tumors. A low α/β-ratio (1-6 Gy) is often observed for radioresistant cells or late responding tissue types (Hall & Giaccia 2011).

The sigmoid shaped dose-response curve characteristic for clinical endpoints, i.e., local tumor control or normal tissue complication can be derived from the clonogenic cell survival curve assuming a certain number of functional cells which need to be inactivated in order to have a response of the tumor or organ regarded (McNally & Sheldon 1977; Dawson & Hillen 2006).

A common method in radiotherapy is the fractionation of the total prescribed dose to the tumor volume in order to enhance the differential effect between tumor and normal tissue response, i.e., to decrease side effects while keeping the effect to the tumor constant. Advantage is taken here from the difference of early and late responding tissues to the same fractionation pattern. For dose response curves with a pronounced shoulder as observed for rather late responding normal tissues, the effect is more sensitive to a change in the dose per fraction. In this case more severe effects for a higher dose per fraction are expected with respect to the same prescribed total dose. In contrast, the dose response curves of early responding tissues or most tumors are typically characterized by only a slight shoulder, the linear component is dominating and indicates a less pronounced dependence on the fraction dose (Thames et al. 1982). Thus the optimal fractionation schedule is mainly determined by the late responding normal tissue (Hall & Giaccia 2011: 395).

The isoeffective dose D_{IsoE} is an appropriate measure to compare the outcome of different fractionation regimens. It describes the total dose needed in a reference fractionation regimen to end up with the same effectiveness as the fractionation regimen with the total dose D and the fraction dose d (Wambersie et al. 2006).

$$D_{IsoE} = \frac{D(1 + d \cdot \beta/\alpha)}{1 + d_{ref} \cdot \beta/\alpha}$$

Here, d_{ref} describes the fraction dose of the reference fractionation regimen. Another measure of effectiveness based on the assumptions of the LQ-model is the equivalent uniform dose (EUD) which is useful to estimate the effect of a defined spatial dose distribution (Niemierko 1997).

$$EUD = -\left(\frac{\alpha}{2\beta}\right) + \sqrt{-\frac{ln\bar{E}}{\beta} + (\alpha/2\beta)^2}$$

The EUD is corresponding to the dose leading to the mean radiobiological effect $\bar{E}$ in a defined volume (target) and is useful to describe the impact of a heterogeneous dose distribution as it occurs especially in the normal tissue surrounding the tumor volume.

The LQ-parameters α and β or at least the α/β-ratio of the photon dose-response curve are needed to calculate the EUD and the isoeffective dose.

Enhanced biological effectiveness of ion beams

Ion radiation induces increased radiation damage in cells compared to photons, In general, the higher effectiveness becomes visible in dose response curves as an increased linear coefficient α of the LQ-model whereas the change in the quadratic component, i.e., the coefficient β, is less pronounced and is observed only for very high-LET values. The relative biological effectiveness (RBE) is defined as the dose ratio of a reference irradiation like photons to ions resulting in the same biological effect.

$$\mathrm{RBE} = \frac{D_{ref}}{D_{ion}}\bigg|_{IsoE}$$

The increased effectiveness can be explained by the different microscopic energy deposition patterns of photons and ions, respectively. On the level of the cell nucleus, photons show a rather sparsely, but homogenous energy distribution. Ions on the contrary show a concentrated energy distribution along the ion trajectory. The correspondingly higher ionization density in the track center induces damage, which is believed to be more difficult to repair for the cell, resulting in a higher effectiveness of high-LET irradiation like, e.g., carbon ions in the Bragg peak region.

The RBE is a complex quantity and depends on several variables such as the LET of the ion, which is the reason for a higher RBE in the Bragg peak region than in the entrance channel. This differential behavior of the RBE in the Bragg peak and entrance channel region poses the biological advantage of high-LET irradiation such as heavier ions, compared to low-LET irradiation like photons. The extent of it though depends on the radiosensitivity of the cells or tissues irradiated (Fokas et al. 2009). A cell or tissue type with a rather small α/β-ratio for photon irradiation shows a more distinctive response to high-LET compared to low-LET irradiation. For a high α/β-ratio a smaller difference between low-LET and high-LET irradiation can be observed. Weyrather et al. (1999) and Friedrich et al. (2013a) have shown that there is an empirical linear relationship of β/α to the RBE, i.e., the RBE increases with the inverse of the α/β-ratio. The RBE also depends on the ion type since ionization densities are different for the same range in water. Furthermore, RBE depends on the effect level regarded, which is dependent on the applied dose. Thus, the RBE is dependent on the fractionation schedule, i.e., on the dose per fraction.

I.III. Treatment planning in radiotherapy

Dose optimization in treatment planning for photon and ion beam radiotherapy requires delineation of the tumor volume and relevant organs at risk (OAR). The definition of the planning target volume (PTV) is based on the macroscopic tumor extension, i.e., the gross target volume (GTV) and the subclinical spread of the tumor accounted for by an

extra margin, i.e., the clinical target volume (CTV) (ICRU 1999a and 1999b). The localization of the PTV and relevant OARs is assessed by computer tomography (CT) and magnetic resonance (MR) images. The optimization is performed for a prescribed fraction dose to the tumor volume and thereby takes into account the tolerance doses of the surrounding normal tissues. The number of fields contributing to the prescribed dose and the corresponding beam direction is defined by the aim to spare the OAR as much as possible.

Treatment planning objective in radiotherapy

In conventional radiotherapy with photons the treatment planning is concentrated on the delivery of a prescribed physical absorbed dose to the tumor volume. Dosimetry procedures ensure the accuracy of the applied dose to the patient. The fractionation regimen takes into account the radiosensitivity of the tumor and the surrounding normal tissues, which are typically derived from experience and clinical studies. Biological modeling approaches in terms of the LQ-model, tumor control probability (TCP)- and normal tissue complication probability (NTCP)-modeling and effective dose prescriptions can be used to estimate the effectiveness of the applied physical dose and the corresponding dose response relationships (Niemierko 1997). The α/β-ratio is a widely used quantity for this purpose however determination of the α/β-ratio for a certain tissue and endpoint is afflicted with large uncertainties. To determine α/β-ratio clinical studies applying different fractionation regimens but resulting in the same outcome are needed (Douglas & Fowler 1976). Otherwise α/β-ratios can be determined from *in-vitro* or *in-vivo* experiments and transferred to clinical endpoints, which again comprises uncertainties following from the environmental differences.

At present, the individual patient radiosensitivity is not taken into account for the planning procedure and the clinically used fractionation regimens are based on the outcome of large patient collectives providing profound knowledge about the dose response relationship of the endpoint under consideration. An important aspect of planning is the reduction of NTCP that is now possible due to the improved dose delivery with IMRT methods, which lead to a high tumor conformity (Pirzkall et al. 2000). The focus or future direction is thus to reduce side effects by incorporation of outcome predictions instead of only dose values. The difficulty is a largely inhomogeneous dose to the surrounding tissues and OARs, which makes the proper assessment of effective dose values to evaluate the NTCP increasingly important (Wu et al. 2002).

The introduction of biological optimization in treatment planning and the consideration of the patient specific radiosensitivity to further improve the outcome of radiotherapy and reduce side effects is discussed in the literature (Brahme 1995; Wang et al. 1995;

Bortfeld et al. 1996; Peacock et al. 1998; Brahme 1999; Stewart & Li 2007). Especially in the case of large tumors, which more often comprise a hypoxic region, it is useful since the responsiveness of the tumor is dominated by the most radioresistant, i.e. the hypoxic, part of it. Commercial treatment planning systems already using biological based optimization and including measures like the EUD, TCP and NTCP have shown to better spare OAR in comparison to the standard dose-volume method (Semenenko et al. 2008; Qi et al. 2009; Li et al. 2012).

In contrast to conventional radiotherapy with photons, the effectiveness of ions is strongly dependent on the position in the treatment field and the applied physical dose is not directly related to the responsiveness of the irradiated tissue. Thus, the application of ions, especially heavier ions like carbon, requires the consideration of the enhanced biological effectiveness at every position in the irradiated tissue in the treatment planning procedure to not harm the normal tissue or underestimate the dose in the target volume to the expense of the local tumor control. Due to a lack of clinical data allowing to deduce the RBE distribution with the required spatial resolution the effectiveness needs to be estimated from experimental data or by means of biophysical models. In the clinical application of ion beams different approaches are followed to account for the enhanced effectiveness in terms of RBE. In proton beam therapy the RBE is considered by multiplying the physical dose distribution with a constant value of 1.1. In the Japanese ion beam therapy centers the estimation of RBE of carbon ions for the irradiated tissue is based on the radiosensitivity of human salivary gland (HSG) cells and the clinical experience with neutron irradiation (Kanai et al. 1999). The work presented in this thesis focuses on the LEM, which is used to predict the RBE for the biological optimization of the prescribed dose.

Biological based treatment planning with TRIP98

The treatment planning software TRiP98 (TReatment Planning for Particles, 1998 edition) was developed at the GSI for radiotherapy with heavy ions, especially with carbon ions (Krämer et al. 2000; Krämer & Scholz 2000; Krämer & Durante 2010). It was used in the pilot study at GSI and is the basis for the commercially developed therapy planning system at the HIT, syngo PT Planning (Siemens Healthcare). It is specifically designed for applications using a full active beam delivery system with active energy variation to modulate the depth position of the Bragg peak and lateral raster scanning by means of horizontal and vertical magnetic deflection of the ion beam (Haberer et al. 1993). Further it is the first treatment planning software allowing a full biological optimization of the prescribed dose for ion beam therapy (Jäkel et al. 2001).

The prescribed dose to the PTV is a RBE-weighted dose and thus reflects a photon equivalent dose. For the optimization of the RBE-weighted dose, the PTV is divided for each field into iso-energy slices corresponding to a constant initial energy of the ions. Slice-by-slice a certain number of ions is prescribed to the vertically and horizontally arranged raster spots to achieve a homogeneous RBE-weighted dose distribution. In depth, the monoenergetic Bragg curves are overlaid and generate the so-called spread out Bragg peak (SOBP; fig. 2). Additionally, the method enables an intensity modulation by independently varying the particle number, i.e., dose to each raster spot.

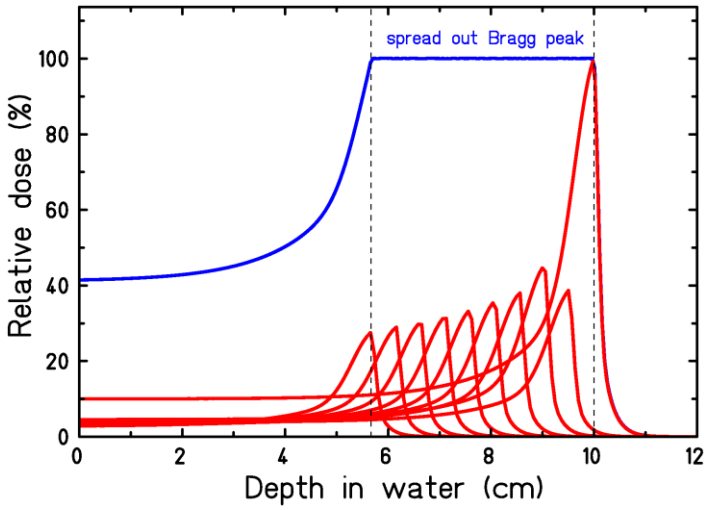

Figure 2: The superposition of fluence-weighted Bragg curves (red) forms the SOBP (blue) of the prescribed dose in the PTV. The relative weighting of the monoenergetic Bragg curves is determined by a dose optimization within the treatment planning system. (Courtesy of Wilma Kraft-Weyrather, GSI Darmstadt, Germany)

The planning procedure requires the 3-dimensional information of the particle composition at each position in the field. This includes the energy spectra of the primary particles, i.e., the projectile, and all projectile fragments. Information about the energy spectra of each particle in the irradiated volume is not only important for the calculation of the physical absorbed dose but also for the calculation of the corresponding RBE-weighted dose. The RBE is predicted by the LEM, which derives the effect of the ion beam from the effect of conventional photon radiation on the irradiated tissue. The LEM is described in more detail in the following subsection.

With TRiP98 it is also possible to perform a simultaneous biological optimization of multiple fields, i.e., a multi-field optimization of the prescribed RBE-weighted dose in the PTV (Gemmel et al. 2008). The difficulty here is that the RBE must be considered for the dose of the superimposed fields and not for each individual field since only the final particle composition in the mixed irradiation field and dose-level determines an accurate RBE. Thus RBE needs to be considered for every iteration step, which is the core of the biological optimization.

Prediction of RBE with the Local Effect Model (LEM)

For the GSI pilot project and currently at the HIT the RBE prediction is based on the first version of the LEM (Scholz et al. 1997). The two main components of the model are the dose-response of a considered endpoint to photon irradiation and the amorphous track structure of the ion beam, i.e., the radial dose distribution of the track. The basic assumption of the model is that local damage is fully determined by the local energy deposition, but otherwise is independent from the radiation type. In contrast to photons, ions produce a rather inhomogeneous dose distribution with a dense energy deposition pattern close to the track center and a more sparse, photon like energy deposition pattern with increasing distance to the track center. The dose response of the photon irradiation that is used as input to the model is described by the LQ-model and extended with a transition to a linear relationship for doses exceeding a threshold dose D_t.

The focus in the development of LEM I was to correctly represent the RBE in therapeutically relevant carbon ion SOBP. Otherwise, it showed to have certain limitations with respect to the accuracy of the RBE predictions in the entrance region and for lighter ions. The use of parameters that allow accurate representation of RBE in the carbon SOBP lead to an overestimation of RBE in the entrance region and a general overestimation for lighter ions, in that case for both the SOBP and the entrance region. However, reliable RBE predictions for lighter ions like protons and helium with a common input parameter set are desirable to allow direct treatment plan comparisons for different ion beams. Therefore, model improvements have been gradually implemented (Elsässer & Scholz 2007; Elsässer et al. 2008). With the latest model version LEM IV (Elsässer et al. 2010) the RBE can be predicted with similar accuracy for all positions in the treatment field and over the whole range of clinically relevant ions with a common set of input parameters.

In the LEM IV a two-step procedure is used to determine the biological effect. In a first step the local damage distribution in terms of double strand breaks (DSB) within individual ion tracks is determined. In the second step the distribution of these DSB within the DNA, specifically within megabase pair chromatin loops is determined (Friedrich et al. 2012). Hence, an intermediate step is introduced as compared to the LEM I for which the local dose distribution is converted into a spatial distribution of DSB. This approach allows a more mechanistic interpretation of the induction of cell death. Subsequently, the RBE is calculated and stored in a tissue and endpoint specific RBE-table which is used in TRiP98 to calculate the RBE in the mixed irradiation field. In the RBE-table the RBE is sorted by ion type from protons to neon with energies ranging from 0.1 to 1000 MeV/u in 40 logarithmically equidistant energy steps.

II. Summary of the published results (cumulative)

II.I. Proof of consistency and comparison with *in-vivo* experiments

The comparison of clinical data for different beam qualities and the construction of common dose response curves require the accurate prediction of RBE-weighted and isoeffective doses. A compilation of 5-year local control for the treatment of skull base chordoma with conventional and ion beam radiotherapy and the resulting dose response relationship is published in Schulz-Ertner et al. (2007). The compilation includes the local control probability obtained in the GSI pilot project corresponding to isoeffective doses based on RBE predictions of the LEM I. The isoeffective dose predictions are in accordance with other ion beam studies by Castro et al. (1994) at the Lawrence Berkeley Laboratory (LBL) using helium and neon ions with the same local tumor control of 63 %. The dose response can be well described by a sigmoid shaped curve. At higher doses the curve is mainly determined by the clinical results obtained with ion beam therapy. Hence, to establish a common dose response curve one needs to consider the RBE, whereby uncertainties and inadequate determination of RBE can alter the dose response relationship due to the corresponding shift on the dose axis. The question arises whether the LEM IV can describe the dose response relationship obtained from clinical data published in the literature as good as the LEM I does. Thus, it was of particular interest to analyze consequences of the model improvements from LEM I to LEM IV in therapeutic relevant situations to demonstrate the applicability of the LEM IV for patient treatment.

Thus, the main goal of ***article 1*** was to compare the LEM IV against LEM I under treatment-like conditions for idealized target geometries. In order to compare the two models on the level of RBE prediction the underlying physical dose distribution had to be the same. Therefore, the dose distribution as applied in the GSI pilot project was used in which the RBE-weighted dose was optimized based on the LEM I. The resulting physical dose distribution further served as a reference for the LEM IV recalculations. Concerning the tissue specification as represented by the photon input parameters of the LEM IV, rather small α/β-ratios of 2 Gy and 2.45 Gy are used **(RBE-table AB2 IV and AB2.45 IV; tab. 1, *article 1*)**, in line with the known characteristics of central nervous system (CNS) tissue types (Karger et al. 2006; Hall & Giaccia 2011:396) and with the α/β-ratio of the photon input parameters applied in the GSI pilot project **(RBE-table AB2 I; tab. 1, *article 1*)**. The assumption of a small α/β-ratio for chordoma is further supported by the α/β-ratio of 2.45 Gy, evaluated for local control of

chordoma from clinical studies using hypofractionated photon radiotherapy (Henderson et al. 2009).

Figure 1a in *article 1* illustrates that the resulting RBE-weighted dose distribution based on LEM IV shows a significant rise within the SOBP using the reference physical dose profile. This is due to the fact that the RBE predicted by the LEM IV shows a steeper gradient of RBE with LET than compared to LEM I. The LET is highest at the distal end of the SOBP due to the pronounced contribution of high-LET ion tracks and leads to a sharp increase of the RBE-weighted dose. For the 2-field optimization **(fig. 1b, *article 1*)** the RBE-weighted dose profile is homogenized but the higher sensitivity on LET is still visible. Nevertheless, the similarity of the EUD and the mean RBE-weighted dose based on the LEM IV predictions for the same target volume dimension showed that the inhomogeneity of the RBE-weighted dose distribution is not reflected in the mean effectiveness of the irradiation **(fig. 2, *article 1*)**.

We were able to show **(fig. 5, *article 1*)** that the higher RBE in the distal part of the SOBP predicted by the LEM IV is in better agreement with the RBE obtained in the *in-vivo* experiments by Karger et al. (2006). The experiments analyzing the tolerance of the rat spinal cord after photon and carbon ion irradiation with different fractionation schedules aimed to determine the RBE and revealed that the RBE predicted by the LEM I was underestimated by about 25 % in the center of a 1 cm SOBP, whereas for LEM IV the deviation are on average less than 10 %. The measurements represent the RBE in the distal part of the SOBP independent on the dimension, i.e., the RBE at around 5 mm from the distal end in any SOBP.

The consistency of the LEM IV based RBE-weighted dose prediction was further verified by the comparison with the 5-year local control data for chordoma of the skull-base compiled by Schulz-Ertner et al. (2007). For this purpose, the isoeffective doses were calculated for two different endpoints, i.e., for two slightly different α/β-ratios of 2 Gy and 2.45 Gy **(RBE-table AB2 IV and AB2.45 IV; tab. 1, *article 1*).** Since the discrepancy between LEM I and LEM IV has shown to be strongly depended on the tumor dimension **(fig. 1 and 2, *article 1*)**, the isoeffective doses were calculated for the median (80.3 ml), minimal (13.9 ml) and maximal (594.2 ml) tumor volume treated in the clinical study respectively.

Figure 4 in *article 1* shows the compilation of the 5-year local control data including the dose-response of carbon ion therapy for skull-base chordoma in the GSI pilot project with 63 % and 100% local control for two different fractionation regimens respectively. The isoeffective doses predicted by the LEM I have shown to be in good agreement with the dose prescriptions of other studies leading to a similar outcome (Castro et al. 1994; Terahara et al. 1999; Hug et al. 2000). Even though the variability

with tumor volume is large, the isoeffective doses for the median tumor volumes based on RBE predictions of the LEM I and LEM IV deviate by less than 5 % for the two considered α/β-ratios. This agreement of the isoeffective doses confirms the capability of the LEM IV to consistently describe the clinical outcome.

II.II. Conversion of institutional dependent RBE-weighted doses

From the comparison with the compiled clinical data of Schulz-Ertner et al. (2007) the question arises to what extent the RBE-weighted doses estimated in other institutions are comparable if they rely on a different approach. This is the case for protons, when a constant RBE is assumed, or for the clinical trials with helium at the LBL where only a depth dependent RBE is considered (Castro et al. 1994). For the comparison of clinical data though, it is of interest to convert RBE-weighted doses predicted by different models for a better understanding and comparison of dose-effect relationships. Since the HIMAC approach is applied in patient treatment at the NIRS for a long time and many different types of tumors the comparison to the GSI/HIT approach based on the LEM is of great interest to compare clinical studies and dose-effect relationships and to utilize well-experienced fractionation schedules applied. In ***article 2*** a method is introduced to convert and compare RBE-weighted doses based on the HIMAC and GSI/HIT approach. In comparison to the LEM the HIMAC approach only gives a depth dependent RBE which is based on the LET distribution but neglects the dose dependence as well as the tissue type dependence. The comparison was done for both the LEM I and LEM IV.

To compare the two approaches, in a first step the HIMAC depth dose profile based on passive beam shaping was reconstructed as described in ***article 2***. The resulting physical dose profile served as reference to compare the RBE-weighted dose distribution resulting from the application of the LEM I and LEM IV, respectively. Since the tissue under consideration influences the RBE-weighted dose, the evaluated conversion factors are specific for the RBE-tables based on LEM I and LEM IV used in the present comparison. However, the conversion factors can be calculated for any kind of tissue and endpoint if the required photon input paramters for the LEM are available.

The resulting RBE-weighted dose distribution based on LEM I and LEM IV are different in shape and magnitude as can be seen in **fig. 2 of *article 2*** but the mean and median RBE-weighted dose are very similar **(fig. 3c and tab. 1, *article 2*)**. Since the goal of a biological optimization is a homogeneous RBE-weighted target dose not only the shift in RBE-weighted dose is being compared to the HIMAC approach but also the homogeneity in the target volume expressed with the EUD. Typically, the deviation of

the EUD from the median RBE-weighted dose is less than 5 % **(tab. 1, *article 2*),** in agreement with the results obtained in ***article 1***.

The conversion factors between HIMAC and LEM turned out to be strongly dependent on the fraction dose and can range from 1.76 to 0.46 for prescribed HIMAC doses from 1 to 60 Gy. At a prescribed HIMAC dose of around 5 Gy (RBE) the conversion factor is 1 leading to similar LEM based RBE-weighted doses in this dose region **(fig. 3 and 4, tab. 2, *article 2*).** The bandwidth of conversion factors demonstrates the need for approriate mapping with treatment planning studies.

With the conversion factors it is now possible to compare the outcome of clinical studies for common dose prescriptions. For instance, the conversion factor for the fractionation schedule of 20 x 3 Gy (RBE) applied for the majority of the patients with skull-base chordoma in the GSI pilot project would be approximately 1.2. This corresponds to a prescribed HIMAC dose of 20 x 2.5 Gy (RBE) and in terms of an isoeffective dose for 2 Gy per fraction to 56.25 Gy (IsoE). The estimated isoeffective dose is considerably lower than the 75 Gy (IsoE) and 76.75 Gy (IsoE) resulting from LEM I and LEM IV predictions respectively. Regarding the local control curve shown in Schulz-Ertner et al. (2007) and ***article 1*** the expected TCP for 56.25 Gy (IsoE) would be lower, comparable to what has been observed in conventional radiotherapy with photons (IMRT).

The HIMAC patients are more often treated with low fraction numbers and higher dose per fraction, therefore it can be expected that the doses converted to the LEM approach are considerably lower and can differ by up to a factor of 2 to the prescribed HIMAC dose. This is well seen from the comparison with the HIMAC single fraction regime of 48 Gy (RBE) prescribed HIMAC dose for non-small-cell lung cancer (NSCLC) (Tsujii & Kamada 2012). To the knowledge from conventional radiotherapy, 48 Gy (RBE) would exceed the tolerance doses of many normal tissues and OAR but converted into a LEM I based median RBE-weighted dose of 23.1 Gy (RBE) the fractionation regimen shows to be within the limit of tolerance doses. This predicted RBE-weighted dose corresponds to a rather radioresistant tissue type with an α/β-ratio of 2 Gy. For rather radiosensitive tissue types the predicted dose is expected to be even lower than the 23.1 Gy (RBE).

This examples show that caution is necessary if dose-response relationship are based on different biological models and tools to convert prescribed doses are necessary especially in the context of heavy ion therapy.

II.III. Sensitivity of RBE on the LEM input parameters

In order to estimate the uncertainty of the RBE the LEM inherent RBE sensitivity to the input parameters was assessed. In ***article 1*** the sensitivity of the RBE-weighted dose on the photon input parameters was evaluated. A modification of the parameters α, β and D_t by 25 % affected the RBE-weighted dose by less than 10 % **(tab. 3, *article 1)***. This variation is in the order of the uncertainty inherent to clinical data.

In ***article 3*** the sensitivity of the RBE and RBE-weighted dose was extensively analyzed for the input parameters of the LEM **(tab. 1*, article 3*)**. For the parameter sets two α/β-ratios were chosen, one describing a rather radioresistant late responding cell - or tissue type with the parameters α = 0.1 Gy^{-1}, β = 0.05 Gy^{-2} and D_t = 8 Gy as design parameters for α/β = 2 Gy and one rather radiosensitive early responding cell- or tissue type with α = 0.5 Gy^{-1}, β = 0.05 Gy^{-2} and D_t = 14 Gy for α/β = 10 Gy **(*article 3*)**. The two α/β-ratios of 2 and 10 Gy represent the typical range of values for relevant radio-oncological endpoints, although in some cases values exceeding this range are observed. For example, for prostate a very low α/β-ratio of 1.5 Gy is reported and for liver a very high value of 15 Gy (Suit et al. 2010). The choice of the parameter D_t was inspired by an empirical linear relationship between α/β-ratio and D_t which was found by Friedrich et al. (2013a).

The sensitivity analysis has been carried out for irradiation under track segment conditions, i.e. for monoenergetic beams with well-defined energy and LET, and for irradiation in a mixed field within a SOBP. For the RBE under track segment conditions it can be seen in **fig. 1 and 2 of *article 3*** that for a parameter variation of 25 % the RBE in general changes less than 25 %. The RBE at the 10 % effect level (RBE_{10}) is typically less sensitive to parameter variations compared to the RBE for the initial slope of the effect curve (RBE_α). Regarding the RBE_{10} only for the variation in the nuclear radii r_n the RBE change is larger than 25 % for high LET values above 200 keV/µm.

For the case of a mixed field irradiation within a SOBP, due to fragmentation, straggling and scattering several particle species, each having an individual energy distribution, may contribute to the overall dose deposited. Because of this mixing in the extended target volumes the sensitivity of RBE to its input parameters is damped as compared to the sensitivity observed for monoenergetic ion beams. Instead of the LET dependence for the mixed irradiation field the depth dependence was regarded. In compliance with the clinical routine the analysis focused on a 2-field optimization to 3 Gy (RBE) for the reference cases as well as for every input parameter variation. **Figure 3 and 4 in *article 3*** show the RBE sensitivity for the different input parameters. The results of

single field optimizations have also been studied extensively and are briefly discussed in the article.

Regarding the 2-field optimizations the largest variation is observed for the chromatin loop size parameter l_{DSB} defining the clustering properties of DSB and thus the lethality ascribed to a given pattern of DSB. In general the RBE sensitivity is higher for the low reference α/β-ratio, i.e., 2 Gy, but for all parameters the RBE variation is less than 25 %. This means that the variation of the RBE values depends typically less than proportional on the variation of the input parameters. The damping of the RBE sensitivity in the mixed irradiation field compared to the monoenergetic beam is a consequence of the broader LET distribution within the SOBP. This can be concluded from the fact that the RBE in the SOBP center is even damped compared to the RBE of a monoenergetic beam with comparable LET of about 50 keV/µm. The RBE in the SOBP is in general lower compared to the RBE for a monoenergetic beam with the same LET and the damping of RBE sensitivity is a consequence of an overall smaller RBE.

II.IV. Proton RBE and assessment of uncertainty

The RBE is not only a matter of heavier ions like carbon but also for the lighter ions. The study presented in ***article 2*** has shown that differences in the RBE prediction can lead to different assumptions of the dose effect relationship, assumed tolerance doses for normal tissues and modified local control relationships. Thus it is important to try to describe these dependencies as accurate as possible. In current clinical practice the RBE of protons is considered to have a constant value of 1.1 independent on the depth distribution in the SOBP and general RBE dependencies. Paganetti et al. (2002) showed by a large compilation of *in-vivo* experiments that the biological effectiveness of protons in tissue is on average very similar to that of x-rays for in vivo endpoints for most of their path. This supports the reasoning to use in clinical practice a constant RBE of 1.1. Nevertheless neglecting the variability along the SOBP can lead to errors in the interpretation of clinical data and to an unnecessary dose to the surrounding tissue, e.g., by an extension of the effective range of the proton beam. The capability of LEM IV to predict the RBE for protons up to carbon ions with sufficient accuracy (Elsässer et al. 2010), gave rise to a systematic analysis of the proton RBE published in ***article 4***. In this analysis, we focus on the RBE and RBE-weighted dose at the distal end of the SOBP, since LET values increase towards the distal end and thus RBE effects are expected to be particularly pronounced in this region.

Validation by means of *in-vitro* data showed that the RBE along a proton SOBP predicted by the LEM IV is in accordance with the experimental observed RBE. The

measured and predicted RBE values for the two experiments of Tang et al. (1997) and Bettega et al. (2000) are shown in **fig. 2 of *article 4***. It was important to show that both the dose-level dependence of the RBE **(fig. 2a, *article 4*)** and the steep increase of RBE due to the high LET at the distal end and in the distal penumbra **(fig. 2b, *article 4*)** are well represented.

Furthermore the biological range extension of the proton beam was analysed which describes the extension of the SOBP due to the enhanced RBE in the distal penumbra compared to the constant RBE of 1.1. The range extension was characterized in dependence on physical factors like the dose-level, initial beam energy, tumor dimension and depth position as well as on biological factors like the tissue type in tumor and normal tissue. For the systematic analysis the photon input paramter sets described in the last section with α/β-ratios of 2 and 10 Gy are used. An important result of the analysis was that the biological extension is strongly influenced by the gradient of the distal dose penumbra, i.e., a flat penumbra leads to a more pronounced extension than a steep one, although a steep gradient goes along with a higher distal RBE-weighted dose compared to a shallow one. This anti-correlation is shown in **fig. 5 of *article 4***. The difference in the distal gradient can be caused by several physical configurations like the depth modulation system, i.e., if it is a passive or active energy variation. The main difference between active and passive variation is the initial energy used for irradiation. For a passive modulation normally a fixed and relatively high initial energy is used. The resulting depth dose distribution for higher energies has a wider distal penumbra due to the enhanced range straggling since the beam passes more material until it stops and is subject to more scattering processes. Lower energies as they can be used in active depth modulation with flexible initial energy show a sharper distal penumbra with a higher maximum LET leading to a higher RBE-weighted dose at the distal end of the SOBP. **Figure 7 in *article 4*** schematically explains the influence of the gradient on the biological range extension.

Similar to what is done in carbon ion therapy, the biological range extension can be accounted for by a biological optimization, which leads to a decreased physical dose towards the distal end of the SOBP. The study showed that a reduction of the physical dose at the distal end is also necessary to decrease disagreement in the range and RBE-weighted dose prediction. The estimated and actual dose can be largely different and due to generous margins in proton beam therapy the maximum difference at the edges of the SOBP also affects parts of the surrounding normal tissue.

The range uncertainties and extensions have also been addressed by Gensheimer et al. (2010) using MRI measurements after irradiation of the lumbar spine with protons in the course of medulloblastoma treatments. They were able to directly determine the

biologically effective range in the patients and reported an average overshoot of the proton beam in the lumbar spine of 1.9 mm (0.8–3.1 mm). A small part of the overshoot (less than 1mm) was attributed to the increased RBE in the distal penumbra according to considerations by Paganetti (1998). Nonetheless, a discrepancy to the actually measured overshoot can be observed. The results presented in ***article 4*** may fully explain the overshoot they have observed with a predicted biological range extension of 1.6–3 mm for 235 MeV and 1.1–1.8 mm for 160 MeV (energies typically used), at the 50 % isodose considering a prescribed RBE-weighted dose (RBE = 1.1) of 2 Gy (RBE). The given bandwidth of biological range extensions describes the dependence on the radiosensitivity of the tissue type.

III. Aim and contribution

Ion beam therapy requires the consideration of RBE to estimate a reliable prescribed dose to the tumor volume. RBE is a complex quantity and the accuracy of the RBE prediction relies on a proper modeling taking all the dependencies of RBE into account. The work presented here aims at analyzing the influence of enhancements in the RBE model currently used for clinical application to outline the potential uncertainties occurring when disregarding the complexity of RBE in treatment planning and the consequences for the interpretation of clinical and experimental data.

III.I. Article 1

Impact of enhancements in the local effect model (LEM) on the predicted RBE-weighted target dose distribution in carbon ion therapy

The publication deals with the differences occurring in the RBE-weighted dose distribution by the application of the improved version of the LEM. I conducted all the treatment planning studies and analyzed the RBE-weighted dose distributions including the calculation and comparison of the EUD, the sensitivity analysis of the photon input parameters, the comparison with the *in-vivo* experiment by Dr. Christian Karger et al. and the consistency check with the 5-year TCP for chordoma of the skull base. The design of the research project was done together with Dr. Michael Scholz. I wrote the manuscript with advises from Dr. Michael Scholz and Dr. Thomas Friedrich concerning the structure and interpretation of the results. Dr. Michael Krämer assisted me with concerns related to the treatment planning software TRiP98. Dr. Christian Karger, Prof. Dr. Klemens Zink, Prof. Dr. Marco Durante and Prof. Dr. Engenhart-Cabillic contribute with ideas and corrections to the manuscript.

III.II. Article 2

Mapping of RBE-weighted doses between HIMAC- and LEM-based treatment planning systems for carbon ion therapy

The work of Dr. Olaf Steinsträter in the department of Prof. Dr. Marco Durante and in the group of Dr. Michael Scholz is partly based on systematic analyzes which I performed in previous work. My preliminary work consisted of the assessment of photon input parameters for the LEM and systematic dependencies of RBE. Moreover I had advisory functions in the realization of the work concerning the introduction to biological based treatment planning with TRiP98 and the interpretation of the results.

III.III. Article 3

Sensitivity analysis of the relative biological effectiveness predicted by the local effect model

I supported the work of Dr. Thomas Friedrich in the department of Prof. Dr. Marco Durante and in the group of Dr. Michael Scholz with the sensitivity analysis of the RBE for the therapy cases, i.e., within the SOBP representing a mixed irradiation field. Moreover I partly wrote the manuscript and was involved in the interpretation of the results.

III.IV. Article 4

Physical and biological factors determining the effective proton range

I did all the systematic analysis and introduced the biological treatment planning for protons. I benchmarked the physical base data needed and compared my results with experiments from the literature where two of them are shown in the manuscript. I did the analysis of the biological range extension and compared my results to other model predictions and clinical data from the literature. I wrote the manuscript and interpreted and discussed the results with constructive ideas and improvements of Dr. Michael Scholz and Dr. Thomas Friedrich. Dr. Michael Krämer has supported me with any questions regarding the treatment planning software TRiP98 and modeling of the proton base data. Prof. Dr. Klemens Zink, Prof. Dr. Marco Durante and Prof. Dr. Engenhart-Cabillic contribute with ideas, fruitful discussions and corrections to the manuscript.

Hiermit bestätige ich die Richtigkeit der gemachten Angaben bezüglich des Eigenanteiles von Rebecca Grün an den aufgeführten Publikationen.

Marburg, Februar 2014

Rebecca Antonia Grün (Autorin)	Prof. Dr. Rita Engenhart-Cabillic (Betreuerin)
Prof. Dr. Klemens Zink (Betreuer)	Dr. Michael Scholz (Externer Betreuer)

IV. Discussion

IV.I. General aspects of modeling dose response in radiotherapy

Ion beam therapy is no standard treatment procedure in radiotherapy but especially for certain types of malignancies like radioresistant head and neck and CNS tumors a promising alternative to conventional radiotherapy with photons (Suit et al. 2010). To estimate the expected benefit from ion beam therapy, accurate modeling of the RBE in tumor and normal tissue is necessary. The RBE is strongly dependent on the dose level, the position in the treatment field and the tumor and normal tissue types involved in the field. Within the framework of the LEM the dose response known from conventional radiation with photons is used to estimate the RBE for ion beams. Whereas for the development of the LEM I the main goal was to accurately predict the effectiveness for carbon ions in the target volume, the improvements implemented in the LEM IV now enable the exploration of RBE dependencies for the whole set of clinically relevant particle beams from protons to carbon ions with similar accuracy. Hence, it is possible to assess RBE-weighted dose relationships and the expected therapeutic gain more correctly.

In general, modeling can be an important tool to estimate the potential benefit from proton or heavy ion radiotherapy compared to conventional radiotherapy. For example, Langendijk et al. (2013) report about the approach followed by the Dutch Health Council where they compare toxicity rates for proton and photon treatment with validated NTCP models to estimate a patient-specific benefit from the application of protons. The approach is used to preselect patients who would have a decisive advantage of proton therapy in terms of a drastically reduced NTCP compared to conventional radiotherapy with photons. This concept can be transferred to treatment planning studies based on RBE modeling approaches to choose the most likely optimal ion beam species for a given treatment situation and thus to preselect patients for the different options of treatments with protons, helium or carbon ions. It is especially favorable for pediatric patients for whom the integral dose needs to be kept as low as possible (Johnstone et al. 2013). However, this approach will not replace randomized clinical trials since hypotheses need to be proved but rather allows distinguishing those patients who would have a clear benefit from a certain radiation modality.

Although improvements of the LEM IV compared to previous model versions have been clearly demonstrated by comparison with *in-vitro* and *in-vivo* experimental data, before potential application of the LEM IV in clinical routine it was important to investigate the consistency with existing clinical data. The compilation of local control

rates for chordoma of the skull base by Schulz-Ertner et al. (2007) including the outcome of the GSI pilot project was the starting point for this investigation. It was shown that for the treatment of radioresistant chordoma of the skull-base the predicted RBE-weighted dose of the LEM IV is comparable to that of LEM I with less than 5 % difference regarding the median tumor volume. On average the predictions of LEM IV and LEM I deviate by less than 10 % for radioresistant tumors with a low α/β-ratio. With regard to the comparably low patient statistics of the TCP compilation, i.e., the large uncertainty of the clinical data available for treatment of skull-base chordoma, both models can describe the clinical outcome with sufficient accuracy **(*article 1*)**.

The transition from LEM I to LEM IV in treatment planning does not imply a drastically adjustment of the physical absorbed dose. The gradient of the physical depth dose distribution though would differ due to the steeper RBE gradient predicted by the LEM IV as compared to LEM I. However, the gradient of the physical dose is dependent on the field configuration and is largely compensated by the application of two opposing fields. With the LEM IV, limitations of the LEM I have been overcome like, e.g., the overestimation of RBE in the entrance channel that could lead to an undesired restriction of the tumor dose. Furthermore, the input parameter set of the LEM IV is not any longer ion specific but a common, consistent set of parameters can be applied for all ions from protons to carbon ions. Since the comparison of LEM I and LEM IV was performed using idealized target geometries it remains to be elucidated how far these results can be transferred to real patient plans.

Schlampp et al. (2011) analyzed the NTCP for the temporal lobes based on the LEM I predictions in the course of the treatment of skull-base chordoma with carbon ions in the GSI pilot project and showed that they are consistent with clinical tolerance data from photon and proton irradiation. In a study by Gillmann et al. (2014, in press) the tolerance doses were recalculated with the LEM IV. The recalculation showed that the RBE-weighted dose at the edges is sharply increasing leading to possibly higher predicted dose to the temporal lobes that are located close to or even within the tumor volume. Since the predicted tolerance doses based on the LEM I have been considered consistent with the corresponding clinical photon data, the predicted tolerance doses based on LEM IV are consequently higher than those observed in conventional photon radiotherapy. However, as will be discussed in a later section, actually higher tolerance doses might be expected in the case of ion beam therapy due to the specific topological properties of the high-LET and thus high-RBE volume that is located as a rim at the distal edges of the individual treatment fields.

IV.II. Modeling biological effectiveness in hypofractionated treatment regimens

Especially with heavier ions like carbon hypofractionation regimens are exploited to decrease the overall treatment time. The HIMAC uses carbon ions for hypofractionation and even single dose schedules to treat for example NSCLC (Miyamoto et al. 2007) or hepatocellular cancer (HCC) (Kato et al. 2004; Imada et al. 2010). Hypofractionation schedules are also a future direction for the facilities in Europe although careful assessment of the normal tissue sensitivity in the entrance channel is needed. The analysis presented in ***article 2*** and Fossati et al. (2012) demonstrated that equally prescribed clinical doses (i.e., RBE-weighted doses) do not necessarily lead to the same outcome since the underlying RBE model is different and so is the corresponding physical absorbed dose. Especially when going to hypofractionation, the results in ***article 2*** showed that the prescribed HIMAC dose and the RBE-weighted dose predicted by the LEM can deviate by a factor of 2 which means that either the HIMAC dose is overestimated or the RBE-weighted dose predicted by the LEM is underestimated.

However, to estimate a proper dose-response relationship and explore fractionation regimens from different insitutions, modeling is needed and the responsiveness needs to be derived from the predictions of the same biological model. Hypofractionation regimens with scanned carbon beams are implemented at the HIT too (Habermehl et al. 2013). They treated HCC of 6 patients with a fractionation regimen of 4 x 10 Gy (RBE) based on the HIMAC approach. Since treatment planning at HIT is based on the LEM I, the prescribed dose was converted and resulted in an applied 4 x 8 Gy (RBE) optimized RBE-weighted dose to the target volume. In total the conversion resulted in a 20 % lower RBE-weighted dose to the tumor compared to the prescribed HIMAC dose even though the underlying physical dose is similar. Furthermore, in the clinical application of the LEM I, currently an α/β-ratio of 2 Gy based on the radioresistant skull base chordoma and chondrosarcoma treated in the GSI pilot project is considered. However, HCC is a rather radiosensitive tumor type which is estimated with an α/β-ratio of around 15 Gy (Tai et al. 2008). Thus, the RBE can be even lower than currently considered with the LEM I. Therefore, the RBE-weighted dose might be even lower than the LEM-based prescribed dose of 8 Gy (RBE) at the HIT or the prescribed HIMAC dose of 10 Gy (RBE) per fraction currently used. Hence, regarding dose effect relationships for tumor and normal tissues caution is advised to compare clinical studies based on different RBE modeling approaches epsecially for hypofractionated treatment regimens.

IV.III. Proton RBE in treatment planning: gain in conformity

The variability of the proton RBE is neglected for clinical application with the argument that it is rather small with a constant RBE of 1.1 and that critical structures can be spared by range margins and field configurations where the distal edge is not pointing towards an OAR. But this compromises precision and conformity of the treatment and sets some unnecessary restrictions to proton radiotherapy. Recently a treatment planning comparison of Tang et al. (2012) for prostate cancer treatment comparing anterior fields with the current standard of parallel-opposed lateral fields showed that anterior or anterior-oblique fields offer a better solution regarding organ sparing and the integral dose, but are not used so far due to the range uncertainty of the proton beam. At present in many proton facilities 3.5 % uncertainty of the proton range plus extra additional 1-3 mm is considered in treatment planning (Goitein 1985; Paganetti 2012). In the case of prostate treatments with proton ranges of approximately 15 cm this corresponds to more than a 5 mm extra range and would deliver high dose to the anterior rectal wall. One part of the range uncertainty could be attributed to the increased RBE at the distal edge. Gensheimer et al. (2010) identified an unexpected systematic overshoot of the proton beam in the treatment of medulloplastoma patients, which could not be explained on the basis of the expectation values discussed for the range extension in the paper. With the comparison of the LEM IV predictions to the results obtained by Gensheimer et al. (2010) we could show that the biological range extension accompanied by the increased RBE in the distal penumbra was underestimated by Gensheimer et al. (2010) and thus could explain the systematic overshoot.

Instead to account for the increased RBE at the distal end of a proton SOBP and prevent the risk of high-LET dose contributions close to an OAR, homogenisation of the LET is considered (Paganetti 2013). However, the LET can only substantially homogenized by the application of parallel opposed fields possibly limiting the scope of field configurations and thus the sparing of critical structures as outlined by Tang et al. (2012). Taking the variable RBE along the SOBP into account would improve the accuracy of the treatment planning with protons and safety margins could be reduced.

Another aspect why proton RBE should be considered for patient treatment like for the heavier ions is the potential false estimation of tolerance doses. For the RBE-weighted dose at the distal edge of the SOBP a considerable deviation from the clinically used constant RBE of 1.1 is expected in line with the results of *in-vitro* cell experiments (Courdi et al. 1994; Wouters et al. 1996; Tang et al. 1997; Bettega et al. 2000). The RBE can be more than twice as high leading to corresponding higher RBE-weighted

doses. Surprisingly, the increased proton RBE seems not to lead to severe side effects reflected in the NTCP.

A potential explanation might be that actually tolerance doses are increased due to a volume effect related to the specific topology of the high-RBE volumes in ion beam therapy. The total high-RBE volume at the distal end of the treatment field is rather small and in general not a compact, but rather flat, shell-shaped volume. In order to assess potential volume effects, in clinical practice the tissue organization especially for OAR is often discussed in terms of serial or parallel organization (Källman et al. 1992). The parallel organized tissues are supposed to show a rather proportional response to dose and volume irradiated whereas serial organized tissues are known to show rather a threshold response to irradiation (Withers et al. 1988; ICRU 1999a). Contradictory to the clinical dogma are the experiments reported by Bijl et al. with the rat spinal cord, a highly serial organized organ, which indicate a significant increase of the tolerance dose for very small volumes (Bijl et al. 2002; Bijl et al. 2003; van Luijk et al. 2005). A reason for this pronounced volume effect, although observed in serial organized tissue, could be the sufficient contact to the unirradiated normal tissue in the case of irradiated small volumes. This is also the case for the highly effective but thin shell-shaped irradiated volumes as they occur at the distal edge of a proton SOBP. The tolerance dose in that case could then be higher as compared to the same total volume having a more compact shape. This could also explain the marginal side effects seen for the temporal lobes in the pilot study with carbon ions even though higher doses are predicted by the LEM IV. Here again, only a small volume with a comparably flat topology, receives a very highly effective dose. According to the results reported by Bijl et al., the short distance to surrounding healthy tissue might lead to a more pronounced recovery and thus correspondingly higher tolerance doses.

IV.IV. Importance of RBE robustness for clinical routine

The robustness of treatment plans is an important issue in radiotherapy and for ion beam therapy this additionally means to keep RBE uncertainties small. Thus, reliable RBE model predictions are needed. ***Article 3*** dealt with the LEM inherent sensitivity of the RBE prediction. Separately for each input parameter the RBE sensitivity was analyzed by means of a ± 25 % variation. The variation of RBE resulting from the parameter alteration turned out to be large but depends still less than proportional on the input parameters **(*article 3*)**. However, in combination all parameters, which are independent on the experiment or clinical situation to be modeled, form a consistent input parameter set and systematic uncertainties of the LEM are minimized by a fit to experimental data taken from Furusawa et al. (2000) and Suzuki et al. (2000). We

found out that the uncertainty is mainly originating from the uncertainty of the photon input parameters α, β and D_t.

Consequently, this is not a specific problem for ion beam therapy, but a general problem of modeling, also in conventional photon therapy, since the description of the dose response relationship of cell- or tissue types to radiation relies on the knowledge of the LQ-parameters or any equivalent parameterization. Hence, in order to minimize the uncertainties accurate estimations of the α/β-ratio for the considered endpoint are required. For clinical endpoints also the inter-patient variability of dose response plays a role. The variable radiosensitivity can be taken into account by a mean value or by a parameter distribution. A parameter distribution implies the flattening of the sigmoid local control curve which is in better agreement with the local control probability observed in clinical trials with large patient numbers (Daşu et al. 2003; Kanai et al. 2006). However, as shown in ***article 1*** **and** ***article 3*** a parameter variation, which also reflects an inter-patient variability, has a higher impact on the photon than on the ion beam dose response relationship.

As shown in ***article 3*** the RBE uncertainty is dependent on the absolute RBE. For clinical practice this can mean that a high RBE usually observed for heavy ions and small photon α/β-ratios also has larger uncertainties as compared to low-LET particles like protons and tumors with a high photon α/β-ratio, showing a small RBE but also correspondingly smaller uncertainties in the RBE. Hence, in this respect protons and heavier ions both have advantages for the clinical application. Heavier ions like carbon offer a beneficial high RBE in the target volume having a better sparing effect to the normal tissue but higher RBE uncertainty. In contrast, for protons the RBE is afflicted with less uncertainties. A promising method to decrease the RBE uncertainty, proposed in the literature, can be the homogenization of LET resulting in an overall reduction of the dose-mean LET[1] (Krämer & Jäckel 2005; Bassler et al. 2010; Grassberger et al. 2011; Böhlen et al. 2012). The reduction of the LET gradient within a carbon SOBP and thus the homogenization of the RBE-weighted dose comparing a single field iradiation to an irradiation with two opposing fields is demonstrated in **fig. 1 of** ***article 1***. Hence, as also mentioned in subchapter IV.III, a homogenization of the LET relies on the application of multiple fields, at best, parallel opposed fields, but comprises higher integral dose compared to a single field irradiation.

IV.V. Other RBE models

The comparison of the LEM to other models potentially applicable in treatment planning, as, e.g., the microdosimteric kinetic model (MKM) (Inaniwa et al. 2010; Sato &

[1] Sum of the LET of each beam component weighted by its relative contribution to the total dose

Furusawa 2012) or the reformulation of the LQ-model presented by Carabe and Jones (Carabe-Fernandez et al. 2007; Jones et al. 2012) is of great interest. Especially the comparison with the MKM is promising since NIRS is now starting to use the MKM for the patient treatment together with a scanning system. One difficulty to compare different treatment planning approaches is that generally they differ in both the phyiscal description of the treatment field and the approach to estimate the RBE. However, the detailed comparison of the RBE models requires use of the same physical dose distributions. In ***article 2*** a method is presented to compare the HIMAC approach, to the LEM approach by using the same physical depth dose profile. The physical dose was reconstructed based on TRiP98 with the aim to result in the same shape of the SOBP along depth. However, the differences in the beam modulation systems, i.e., passive vs. raster scanning system, were neglected. This can involve differences in the particle and fragment composition that might additonaly influence the RBE. Thus, it is of interest to use really identical physical dose distributions for the comparison of the LEM with the HIMAC approach and other RBE models. Steinsträter et al. (GSI project) implemented a method to apply other RBE models within the framework of TRiP98 and the underlying physical beam model, thus allowing for a direct comparison of the different biological modelling approaches.

The model presented by Carabe and Jones for example, which is only applicable for protons, will be worth a comparison. In Carabe et al. (2012) they investigated the biological range extension based on this model in terms of tissue type and dose-level, similarly to our analysis **(*article 4*).** However, the results are qualitatively and quantitatively quite different since they even observe negative biological range extensions which imply an RBE smaller than 1.1 at the distal edge. In contrast to the LEM, the parameterization of RBE_{max} and RBE_{min} used by Carabe et al. (2012) can even lead to RBE values below 1.

Furthermore, the dose dependence of RBE according to the model in Carabe et al. (2012) is inverted compared to the dose dependence predicted by the LEM. For the LEM the RBE is decreasing with increasing dose per fraction, which is in agreement with experimental results. This behaviour was demonstrated in ***article 4*** by comparison of the LEM predictions with experimental results for different dose-levels as reported by Tang et al. (1997). Instead, the parameterization used by Carabe et al. (2012), i.e., RBE_{min} and RBE_{max}, shows a contradictory behaviour regarding their meaning. The parameter RBE_{max} which represents the RBE in the limit of small doses can be smaller than 1 for $LET \rightarrow 0$. It can be even smaller than RBE_{min}, representing the limiting RBE value for very high doses, which has a limiting value of 1.09 for $LET \rightarrow 0$. Consequently, this can lead to an increase of the RBE for increasing dose, and

therefore the dose dependence of RBE might be inverted compared to the LEM. Thus, further detailed comparison is needed to elucidate the impact of specific model properties on the RBE since it has a significant influence on the range extension of protons.

IV.VI. Outlook

The future direction of ion beam therapy goes towards the exploration of the advantages of different ion types. At HIT the application of oxygen and helium ions additional to carbon and protons is proposed (Jäkel et al. 2003). Brahme (2004) also discussed the flexibility of using different ion species in therapy matching with the treatment scenario and proposed the use of two to three different ions with low, intermediate and high LET, respectively. Oxygen ions offer the additional advantage of a high LET particularly effective to hypoxic tumors because of the reduced OER and to cancer stem cells (CSC) and can be an alternative to carbon ions (Durante 2014; Scifoni et al. 2013; Bassler et al. 2014). Helium ions are considered to have a RBE comparable to that of protons but show less lateral scattering in tissue and thus a better dose conformation. When comparing the various ion species the differential RBE-weighted dose between SOBP and entrance channel is an important measure since it defines the therapeutic window between a high local control of the tumor on the one hand and a reasonably small NTCP on the other hand.

The work presented in this thesis demonstrated that the LEM IV is capable to give consistent RBE predictions for the clinical situation. The LEM can thus be used to assess the expected differential RBE-weighted doses, reflecting the therapeutic gain of a given treatment scenario. The differential effect depends on physical properties like depth dose profile or dose-level as well as on biological properties like the combination of tumor and surrounding tissue type.

Protons for example show an overall lower RBE but a beneficial physical depth dose profile in terms of peak to entrance channel ratio compared to carbon ions. This is due to the fact that no projectile fragments are produced which contribute to the dose distribution. In this regard it should be noted that target fragments contribute to the dose as well, but are in general not yet considered in treatment planning. Up to now, only projectile fragments are considered in ion beam therapy. However, the biological effectiveness of these mainly low-energetic target projectiles is worth to investigate since especially for protons they may contribute to a slightly enhance RBE even in the entrance region.

In addition to a much lower multiple scattering compared to protons, carbon ions are considered to show a high differential RBE. Thus, it needs to be elucidated for which

clinical cases the advantage of a high differential carbon ion RBE and of the better lateral dose conformation overcompensates the less beneficial longitudinal depth dose profile of carbon ions as compared to protons. Accordingly, ongoing work at GSI includes biological optimized treatment planning studies to compare therapy relevant ion species concerning their physical and biological properties with special regard to their therapeutic gain.

A particular question arising in this framework is to what extent hypofractionation regimens influence the differential RBE. In general RBE is decreasing with increasing dose per fraction, and thus the differential effects are expected to be diminished for hypofractionation regimens. However, if tumor conformity is of primary concern, in any case carbon ions are expected to be favourable in particular for radioresistant and hypoxic tumors allowing to simultaneously reducing the integral dose and thus the burden to the normal tissue.

A major challenge for the reliable estimation of RBE values at present remains the limited knowledge of the tissue characteristics in terms of radiosensitivity as commonly described by the photon α/β-ratio. This challenge, however, is not specific to ion beam therapy, but also is of relevance for conventional photon therapy. Since for a reliable RBE prediction a correct estimation of the photon dose-response parameters is essential, all the uncertainties concerning the dose response description inherent to conventional photon therapy are automatically transferred to ion beam therapy. Thus, RBE prediction can only be as good as the corresponding description of the tissue characteristics in terms of the photon dose-response parameters. Fortunately, in particular in the framework of stereotactic body radiation therapy (SBRT) a lot of efforts is put into studies to better characterize clinical dose-response relationships after photon radiation (Park et al. 2008; Wennberg & Lax 2013; Song et al. 2013). These studies mainly are motivated by the fact that the linear-quadratic model is not strictly valid at high doses, and thus the extrapolations based on the linear-quadratic parameters that are derived from lower doses per fraction are not expected to be accurate (Kirkpatrick et al. 2008; Otsuka et al. 2011). The better description of dose-response curves at high doses perfectly fits to the needs for the application of the LEM, where also the input photon dose response curve is parameterized in the form of a modified linear-quadratic model, characterized by a transition to a purely linear shape at high dose. In that respect, further improvements in the estimation of clinical RBE values will largely profit from the analysis of clinical data performed in the framework of SBRT.

V. References

Bassler N, Jäkel O, Søndergaard CS and Petersen JB (2010). Dose- and LET-painting with particle therapy. *Acta Oncol* 49:1170–6.

Bassler N, Toftegaard J, Lühr A, Singers Sørensen B, Scifoni E, Krämer M, Jäkel O, Saksø Mortensen L, Overgaard J, Petersen JB (2014). LET-painting increases tumour control probability in hypoxic tumours. *Acta Oncol* 53:25–32.

Bettega D, Calzolari P, Chauvel P, Courdi A, Herault, J, Iborra, N, Marchesini, R, Massariello, P, Poli, GL and Tallone L (2000). Radiobiological studies on the 65 MeV therapeutic proton beam at Nice using human tumour cells. *Int J Radiat Biol* 76:1297–303.

Bijl HP, van Luijk P, Coppes RP, Schippers JM, Konings AWT and van der Kogel AJ (2002). Dose-volume effects in the rat cervical spinal cord after proton irradiation. *Int J Radiat Oncol Biol Phys* 52:205–11.

Bijl, HP, van Luijk P, Coppes RP, Schippers JM, Konings AW and van der Kogel AJ (2003). Unexpected changes of rat cervical spinal cord tolerance caused by inhomogeneous dose distributions. *Int J Radiat Oncol* 57:274–81.

Böhlen TT, Brons S, Dosanjh M, Ferrari A, Fossati P, Haberer T, Patera V and Mairani A (2012). Investigating the robustness of ion beam therapy treatment plans to uncertainties in biological treatment parameters. *Phys Med Biol* 57:7983–8004.

Bortfeld T, Schlegel,W, Dykstra C, Levegrün S and Preiser K (1996). Physical vs. biological objectives for treatment plan optimization. *Radiat Oncol*, 40:185–9.

Brahme A (1995). Treatment optimization using physical and radiobiological objective functions. Radiation Therapy Physics 209–46, edited by Smith A R. *Springer*, Berlin.

Brahme A (1999). Biologically Based Treatment Planning. *Acta Oncol* 13:61–68.

Brahme A (2004). Recent advances in light ion radiation therapy. *Int J Radiat Oncol* 58:603–16.

Carabe A, Moteabbed M, Depauw N, Schuemann J and Paganetti H (2012). Range uncertainty in proton therapy due to variable biological effectiveness. *Phys Med Biol* 57:1159–72.

Carabe-Fernandez A, Dale RG and Jones B (2007). The incorporation of the concept of minimum RBE (RBE min) into the linear-quadratic model and the potential for improved radiobiological analysis of high-LET treatments. *Int J Radiat Biol* 83:27–39.

Castro J, Saunders W and Tobias C (1982). Treatment of cancer with heavy charged particles. *Int J Radiat Oncol* 8:2191–8.

Castro J, Linstadt D and Bahary J (1994). Experience in charged particle irradiation of tumors of the skull base:1977–1992. *Int J Radiat Oncol* 29:647–55.

Combs SE, Jäkel O, Haberer T, Debus J (2010). Particle therapy at the Heidelberg Ion Therapy Center (HIT) - Integrated research-driven university-hospital-based radiation oncology service in Heidelberg, Germany. *Radiat Oncol* 95:41–4.

Courdi A, Brassart N, Hérault J and Chauvel P (1994). The depth-dependent radiation response of human melanoma cells exposed to 65 MeV protons. *Br J Radiol* 67:800–4.

Daşu A, Toma-Daşu I and Fowler JF (2003). Should single or distributed parameters be used to explain the steepness of tumour control probability curves? *Phys Med Biol* 48:387–97.

Dawson A and Hillen T (2006). Derivation of the Tumour Control Probability (TCP) from a Cell Cycle Model. *Comput Math Methods Med* 7:121–41.

DeLaney TF and Kooy HM (2007). Proton and Charged Particle Radiotherapy. Lippincott Williams & Wilkins, 1st edition.

Ding L, Park S, Peyton M, Girard L, Xie Y, Minna JD and Story MD (2013). Distinct transcriptome profiles identified in normal human bronchial epithelial cells after exposure to γ-rays and different elemental particles of high Z and energy. *BMC Genomics* 14:372–1–13.

DKFZ Deutsches Krebsforschungszentrum (2013). Krebsatlas. Die häufigsten Todesursachengruppen in Deutschland 2010. Accessed 3 december 2013, http://www.dkfz.de/de/krebsatlas/gesamt/mort_2.html.

Douglas BG and Fowler JF (1976). The effect of multiple small doses of X rays on skin reactions in the mouse and a basic interpretation. *Radiat Res* 66:401–26.

Durante M (2014). New challenges in high-energy particle radiobiology. *Brit J Radiol* doi:10.1259/bjr.20130626.

Elsässer T and Scholz M (2007). Cluster effects within the local effect model. *Radiat Res* 167:319–29.

Elsässer T, Krämer M and Scholz M (2008). Accuracy of the local effect model for the prediction of biologic effects of carbon ion beams in vitro and in vivo. *Int J Radiat Oncol Biol Phys* 71:866–72.

Elsässer T, Kraft-Weyrather W, Friedrich T, Durante M, Iancu G, Krämer M, Kragl G, Brons S, Winter M, Weber KJ and Scholz M (2010). Quantification of the relative biological effectiveness for ion beam radiotherapy: Direct experimental comparison of proton and carbon ion beams and a novel approach for treatment planning. *Int J Radiat Oncol Biol Phys* 78:1177–83.

Fokas E, Kraft G, An H and Engenhart-Cabillic R (2009). Ion beam radiobiology and cancer: time to update ourselves. *Biochim Biophys Acta* 1796:216–29.

Fossati P, Molinelli S, Matsufuji N, Ciocca M, Mirandola A, Mairani A, Mizoe J, Hasegawa A, Imai R, Kamada T, Orecchia R and Tsujii H (2012). Dose prescription in carbon ion radiotherapy: a planning study to compare NIRS and LEM approaches with a clinically-oriented strategy. *Phys Med Biol* 57:7543–54.

Friedrich T, Durante M and Scholz M (2012). Modeling cell survival after photon irradiation based on double-strand break clustering in megabase pair chromatin loops. *Radiat Res* 178:385–94.

Friedrich T, Grün R, Scholz U, Elsässer T, Durante M and Scholz M (2013). Sensitivity analysis of the relative biological effectiveness predicted by the local effect model. *Phys Med Biol* 58:6827–49.

Friedrich T, Scholz U, Elsässer T, Durante M and Scholz M (2013). Systematic analysis of RBE and related quantities using a database of cell survival experiments with ion beam irradiation. *J Radiat Res* 54:494–514.

Furusawa Y, Fukutsu K, Aoki M and Itsukaichi H (2000). Inactivation of aerobic and hypoxic cells from three different cell lines by accelerated 3He-, 12C-and 20Ne-ion beams. *Radiat Res* 496:485–96.

Gemmel A, Hasch B, Ellerbrock M, Weyrather WK and Krämer M (2008). Biological dose optimization with multiple ion fields. *Phys Med Biol* 53:6991–7012.

Gensheimer MF, Yock TI, Liebsch NJ, Sharp GC, Paganetti H, Madan N, Grant PE and Bortfeld T (2010). In vivo proton beam range verification using spine MRI changes. *Int J Radiat Oncol Biol Phys* 78:268–75.

Gillmann.C, Jäkel O, Schlampp I and Karger CP (2014). Temporal lobe reactions after carbon ion radiation therapy: Comparison of relative biological effectiveness-weighted tolerance doses predicted by local effect models I and IV. *Int J Radiat Oncol Biol Phys* (in press).

Goitein M (1985). Calculation of the uncertainty in the dose delivered during radiation therapy. *Med Phys* 12:608–12.

Grassberger C, Trofimov A, Lomax A and Paganetti H (2011). Variations in linear energy transfer within clinical proton therapy fields and the potential for biological treatment planning. *Int J Radiat Oncol Biol Phys* 80:1559–66.

Grün R, Friedrich T, Elsässer T, Krämer M, Zink K, Karger CP, Durante M, Engenhart-Cabillic R and Scholz M (2012). Impact of enhancements in the local effect model (LEM) on the predicted RBE-weighted target dose distribution in carbon ion therapy. *Phys Med Biol* 57:7261–74.

Grün R, Friedrich T, Krämer M, Zink K, Durante M, Engenhart-Cabillic R, Scholz M and (2013). Physical and biological factors determining the effective proton range. *Med Phys* 40:111716–1–10.

Haberer T, Becher W, Schardt D and Kraft G (1993). Magnetic scanning system for heavy ion therapy. *Nucl Instrum Methods Phys Res A 330:296–305.*

Habermehl D, Debus J, Ganten T, Ganten MK, Bauer J, Brecht IC, Brons S, Haberer T, Haertig M, Jäkel O, Parodi K, Welzel T and Combs SE (2013). Hypofractionated carbon ion therapy delivered with scanned ion beams for patients with hepatocellular carcinoma - feasibility and clinical response. *Radiat Oncol* 8:59–1–8.

Hall EJ and Giaccia AJ (2011). Radiobiology for the radiologist. Lippincott Williams & Wilkins, 7th edition.

Henderson FC, McCool K, Seigle J, Jean W, Harter W and Gagnon GJ (2009). Treatment of Chordomas with CyberKnife: Georgetown University Experience and Treatment Recommendations. *Neurosurgery* 64:A44–53.

ICRU (1999a). Prescribing, Recording and Reporting Photon Beam Therapy. Report 50. Bethesda, MD: International Commission on Radiation Units and Measurements.

ICRU (1999b). Prescribing, Recording and Reporting Photon Beam Therapy (Supplement to ICRU Report 50). Report 62. Bethesda, MD: International Commission on Radiation Units and Measurements.

Imada H, Kato H, Yasuda S, Yamada S, Yanagi T, Kishimoto R, Kandatsu S, Mizoe J, Kamada T, Yokosuka O and Tsujii H (2010). Comparison of efficacy and toxicity of short-course carbon ion radiotherapy for hepatocellular carcinoma depending on their proximity to the porta hepatis. *Radiother Oncol* 96:231–5.

Inaniwa T, Furukawa T, Kase Y, Matsufuji N, Toshito T, Matsumoto Y, Furusawa Y and Noda K (2010). Treatment planning for a scanned carbon beam with a modified microdosimetric kinetic model. *Phys Med Biol* 55:6721–37.

Jäkel O, Krämer M, Karger, CP and Debus, J (2001). Treatment planning for heavy ion radiotherapy: clinical implementation and application. *Phys Med Biol* 46:1101–16.

Jäkel O, Schulz-Ertner D, Karger CP, Nikoghosyan A, Debus J (2003). Heavy ion therapy: status and perspectives. *Technol Cancer Res Treat* 2:377–87.

Johnstone PAS, McMullen KP, Buchsbaum JC, Douglas JG and Helft P (2013). Pediatric CSI: are protons the only ethical approach? *Int J Radiat Oncol Biol Phys* 87:228–30.

Jones B, Wilson P, Nagano A, Fenwick J and Mckenna, G (2012). Dilemmas concerning dose distribution and the influence of relative biological effect in proton beam therapy of medulloblastoma. *Brit J Radiol 85:e912–8*.

Källman P, Agren A and Brahme A (1992). Tumour and normal tissue responses to fractionated non-uniform dose delivery. *Int J Radiat Biol* 62:249–62.

Kanai T, Endo M, Minohara S, Miyahara N, Koyama-ito H, Tomura H, Matsufuji N, Futami Y, Fukumura A, Hiraoka T, Furusawa Y, Ando K, Suzuki M, Soga F and Kawachi, K (1999). Biophysical characteristics of HIMAC clinical irradiation system for heavy-ion radiation therapy. *Int J Radiat Oncol Biol Phys* 44:201–10.

Kanai T, Matsufuji N, Miyamoto T, Mizoe J, Kamada T, Tsuji H, Kato H, Baba M and Tsujii H (2006). Examination of GyE system for HIMAC carbon therapy. *Int J Radiat Oncol Biol Phys* 64:650–6.

Karger CP, Peschke P, Sanchez-Brandelik R, Scholz M and Debus J (2006). Radiation tolerance of the rat spinal cord after 6 and 18 fractions of photons and carbon ions: experimental results and clinical implications. *Int J Radiat Oncol Biol Phys* 66:1488–97.

Kato H, Tsujii H, Miyamoto T, Mizoe J, Kamada T, Tsuji H, Yamada S, Kandatsu S, Yoshikawa K, Obata T, Ezawa H, Morita S, Tomizawa M, Morimoto N, Fujita J and Ohto M (2004). Results of the first prospective study of carbon ion radiotherapy for hepatocellular carcinoma with liver cirrhosis. *Int J Radiat Oncol Biol Phys* 59:1468–76.

Kellerer AM and Rossi HH (1971). RBE and the primary mechanism of radiation action. *Radiat Res* 47:15–34.

Kirkpatrick JP, Meyer JJ and Marks LB (2008). The linear-quadratic model is inappropriate to model high dose per fraction effects in radiosurgery. *Semin Radiat Oncol* 18:240–3.

Kraft G (2000). Tumor therapy with heavy charged particles. *Prog Part Nucl Phys* 45:S473–544.

Krämer M, Jäkel O, Haberer T, Kraft G, Schardt D and Weber U (2000). Treatment planning for heavy-ion radiotherapy: physical beam model and dose optimization. *Phys Med Biol* 45:3299–317.

Krämer M and Scholz M (2000). Treatment planning for heavy-ion radiotherapy: calculation and optimization of biologically effective dose. *Phys Med Biol* 45:3319–30.

Krämer M and Jäckel O (2005). Biological dose optimization using ramp-like dose gradients in ion irradiation field. *Phys Medica* 21:107–11.

Krämer M and Durante M (2010). Ion beam transport calculations and treatment plans in particle therapy. *Eur Phys J D* 60:195–202.

Langendijk JA, Lambin P, De Ruysscher D, Widder J, Bos M and Verheij M (2013). Selection of patients for radiotherapy with protons aiming at reduction of side effects: The model-based approach. *Radiother Oncol* 107:267–73.

Loeffler JS and Durante M (2013). Charged particle therapy-optimization, challenges and future directions. *Nat Rev Clin Oncol* 10:411–24.

McNally N and Sheldon P (1977). The effect of radiation on tumour growth delay, cell survival and cure of the animal using a single tumour system. *Br J Radiol* 50:321–328.

Miyamoto T, Baba M, Yamamoto N, Koto M, Sugawara T, Yashiro T, Kadono K, Ezawa H, Tsujii H, Mizoe JE, Yoshikawa K, Kandatsu S, Fujisawa T (2007). Curative treatment of stage i non-small-cell lung cancer with carbon ion beams using a hypofractionated regimen. *Int J Radiat Oncol Biol Phys* 67:750–8.

Niemierko A (1997). Reporting and analyzing dose distributions: a concept of equivalent uniform dose. *Med Phys* 24:103–10.

Otsuka S, Shibamoto Y, Iwata H, Murata R, Sugie C, Ito M and Ogino H (2011). Compatibility of the linear-quadratic formalism and biologically effective dose concept to high-dose-per-fraction irradiation in a murine tumor. *Int J Radiat Oncol Biol Phys* 81:1538–43.

Paganetti H (1998). Calculation of the spatial variation of relative biological effectiveness in a therapeutic proton field for eye treatment. *Phys Med Biol* 43:2147–57.

Paganetti H, Niemierko A, Ancukiewicz M, Gerweck LE, Goitein M, Loeffler JS and Suit HD (2002). Relative biological effectiveness (RBE) values for proton beam therapy. *Int J Radiat Oncol Biol Phys* 53:407–21.

Paganetti H (2012). Range uncertainties in proton therapy and the role of Monte Carlo simulations. *Phys Med Biol* 57:R99–117.

Paganetti H (2013). Advancing (Proton) Radiation Therapy. *Int J Radiat Oncol* 87:871–3.

Park C, Papiez L, Zhang S, Story M and Timmerman RD (2008). Universal survival curve and single fraction equivalent dose: useful tools in understanding potency of ablative radiotherapy. *Int J Radiat Oncol Biol Phys* 70:847–52.

Peacock J, Nahum A and Steel G (1998). Normal-tissue effects in radiotherapy: Physics meets biology. Report on a workshop held at Hartsfield Manor, Betchworth, Surrey, UK, 14-16 July 1997. *Int J Radiat Biol* 73:341–4.

Pignalosa D and Durante M (2012). Overcoming resistance of cancer stem cells. *Lancet Oncol* 13:e187–8.

Pirzkall A, Carol M, Lohr F, Höss A, Wannenmacher M and Debus J (2000). Comparison of intensity-modulated radiotherapy with conventional conformal radiotherapy for complex-shaped tumors. *Int J Radiat Oncol Biol Phys* 48:1371–80.

Podgorsak EB (2005). Radiation Oncology Physics: A Handbook for Teachers And Students. International Atomic Energy Agency.

PTCOG Particle Therapy Co-Operative Group (2013). Patient Statistics. Accessed 3 december 2013, http://ptcog.web.psi.ch/patient_statistics.html.

Qi XS, Semenenko VA and Li XA (2009). Improved critical structure sparing with biologically based IMRT optimization. *Med Phys* 36:1790–99.

Roelofs E, Engelsman M,. Rasch C, Persoon L, Qamhiyeh S, de Ruysscher D, Verhaegen F, Pijls-Johannesma M and Lambin P (2011). Results of a Multicentric In Silico Clinical Trial (ROCOCO). *J Thorac Oncol* 7:13–19.

Rossi S on behalf of the CNAO Collaboration (2011). The status of CNAO. *Eur Phys J Plus* 126:78–1–39.

Rubin P and Casarett, GW (1968). Clinical radiation pathology as applied to curative radiotherapy. *Cancer* 22:767–78.

Sato T and Furusawa Y (2012). Cell Survival Fraction Estimation Based on the Probability Densities of Domain and Cell Nucleus Specific Energies Using Improved Microdosimetric Kinetic Models. *Radiat Res* 178:341–56.

Schardt D, Elsässer T and Schulz-Ertner D (2010). Heavy-ion tumor therapy: Physical and radiobiological benefits. *Rev Mod Phys* 82:383–425.

Schlampp I, Karger CP, Jäkel O, Scholz M, Didinger B, Nikoghosyan A, Hoess A, Krämer M, Edler L, Debus J and Schulz-Ertner D (2011). Temporal lobe reactions after radiotherapy with carbon ions: incidence and estimation of the relative biological effectiveness by the local effect model. *Int J Radiat Oncol Biol Phys* 80:815–23.

Scholz M, Kellerer AM, Kraft-Weyrather W and Kraft G (1997). Computation of cell survival in heavy ion beams for therapy. The model and its approximation. *Radiat Environ Biophys* 36:59–66.

Schulz-Ertner D, Karger CP, Feuerhake A, Nikoghosyan A, Combs SE, Jäkel O, Edler L, Scholz M and Debus J (2007). Effectiveness of carbon ion radiotherapy in the treatment of skull-base chordomas. *Int J Radiat Oncol Biol Phys* 68:449–57.

Scifoni E, Tinganelli W, Weyrather WK, Durante M, Maier A and Krämer M (2013). Including oxygen enhancement ratio in ion beam treatment planning: model implementation and experimental verification. *Phys Med Biol* 58:3871–95.

Semenenko VA, Reitz B, Day E, Qi XS, Miften M, Li XA (2008). Evaluation of a commercial biologically based IMRT treatment planning system. *Med Phys* 35:5851–60.

Sinclair WK (1966). The shape of radiation survival curves of mammalian cells cultured in vitro. Biophysical Aspects of Radiation Quality, International Atomic Energy Agency Technical Reports Series 58:21–43.

Song CW, Cho LC, Yuan J, Dusenbery KE, Griffin RJ and Levitt SH (2013). Radiobiology of stereotactic body radiation therapy/stereotactic radiosurgery and the linear-quadratic model. *Int J Radiat Oncol Biol Phys* 87:18–9.

Steinsträter O, Grün R, Scholz U, Friedrich T, Durante M and Scholz M (2012). Mapping of RBE-Weighted Doses Between HIMAC- and LEM-Based Treatment Planning Systems for Carbon Ion Therapy. *Int J Radiat Oncol Biol Phys* 84:854–60.

Stewart RD and Li XA (2007). BGRT: Biologically guided radiation therapy-The future is fast approaching! *Med Phys* 34:3739–51.

Suit H, DeLaney T, Goldberg S, Paganetti H, Clasie B, Gerweck L, Niemierko A, Hall E, Flanz J, Hallman J and Trofimov A (2010). Proton vs. carbon ion beams in the definitive radiation treatment of cancer patients. *Radiother Oncol* 95:3–22.

Suzuki M, Kase Y, Yamaguchi H and Kanai T (2000). Relative biological effectiveness for cell-killing effect on various human cell lines irradiated with heavy-ion medical accelerator in Chiba (HIMAC) carbon-ion beams. *Int J Radiat Oncol* 48:241–50.

Tai, A. Erickson B, Khater KA and Li XA , (2008). Estimate of radiobiologic parameters from clinical data for biologically based treatment planning for liver irradiation. *Int J Radiat Oncol Biol Phys* 70:900–7.

Tang JT, Inoue T, Yamazaki H, Fukushima S, Fournier-Bidoz N, Koizumi M, Ozeki S and Hatanaka K (1997). Comparison of radiobiological effective depths in 65 MeV modulated proton beams. *Br J Cancer* 76:220–5.

Tang S, Both S, Bentefour H, Paly JJ, Tochner Z, Efstathiou J and Lu HM (2012). Improvement of prostate treatment by anterior proton fields. *Int J Radiat Oncol Biol Phys* 83:408–18.

Thames HD, Withers HR, Peters LJ and Fletcher GH (1982). Changes in early and late radiation responses with altered dose fractionation: implications for dose-survival relationships. *Int J Radiat Oncol Biol Phys* 8:219–26.

Tsujii H, Mizoe J, Kamada T et al. (2004). Overview of clinical experiences on carbon ion radiotherapy at NIRS. *Radiat Oncol* 73, Supplement 2:S41–S49.

Tsujii H, Mizoe J, Kamada T et al. (2007). Clinical Results of Carbon Ion Radiotherapy at NIRS. *J Radiat Res* 48:A1–13.

Tsujii H and Kamada T (2012). A Review of Update Clinical Results of Carbon Ion Radiotherapy. *Jpn J Clin Oncol* 42:670–85.

Van Luijk P, Bijl HP, Konings AWT, van der Kogel AJ and Schippers JM (2005). Data on dose-volume effects in the rat spinal cord do not support existing NTCP models. *Int J Radiat Oncol Biol Phys* 61:892–900.

Wambersie A, Hendry JH, Andreo P, DeLuca PM, Gahbauer R, Menzel H and Whitmore G (2006). The RBE issues in ion-beam therapy: conclusions of a joint IAEA/ICRU working group regarding quantities and units. *Radiat Prot Dosimetry* 122:463–70.

Wang X H, Mohan R, Jackson A, Leibel SA, Fuks Z, Ling CC (1995). Optimization of intensity-modulated 3D conformal treatment plans based on biological indices. *Radiat Oncol* 37:140–52.

Wennberg B and Lax I (2013). The impact of fractionation in SBRT: analysis with the linear quadratic model and the universal survival curve model. *Acta Oncol* 52:902–9.

Weyrather WK, Ritter S, Scholz M and Kraft G (1999). RBE for carbon track-segment irradiation in cell lines of differing repair capacity. *Int J Radiat Biol* 75:1357–64.

WHO: World Health Organization (2013). Cancer. Accessed 3 december 2013, http://www.who.int/cancer/en/.

Wilson RR (1946). Radiological use of fast protons. *Radiology* 47:487–91.

Withers HR, Taylor JMG and Maciejewski B (1988). Treatment volume and tissue tolerance. *Int J Radiat Oncol Biol Phys* 14:751–9.

Wouters BG, Lam GKY, Oelfke U, Gardey K, Durand RE and Skarsgard LD (1996). Measurements of relative biological effectiveness of the 70 MeV proton beam at TRIUMF using Chinese hamster V79 cells and the high-precision cell sorter assay. *Radiat Res* 146:159–70.

Wu Q, Mohan R, Niemierko A and Schmidt-Ullrich R 2002. Optimization of intensity-modulated radiotherapy plans based on the equivalent uniform dose. *Int J Radiat Oncol Biol Phys* 52:224–35.

VI. Articles

VI.I. Article 1

Impact of enhancements in the local effect model (LEM) on the predicted RBE-weighted target dose distribution in carbon ion therapy

VI.II. Article 2

Mapping of RBE-weighted doses between HIMAC- and LEM-based treatment planning systems for carbon ion therapy

VI.III. Article 3

Sensitivity analysis of the relative biological effectiveness predicted by the local effect model

VI.IV. Article 4

Physical and biological factors determining the effective proton range

Phys. Med. Biol. **57** (2012) 7261–7274 doi:10.1088/0031-9155/57/22/7261

Impact of enhancements in the local effect model (LEM) on the predicted RBE-weighted target dose distribution in carbon ion therapy

R Grün[1,2,3], T Friedrich[1], T Elsässer[1,7], M Krämer[1], K Zink[2,4], C P Karger[5], M Durante[1,6], R Engenhart-Cabillic[3,4] and M Scholz[1]

[1] Department of Biophysics, GSI Helmholtz Centre for Heavy Ion Research, Darmstadt, Germany
[2] Institut für Medizinische Physik und Strahlenschutz, TH-Mittelhessen, Gießen, Germany
[3] Department of Radiotherapy and Radiation Oncology, Philipps-University Marburg, Marburg, Germany
[4] Department of Radiotherapy and Radiation Oncology, University Medical Center Giessen and Marburg, Marburg, Germany
[5] Department of Medical Physics, German Cancer Research Center (DKFZ), Heidelberg, Germany
[6] Department of Condensed Matter Physics, Darmstadt University of Technology, Darmstadt, Germany

E-mail: r.gruen@gsi.de

Received 27 April 2012, in final form 4 September 2012
Published 17 October 2012
Online at stacks.iop.org/PMB/57/7261

Abstract
Biological optimization for treatment planning in carbon ion therapy is currently based on the first version of the local effect model (LEM I). Further developments implemented in the latest version (LEM IV) allowed to predict more accurately the Relative Biological Effectiveness (RBE) *in-vitro*. The main goal of this study is to compare the LEM IV against LEM I under treatment-like conditions for idealized target geometries. Therefore, physical dose distributions resulting from the biological optimization with LEM I were used to recalculate the RBE-weighted dose distribution based on LEM IV. Input parameters representing the clinical endpoints late toxicity in the central nervous system and the tumor control for chordoma were chosen to investigate the impact of changes on the predicted isoeffective dose levels. The recalculated RBE-weighted dose distributions show an increase within the target region, and the mean RBE-weighted dose values are dependent on the geometry and decrease with increasing target dimension. The differences between predictions of LEM IV and LEM I are less than 10% for typical tumor volumes treated in the pilot project at GSI. Median RBE-weighted doses predicted by LEM IV in the target region are consistent with clinically observed dose-response behavior as demonstrated by comparison to the 5-year local control curve for skull base chordoma.

[7] Present address: Siemens AG, Healthcare Sector, Erlangen, Germany.

1. Introduction

Ion beam therapy requires accurate predictions of the relative biological effectiveness (RBE). For treatment planning the clinical relevant RBE of ions in cells and tissue has to be considered to obtain a homogeneous RBE-weighted dose within the target volume. In order to achieve that goal, different strategies have been developed at Heavy Ion Medical Accelerator Japan (HIMAC) and for the pilot project performed at the GSI Helmholtz Centre for Heavy Ion Research (GSI). At HIMAC, an approach based on experimental *in-vitro* data in combination with the clinical experience obtained with neutron beams has been implemented (Kanai *et al* 1997, 1999 and 2006). More recently, this approach has been extended by including biophysical modeling to adapt the treatment planning to treatments using scanned beams (Kase *et al* 2006 and 2008, Inaniwa *et al* 2010).

For the GSI pilot project, the RBE of carbon ions was predicted by the Local Effect Model (LEM I) in conjunction with the treatment planning software TRiP98 (Treatment Planning for Particles, 98 edition) (Scholz *et al* 1997, Krämer *et al* 2000, Schardt *et al* 2010). The LEM can predict the biological effect of ions from the response of cells and tissues to photon radiation. The analysis of the dose-response curves for local control of skull base chordoma and normal tissue reactions observed in the pilot project suggest that the clinical results can be expressed sufficiently accurate by the RBE predictions of the LEM I (Schulz-Ertner *et al* 2007, Schlampp *et al* 2011). Experimental data, however, showed an overestimation of the RBE-weighted dose for light ions in general and for carbon ions in the entrance channel (Karger *et al* 2006, Elsässer *et al* 2008). These differences were not crucial for treatment safety, since the actual RBE-weighted dose in the entrance channel was less than predicted by the model. Nevertheless, a better agreement with the experimental data is important for the general applicability of the model in treatment planning, particularly also for other entities like the RBE-weighted dose in the healthy tissue as well as systematic comparisons between different tumor types and ion species.

Consequently, the LEM has been constantly improved with respect to biological parameters and mechanisms. The LEM I (Scholz *et al* 1997) directly links the local dose deposition pattern in the cell nuclei to the dose-response curve of photons. LEM II (Elsässer and Scholz 2007) and LEM III (Elsässer *et al* 2008) keep on pursuing this approach. In the recent version (LEM IV, Elsässer *et al* 2010, Friedrich *et al* 2012) an intermediate step is introduced: rather than the local dose, the complexity of the radiation damage in terms of microscopic double-strand break distribution on the DNA is considered (Elsässer *et al* 2010, Friedrich *et al* 2012). This damage distribution pattern is assumed to better represent the processes leading to the finally observed biological effect, and consequently should lead to a better prediction of the RBE.

However, despite the changes in the model, predictions of the RBE-weighted dose for the target regions should not be significantly affected to be consistent with the clinical results obtained so far, since these have been demonstrated to be in agreement already with the LEM I (Schulz-Ertner *et al* 2007, Schlampp *et al* 2011). The latest version of the model (LEM IV) has already demonstrated a better description of *in-vitro* data (Elsässer *et al* 2010, Friedrich *et al* 2012) but has not yet been compared in detail with clinical results. Hence, the agreement of the RBE predictions based on LEM IV with those of LEM I as well as with clinical data is investigated. For the comparison with the clinical outcome for the treatment of chordoma of the skull base with carbon ions in the GSI pilot project (Schulz-Ertner *et al* 2007) the clinical endpoints late toxicity in the central nervous system (CNS) evaluated in the rat spinal cord experiment (Karger *et al* 2006) and local control of chordoma evaluated from clinical studies of hypofractionated photon radiotherapy (Henderson *et al* 2009) were considered for

the RBE prediction. Idealized target volumes instead of real patient plans were used to point out the major differences between LEM I and LEM IV. In patient plans other aspects like field configuration, target geometries, margins and inter-patient heterogeneity could smear out the difference between LEM I and LEM IV and make a systematic analysis difficult. Therefore this study concentrates on a systematic analysis with idealized geometries rather than real patient plans which can be transferred to the clinical situation in a further step. A detailed analysis of the individual patient plans as well as the comparison of the LEM to other models of the literature will follow in a separate publication.

2. Materials and methods

2.1. Treatment planning

To compare the predictions of LEM IV against LEM I under treatment-like conditions, idealized target geometries (spheres and cubes) were used to facilitate the systematic comparison of the different LEM versions. The cubic volume has a fixed lateral dimension of 50 $\times$ 50 mm but varies in its dimension along the beam axis. For the spherical volume, the diameter varies between 20 to 100 mm (20 mm steps) and the target point along the beam axis (center of volume) varied from 50 to 200 mm depth (50 mm steps). These target configurations cover the whole spectrum of clinically relevant situations. Treatment plans consisted of two directly opposing fields in line with the majority of field arrangements in the pilot project. The treatment planning system TRiP98 was used to optimize the physical dose distribution with the RBE predictions based on LEM I to achieve a homogeneous RBE-weighted depth dose profile (Krämer *et al* 2000).

For comparison with the previously published dose-response curve for chordoma of the skull base treated in the GSI clinical trial (Schulz-Ertner *et al* 2007, Schulz-Ertner *et al* 2002), the median (80.3 ml), minimum (13.9 ml) and maximum (594.2 ml) tumor volumes representing the patient population were considered. For the analysis, volumes close to the original ones expressed with spheres of 53.5, 29.8 and 104.3 mm diameter respectively were used. These volumes refer to the subvolume (PTV2) of the initial planning target volume (PTV1) to account for the macroscopic tumor as well as a safety margin for localization uncertainty. For this analysis, PTV2 was assumed to cover 65% of PTV1, which was a representative value for the patient population regarded. Treatments were performed with 15 fractions to PTV1 and 5 fractions to PTV2. The RBE-weighted dose per fraction was chosen as 3 Gy (RBE) and 3.5 Gy (RBE), corresponding to the clinically applied values (Schulz-Ertner *et al* 2002).

2.2. RBE data

For clinical application, the LEM is used to calculate energy dependent RBE values for all projectiles from protons to neon which are stored in a so-called 'RBE-table' and used as input for the TRiP98 treatment planning program.

As the LEM derives the biological effect of ions from the dose-response to photon radiation, the biological input parameters of the LEM are the parameters α_γ, β_γ and D_t characterizing the photon dose-response curves according to the linear-quadratic model (LQ model) and extended by the threshold dose D_t (Astrahan 2008) describing the transition into a purely exponential shape (Elsässer and Scholz 2007). The transition dose D_t is necessary because the dose-response curve is needed up to very high doses since the LEM uses instead of a macroscopic dose scale rather the local dose deposition within individual particle traversals.

Table 1. Input parameters for the RBE tables.

RBE table	LEM version	α_γ (Gy^{-1})	β_γ (Gy^{-2})	$\alpha_\gamma/\beta_\gamma$ (Gy)	D_t (Gy)
[a]AB2 I	I	0.1	0.05	2	30
AB2 IV	IV	0.003	0.0015	2	22
AB2.45 IV	IV	0.0081	0.0033	2.45	30

[a] AB is the abbreviation for the photon $\alpha_\gamma/\beta_\gamma$-ratio from the linear-quadratic formula with the number representing the magnitude. The roman number represents the LEM version.

Thus the threshold dose D_t has to be considered even for small fraction sizes, i.e. 3–4 Gy (RBE), to describe the photon-dose response up to high photon doses potentially needed.

For the analysis three different RBE tables were used (table 1) characterized by their α_γ, β_γ and D_t value. All other parameters of the LEM are kept constant and chosen as described in Elsässer *et al* (2010). RBE table AB2 I was used during the clinical trial at GSI. The $\alpha_\gamma/\beta_\gamma$-ratio of 2 Gy was selected as it is characteristic for late toxicity in the CNS (Karger *et al* 2006). Since no data were available for photon $\alpha_\gamma/\beta_\gamma$-ratios of chordoma tumors at the beginning of the pilot project, the particular choice of $\alpha_\gamma/\beta_\gamma = 2$ Gy also for chordomas has been based on more general considerations concerning a potential correlation between the $\alpha_\gamma/\beta_\gamma$-ratio and tumor volume doubling times, as suggested e.g. by the clinical data reported by Battermann *et al* (1981).

The RBE table AB2 IV calculated with the LEM IV is based on the same biological endpoint, i.e. the same $\alpha_\gamma/\beta_\gamma$-ratio of 2 Gy, but the biological input parameters α_γ, β_γ as well as D_t were updated. Lower absolute values of α_γ and β_γ were chosen in accordance with recent findings concerning the observed difference of the absolute LQ-parameters between *in-vitro* and *in-vivo* endpoints independent on the tumor type (endpoint), i.e. the $\alpha_\gamma/\beta_\gamma$-ratio (Tai *et al* 2008, Henderson *et al* 2009).

Recently, also LQ-parameters for tumor control of chordoma became available from clinical studies of hypofractionated photon radiotherapy (Henderson *et al* 2009); as we focus on the analysis of the clinical results for chordoma of the skull base these are used for the third RBE table AB2.45 IV, also calculated with the LEM IV. Here, D_t is increased in line with an analysis of cell survival data suggesting an increase of D_t with increasing photon $\alpha_\gamma/\beta_\gamma$-ratio (Elsässer *et al* 2008).

2.3. Evaluation of the treatment plans

The impact of the model enhancement was investigated based on a reference physical depth dose profile obtained from a biological optimization using the LEM I (AB2 I). The resulting physical depth dose profile is used as input for a recalculation of the RBE-weighted dose based on the new model (AB2 IV and AB2.45 IV). Thus, the physical dose distributions were identical for both profiles and differences in the RBE-weighted dose can be uniquely attributed to the change of the LEM version. We focus here on the analysis of the target volume because clinical data are available, in contrast to the entrance channel where the clinical data are not yet available. Considering the dose volume histogram (DVH), the median and mean RBE-weighted doses were regarded for statistical comparison.

2.4. Local control

To assess the impact of the model enhancement, the dose-response data for 5-year local control of chordoma as compiled by Schulz-Ertner *et al* (2007) were reanalyzed by (i) replacing

the clinical target geometries by the idealized PTV1 and PTV2, and (ii) by recalculating the LEM I-optimized dose distributions with LEM IV using the RBE tables described in table 1.

As the recalculated RBE-weighted dose distributions are inhomogeneous, the equivalent uniform dose (EUD) can be used to further characterize the RBE-weighted dose distribution. If in the case of tumor tissue the corresponding linear-quadratic parameters describe the cell survival, the EUD can be determined from the mean or median survival $\overline{S}$ in the target volume by

$$\mathrm{EUD} = -(\alpha_\gamma/2\beta_\gamma) + \sqrt{-\ln \overline{S}/\beta_\gamma + (\alpha_\gamma/2\beta_\gamma)^2}, \tag{1}$$

where α_γ and β_γ are the photon parameters of the LQ model (Niemierko 1997). Due to the nonlinearity of the dose-response curve, dose fluctuations can have an increased impact on cell survival. This is related to the linear-quadratic dependence of the dose-response curve. Strong deviations from the planned target dose can therefore lead to a disproportionately higher or lower survival rate becoming perceivable in the EUD. Also the median RBE-weighted dose was considered as representative, since it reflects the EUD of the tumor in case of directly opposing fields (Steinsträter *et al* 2012).

For comparison with the dose response curve given in Schulz-Ertner *et al* 2007, the obtained median RBE-weighted doses were recalculated to isoeffective doses using a fractionation schedule of 2 Gy (RBE) per fraction (d_{ref}) according to Wambersie *et al* (2006):

$$D_{\mathrm{IsoE}} = \frac{D \cdot (1 + \beta/\alpha \cdot d)}{1 + \beta/\alpha \cdot d_{\mathrm{ref}}}, \tag{2}$$

where d and D are the actually applied fractional and total RBE-weighted doses, respectively. For the determination of the EUD and the isoeffective dose an $\alpha_\gamma/\beta_\gamma$ -ratio describing the endpoint under consideration is needed; therefore the $\alpha_\gamma/\beta_\gamma$-ratios associated with the RBE tables described in table 1 were used.

3. Results

3.1. Dose analysis of idealized geometries

Using the RBE table AB2 IV for the RBE prediction results in an increase of the RBE-weighted dose towards the distal end of the target volume as illustrated in figure 1(a). This increase can be explained by the more detailed consideration of correlated double strand breaks (DSB) within small subvolumes thus leading to a stronger variation of RBE with LET and consequently a steeper gradient of RBE with depth compared to the LEM I. Moreover it is shown that the shapes of the distal parts of the RBE-weighted depth dose profiles are the same for all investigated target dimensions. This is due to the fact that the composition of the distal part of the SOBP is not affected by adding Bragg peaks at the proximal part when increasing the dimension of the SOBP, apart from an obviously minor contribution of lighter fragments. When two opposing fields are used, as typically applied in the GSI clinical trial, the gradient of the RBE-weighted dose throughout the target region is substantially diminished, (figure 1(b)). The degree of RBE homogenization decreases with increasing target dimension. The configuration with opposing fields leads to the largest LET-homogenization compared to other field configurations like for example a single field or (right) angled fields. Thus for the opposing fields also the largest RBE gradient compensation is observed. For non-opposing field configurations, i.e. angled fields, a less pronounced compensation is expected. For different depth localizations, only minor differences in the shape of the RBE-weighted

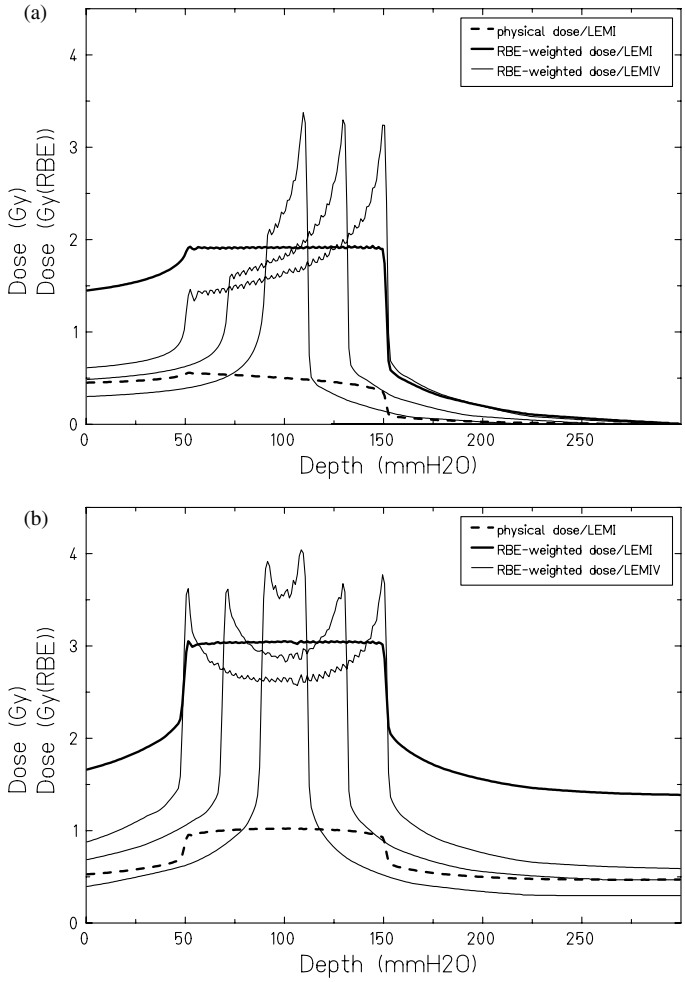

Figure 1. (a) Physical and RBE-weighted depth dose profiles resulting from RBE predictions with the RBE tables AB2 I (100 mm diameter) and AB2 IV. Illustrated is one out of two fields for different spherical target volumes with 20, 60 and 100 mm diameter and an discounter at 100 mm. (b) Superposition of two opposing fields for the same geometrical arrangements as in (a).

depth-dose profiles are observed (data not shown). In table 2 RBE-values for the RBE-tables described in table 1 for an SOBP of 60 mm dimension from 75 to 125 mm depth as shown in figure 1(a) are tabulated to provide detailed information of the RBE for different dose-levels.

In figure 2, the corresponding mean RBE-weighted doses are plotted as a function of the target dimension. For RBE predictions with AB2 IV, the mean RBE-weighted dose decreases with increasing dimension. This can be explained by the underestimation of the RBE-weighted dose as compared to LEM I in the center of the target volume which is increasingly composed of dose contributions with photon like efficiency leading to a decreased RBE and thus leading to an overall decrease in the mean RBE-weighted dose. Consequently, the RBE-weighted dose variation as expressed by the standard deviation increases with increasing dimension (3–7%). As suggested before, the shape of the target volume has an impact on the RBE-weighted dose too. For the spherical volumes a higher RBE-weighted dose is observed as compared to the

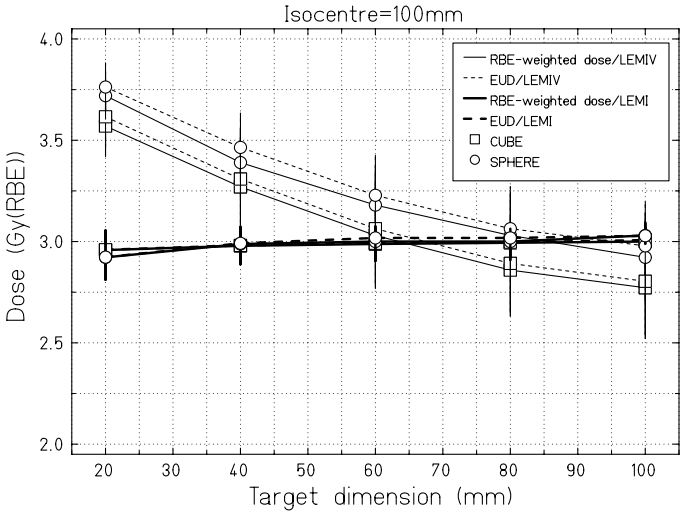

Figure 2. Mean RBE-weighted dose, equivalent uniform dose (EUD) and the corresponding standard deviations for the different spherical and cubic target dimensions at an discounter depth of 100 mm.

Table 2. RBE-values for the RBE-tables described in table 1 for an SOBP of 60 mm dimension from 75 to 125 mm depth as shown in figure 1(a).

	AB2 IV			AB2.45 IV			AB2 I		
Prescribed dose	[c]Proximal	Distal	Mean	Proximal	Distal	Mean	Proximal	Distal	Mean
3 [a]Gy (RBE)	2.13	9.59	4.71	2.11	10.40	4.98	3.047	4.45	3.57
0.5 [b]Gy	2.09	8.61	4.19	1.00	9.18	4.27	3.69	4.99	4.19
1 Gy	1.80	6.45	3.30	1.75	6.92	3.40	2.96	3.86	3.30
2 Gy	1.53	4.75	2.56	1.52	5.13	2.66	2.33	2.93	2.56
5 Gy	1.26	3.13	1.83	1.27	3.40	1.92	1.70	2.011	1.82
10 Gy	1.13	2.28	1.45	1.14	2.48	1.52	1.38	1.52	1.43

[a]The unit Gy (RBE) describes an optimized RBE-weighted dose.
[b]The unit Gy describes an optimized physical dose.
[c]RBE-values are shown for the proximal end (75 mm) and the distal end (125 mm) as well as the mean value from 175 to 125 mm depth.

cubic volumes for a given dimension. Besides the mean RBE-weighted dose also the median is calculated and shows no significant deviation (<3%) from the mean (data not shown).

Apart from the agreement of mean or median RBE-weighted doses as described above, it is of interest to assess the potential impact of the heterogeneity of the RBE-weighted dose distribution in individual fields. Hence, also the equivalent uniform dose (EUD) calculated from the mean cell survival was analyzed (Niemierko 1997). The EUD shows only slight deviations from the mean and median RBE-weighted dose (figure 2). This suggests that the heterogeneity of the RBE-weighted dose distribution has no particular impact in terms of disproportional higher or lower overall effect resulting from an over- or underestimation of the RBE-weighted dose distribution at the distal and proximal end of the target volume, respectively.

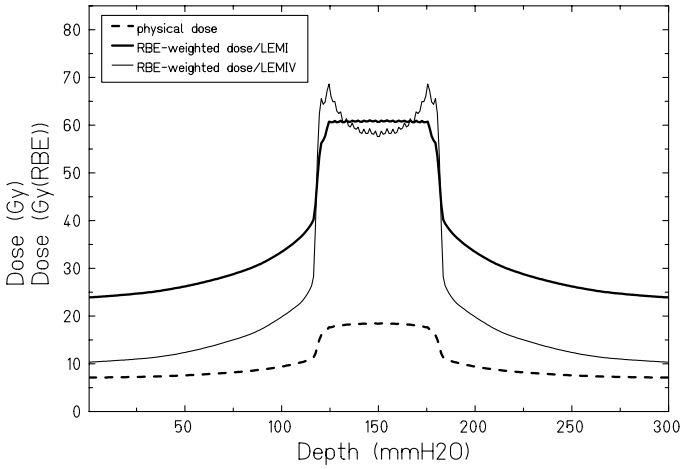

Figure 3. Physical and RBE-weighted depth dose profiles resulting from the RBE predictions with the RBE tables AB2 I and AB2 IV with an optimized RBE-weighted dose of 15 × 3 Gy (RBE) to PTV1 (Ø 61.8 mm) and additional 5 × 3 Gy (RBE) to PTV2 (Ø 53.52 mm) using AB2 I.

3.2. Local control analysis

Comparison of local control rates with other treatment modalities like e.g. modern photon techniques or proton treatments requires the accurate estimation of RBE values. For the clinical evaluation of the LEM IV the consistency of the predicted RBE-weighted dose with the dose-response curve for local control of skull base chordoma as reported by Schulz-Ertner *et al* (2007) is important. For this purpose the isoeffective dose for the reference fractionation schedule of 2 Gy per fraction was chosen to compare different studies in the literature (Schulz-Ertner *et al* 2007).

A RBE-weighted target dose of 60 Gy (RBE) in 15+5 fractions of 3 Gy (RBE) and the linear quadratic parameters corresponding to the RBE table A2 I lead to an isoeffective dose of 75 Gy (IsoE) for a fraction size of 2 Gy in PTV2. The corresponding tumor control probability of 63% has shown to be in good agreement with the results obtained in studies using photon and proton treatments, thus indicating that the estimation of RBE based on LEM I was sufficiently accurate.

When analyzing the impact of the transition to LEM IV, the dependence on the target dimensions as illustrated in figure 2 has to be taken into account. Recalculations of the median isoeffective dose based on the RBE tables AB2 IV and AB2.45 IV were thus performed for idealized PTV1 and PTV2 (spheres). Figure 3 illustrates the physical and RBE-weighted dose distributions as applied in 15 + 5 fractions leading to 60 Gy (RBE) in the idealized PTV2 of 78.3 ml, representing the median value of the patient population (Schulz-Ertner *et al* 2007).

Furthermore, the local control rates of the original clinical collective (Schulz-Ertner *et al* 2007) are plotted against the median isoeffective doses predicted here for the idealized PTV2. These response data points are then compared with the mentioned dose response curve for local control of chordoma (figure 4), which also includes the original response data points from the GSI pilot project (LEM I based doses). Note that the median isoeffective doses attributed to the local control rates within the other studies refer to the median dose applied in the patient population whereas the recalculated doses refer to the median isoeffective dose within the above-described idealized PTV2.

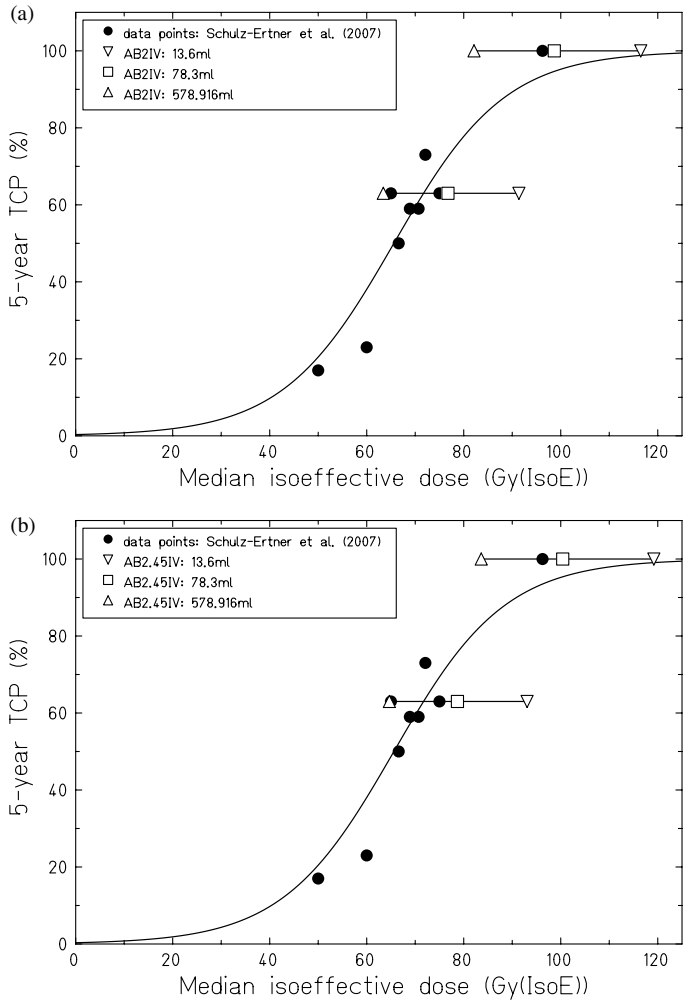

Figure 4. TCP curve published in Schulz-Ertner *et al* (2007) with reanalyzed data points referring to the median isoeffective dose achieved with (a) the RBE table AB2 IV and (b) AB2.45 IV for a idealized PTV2 of 78.3 ml and corresponding PTV1 as well as for a PTV2 of 13.6 ml and 578.9 ml to show the dependence of the isoeffective dose on the target volume dimension.

3.3. Sensitivity

To assess the uncertainties of the photon input data, the sensitivity on variations of α_γ, β_γ and D_t was analyzed (table 3). The RBE-weighted dose was therefore optimized to 3 Gy (RBE) with the corresponding reference RBE-table.

Changing the parameters by 25% results in variations of the RBE-weighted dose by less than 10%, which is in the order of the scatter of the clinical data around the adjusted TCP curve in figure 4. This is thus considered to be sufficiently robust for clinical application.

4. Discussion

To fully exploit the potential advantages of ion beams for therapy requires to prospectively estimate the RBE as accurately as possible for treatment planning. Biophysical models

Table 3. Sensitivity analysis for a 60 mm extended Bragg-peak spreaded from 120 to 180 mm.

Reference RBE-table	Mean (Gy(RBE))	Photon input parameters LEM	Modification (%)	△RBE-weighted dose (%)
AB2 IV	2.99	α_γ	+25	−4.7
			−25	+3.4
		β_γ	+25	+2.4
			−25	−4.7
		D_t	+25	+7.4
			−25	−9.4
AB2.45 IV	2.99	α_γ	+25	−5.2
			−25	+5.5
		β_γ	+25	+3.5
			−25	−6.1
		D_t	+25	+5.5
			−25	−8.0

represent a powerful tool to achieve this goal and have been demonstrated to allow RBE predictions with reasonable accuracy for different endpoints *in-vitro* (Elsässer and Scholz 2007, Inaniwa *et al* 2010), *in-vivo* (Karger *et al* 2006, Debus *et al* 2003) and for clinical applications (Schulz-Ertner *et al* 2007, Schlampp *et al* 2011). Nevertheless, the first version of LEM I implemented in the treatment planning for the GSI pilot project has been shown to have certain limitations with respect to the accuracy of the RBE predictions in the entrance region and for lighter particles like e.g. protons. Subsequent enhancements of the LEM have been demonstrated to substantially improve the accuracy of the model in biological experiments (Elsässer and Scholz 2007, Elsässer *et al* 2008, Elsässer *et al* 2010, Friedrich *et al* 2012).

In agreement with experimental data the latest version, LEM IV, predicts a more pronounced increase of RBE with LET as compared to the LEM I. This leads to the inhomogeneity and the rise of the RBE-weighted dose towards the distal end of the target volume, when the RBE-weighted dose is obtained from the physical dose resulting from the optimization based on LEM I.

In order to estimate the clinical impact of this more pronounced RBE gradient it is important to assess the accuracy of the model predictions for clinically relevant endpoints, e.g. late effects in the CNS. Experiments analyzing the tolerance of the rat spinal cord according to Karger *et al* (2006) revealed that the RBE predicted with the LEM I was underestimated by about 25% in the Bragg-peak region. Using instead the LEMIV-based RBE table AB2 IV with LQ-parameters describing the dose response behavior in the experiment of Karger *et al* (2006) results in a higher RBE which is in much better agreement with the measured values (figure 5). In line with the *in vitro* data presented in Elsässer *et al* (2010), this further demonstrates the improvement of the LEM IV as compared to the LEM I also for *in vivo* data.

Consequently, the question arises whether this steeper gradient of the RBE and the resulting inhomogeneity of the RBE-weighted dose distribution would be clinically significant when reanalyzing the clinical results obtained in the clinical trial with carbon ions at GSI.

Here it is important to note that large parts of the inhomogeneity are already compensated when using two opposing fields, representing the typical situation for the chordoma patients treated at GSI. The remaining inhomogeneity and the corresponding difference of the mean RBE-weighted dose as compared to the LEM I prediction primarily depend on the shape and dimension of the target volume.

For typical tumor volumes as treated within the pilot project, the mean values of the RBE-weighted dose according to LEM IV are very similar compared to those of LEM I

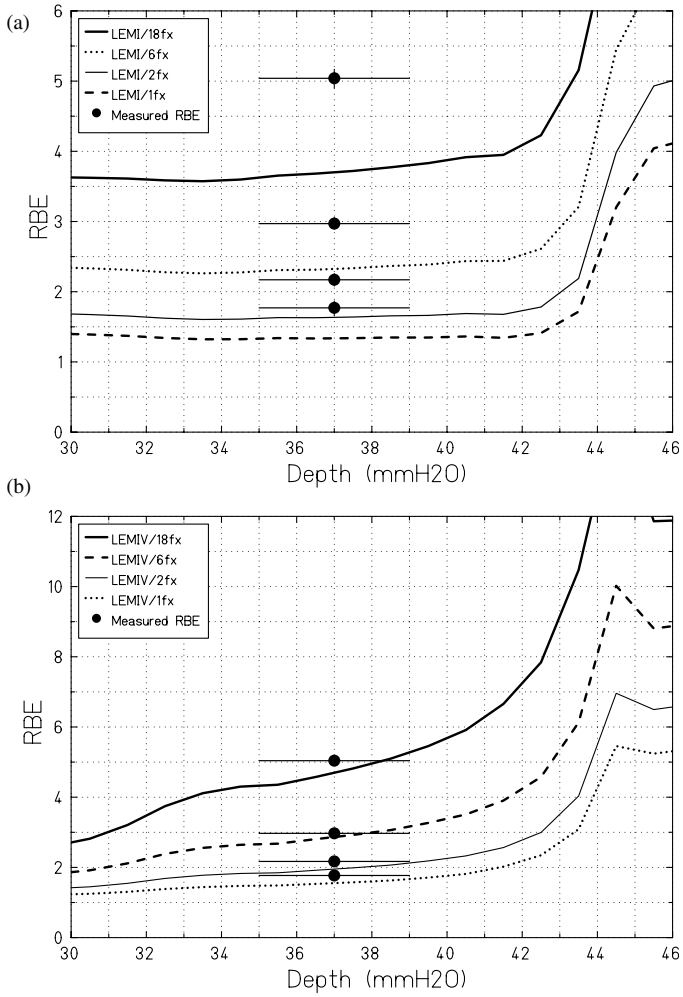

Figure 5. RBE distribution predicted with (a) the RBE table AB2I and (b) the RBE table AB2 IV for the irradiation of the spinal cord in rats according to Karger *et al* (2006) compared to the measured RBE (position uncertainty: ± 2 mm within SOBP). Note that the scales in (a) and (b) differ.

(table 2, figure 2). When taking into account the distribution of tumor volumes for a typical patient population, the smaller volumes would get a larger RBE-weighted dose, whereas for the larger volumes a lower RBE-weighted dose would be expected. This could have an impact on the local control probability of individual patients. In a population-based clinical analysis, however, this larger spread would probably not be detectable within the other uncertainties like e.g. inter-patient heterogeneity of radiation sensitivity, and thus the agreement in the mean values is most important here.

The reanalysis of the isoeffective dose clearly indicates that the transition from LEM I to LEM IV would have no significant impact on the TCP dose-response curve. Since the LQ-parameters α_γ and β_γ published in Henderson *et al* (2009) are very low and also the absolute values published in Tai *et al* (2008) for liver cancer are lower than comparable *in-vitro* data we concluded a trend towards lower absolute values for *in-vivo* endpoints compared to *in-vitro*.

We demonstrated with this study that the dose-response behavior in terms of local control for chordoma and late effects in the CNS can be well described with lower absolute values independent on the $\alpha_\gamma/\beta_\gamma$-ratio. Therefore, the RBE values predicted with LEM IV and the RBE tables AB2 IV as well as the AB2.45 IV with updated parameters are consistent with the available clinical data for local control of chordoma (Schulz-Ertner *et al* 2007).

Besides comparison of the different LEM model versions, comparison to other models potentially applicable in treatment planning, as e.g. the MKM (Inaniwa *et al* 2010) or RMF (Carlson *et al* 2008, Frese *et al* 2012) would be of interest. However, at present a direct comparison of models on the basis of published results is mainly hindered by the fact that the different biological models are used in combination with different physical models that are required to characterize the radiation field. For example, Frese *et al* (2012) use the RFM in combination with a simple physics model that completely neglects nuclear interactions and beam fragmentation. Inaniwa *et al* (2010) use the MKM in combination with a more realistic physics model based on Geant4, which might however differ from the approach implemented in TRiP98. As a consequence, differences in RBE predictions cannot be uniquely attributed to the different biological models, but might also arise from the differences in the underlying physics description. We are thus currently implementing an interface to the TRiP98 environment that will allow to use any biological model that is capable of predicting dose response curves as a function of the particle species and energy or LET. With that, the different models can be compared on the basis of exactly the same physical composition of the radiation field.

The analysis presented here is based on idealized volumes (spheres and cubes) and focuses on a general understanding of the main trends. It remains to be elucidated in how far the conclusions from these idealized geometries can be transferred to the situation of real patient treatment plans. Therefore, LEM IV based recalculations of patient treatment plans are currently performed (Gillmann 2011). Similarly, the impact of the model enhancement on the analysis of normal tissue complications as reported by Schlampp *et al* (2011) will be assessed.

As a consequence of the differences between LEM I and LEM IV, biological optimization in treatment planning based on LEM IV would lead to an increase of the physical dose in the center of the target volume and a reduction of the physical dose at the border as compared to an optimization with LEM I. Implementation of the LEM IV and the replacement of LEM I in treatment planning thus requires a thorough clinical assessment of the balance between the potentially higher effect in the center and reduction of the effect at the field boarders.

5. Conclusion

The differences in the prediction of RBE-weighted doses and isoeffective doses between LEM I and LEM IV for typical tumor volumes, i.e. averaged over the patient population in the GSI pilot project, are less than 10%. Thus, based on the analysis of idealized target geometries, the transition to LEM IV is not expected to lead to significant differences of the TCP dose-response relationship for chordoma as compared to the analysis based on LEM I.

Acknowledgments

The authors would like to thank Oliver Jäkel, PhD and Clarissa Gillmann from the Heidelberger Ionenstrahl-Therapiezentrum (HIT) for their helpful comments on the manuscript. This work is part of HGS-HIRe.

References

Astrahan M 2008 Some implications of linear-quadratic-linear radiation dose-response with regard to hypofractionation *Med. Phys.* **35** 4161–72

Battermann J J, Breur K, Hart G A M and Van Peperzeel H A 1981 Observations on pulmonary metastases in patients after single doses and multiple fractions of fast neutrons and cobalt-60 gamma rays *Eur. J. Cancer* **17** 539–48 PMID: 7297593

Carlson D J, Stewart R D, Semenenko V A and Sandison G A 2008 Combined use of Monte Carlo DNA damage simulations and deterministic repair models to examine putative mechanisms of cell killing *Radiat. Res.* **169** 447–59

Debus J, Scholz M, Haberer T, Peschke P, Jäkel O, Karger C P and Wannenmacher M 2003 Radiation tolerance of the rat spinal cord after single and split doses of photons and carbon ions *Radiat. Res.* **160** 536–42

Elsässer T, Krämer M and Scholz M 2008 Accuracy of the local effect model for the prediction of biologic effects of carbon ion beams *in vitro* and *in vivo Int. J. Radiat. Oncol. Biol. Phys.* **71** 866–72

Elsässer T *et al* 2010 Quantification of the relative biological effectiveness for ion beam radiotherapy: direct experimental comparison of proton and carbon ion beams and a novel approach for treatment planning *Int. J. Radiat. Oncol. Biol. Phys.* **78** 1177–83

Elsässer T and Scholz M 2007 Cluster effects within the local effect model *Radiat. Res.* **167** 319–29

Frese M C, Yu V K, Stewart R D and Carlson D J 2012 A mechanism-based approach to predict the relative biological effectiveness of protons and carbon ions in radiation therapy *Int. J. Radiat. Oncol. Biol. Phys.* **83** 442–50

Friedrich T, Scholz U, Elsässer T, Durante M and Scholz M 2012 Calculation of the biological effects of ion beams based on the microscopic spatial damage distribution pattern *Int. J. Radiat. Biol.* **88** 103–107

Gillmann C 2012 private communication

Henderson F C, McCool K, Seigle J, Jean W, Harter W and Gagnon G J 2009 Treatment of chordomas with CyberKnife: George-town university experience and treatment recommendations *Neurosurgery* **64** A44–53

Inaniwa T, Furukawa T, Kase Y, Matsufuji N, Toshito T, Matsumoto Y, Furusawa Y and Noda K 2010 Treatment planning for a scanned carbon beam with a modified microdosimetric kinetic model *Phys. Med. Biol.* **55** 6721–37

Kanai T *et al* 1999 Biophysical characteristics of HIMAC clinical irradiation system for heavy-ion radiation therapy *Int. J. Radiat. Oncol. Biol. Phys.* **44** 201–10

Kanai T, Furusawa Y, Fukutsu K, Itsukaichi H, Eguchi-Kasai K and Ohara H 1997 Irradiation of mixed beam and design of spread-out Bragg peak for heavy-ion radiotherapy *Radiat. Res.* **147** 78–85

Kanai T, Matsufuji N, Miyamoto T, Mizoe J, Kamada T, Tsuji H, Kato H, Baba M and Tsujii H 2006 Examination of GyE system for HIMAC carbon therapy *Int. J. Radiat. Oncol. Biol. Phys.* **64** 650–6

Karger C P, Peschke P, Sanchez-Brandelik R, Scholz M and Debus J 2006 Radiation tolerance of the rat spinal cord after 6 and 18 fractions of photons and carbon ions: experimental results and clinical implications *Int. J. Radiat. Oncol. Biol. Phys.* **66** 1488–97

Kase Y, Kanai T, Matsufuji N, Furusawa Y, Elsässer T and Scholz M 2008 Biophysical calculation of cell survival probabilities using amorphous track structure models for heavy-ion irradiation *Phys. Med. Biol.* **53** 37–59

Kase Y, Kanematsu N, Kanai T and Matsufuji N 2006 Biological dose calculation with Monte Carlo physics simulation for heavy-ion radiotherapy *Phys. Med. Biol.* **51** N467–75

Krämer M, Jäkel O, Haberer T, Kraft G, Schardt D and Weber U 2000 Treatment Planning for heavy-ion radiotherapy: physical beam model and dose optimization *Phys. Med. Biol.* **45** 3299–317

Niemierko A 1997 Reporting and analyzing dose distributions: a concept of equivalent uniform dose *Med. Phys.* **24** 103–10

Schardt D, Elsässer T and Schulz-Ertner D 2010 Heavy-ion tumor therapy: physical and radiobiological benefits *Rev. Mod. Phys.* **82** 383–425

Schlampp I *et al* 2011 Temporal lobe reactions after radiotherapy with carbon ions: incidence and estimation of the relative biological effectiveness by the local effect model *Int. J. Radiat. Oncol. Biol. Phys.* **80** 815–23

Scholz M, Kellerer A M, Kraft-Weyrather W and Kraft G 2000 Computation of cell survival in heavy ion beams for therapy. The model and its approximation *Radiat. Environ. Biophys.* **36** 59–66

Schulz-Ertner D, Haberer T, Jäkel O, Thilmann C, Krämer M, Enghardt W, Kraft G, Wannenmacher M and Debus J 2002 Radiotherapy for chordomas and low grade chondrosarcomas of the skull base with carbon ions *Int. J. Radiat. Oncol. Biol. Phys.* **53** 36–42

Schulz-Ertner D, Karger C P, Feuerhake A, Nikoghosyan A, Combs S, Jäkel O, Edler L, Scholz M and Debus J 2007 Effectiveness of carbon ion radiotherapy in the treatment of skull-base chordoma *Int. J. Radiat. Oncol. Biol. Phys.* **68** 449–57

Steinsträter O, Grün R, Scholz U, Friedrich T, Durante M and Scholz M 2012 Mapping of RBE-weighted doses between HIMAC- and LEM-based treatment planning systems *Int. J. Radiat. Oncol. Biol. Phys.* (at press) online at http://dx.doi.org/10.1016/j.ijrobp.2012.01.038

Tai A, Erickson B, Khater K A and Allen Li X 2008 Estimate of radiobiologic parameters from clinical data for biologically based treatment planning for liver irradiation *Int. J. Radiat. Oncol. Biol. Phys.* **70** 900–7

Wambersie A *et al* 2006 The RBE issues in ion-beam therapy: conclusions of a joint IAEA/ICRU working group regarding quantities and units *Radiat. Prot. Dosim.* **122** 463–70

International Journal of
Radiation Oncology
biology • physics

www.redjournal.org

Physics Contribution

Mapping of RBE-Weighted Doses Between HIMAC– and LEM–Based Treatment Planning Systems for Carbon Ion Therapy

Olaf Steinsträter, Ph.D.,* Rebecca Grün, M.Sc.,*,†,‡ Uwe Scholz, M.Sc.,*,§ Thomas Friedrich, Ph.D.,* Marco Durante, Ph.D.,*,§ and Michael Scholz, Ph.D.*

**Abteilung Biophysik, GSI Helmholtzzentrum für Schwerionenforschung, Darmstadt, Germany; †Institut für Medizinische Physik und Strahlenschutz, TH-Mittelhessen, Gießen, Germany; ‡Fachbereich Medizin, Philipps-Universität Marburg, Marburg, Germany; and §Institut für Festkörperphysik, Technische Universität Darmstadt, Darmstadt, Germany*

Received Jun 1, 2011, and in revised form Jan 10, 2012. Accepted for publication Jan 12, 2012

Summary

A method was developed to convert clinically prescribed RBE (Relative Biological Effectiveness)-weighted doses from the approach used at the Heavy-Ion Medical Accelerator facility (HIMAC; National Institute of Radiological Science, Japan) to the Local Effect Model–based approach used at GSI Helmholtzzentrum, Germany, and other centers. For interpretation and comparison of clinical trials, this conversion is of extreme importance because, given the different methods to determine the RBE-weighted dose, similar dose values might not necessarily be related to similar clinical outcomes.

Purpose: A method was developed to convert clinically prescribed RBE (Relative Biological Effectiveness)-weighted doses from the approach used at the Heavy-Ion Medical Accelerator (HIMAC) at the National Institute of Radiological Science, Chiba, Japan, to the LEM (Local Effect Model)-based TReatment planning for Particles (TRiP98) approach used in the pilot project at the GSI Helmholtzzentrum, Darmstadt, and the Heidelberg Ion-Beam Therapy Center (HIT).

Methods and Materials: The proposed conversion method is based on a simulation of the fixed spread-out Bragg peak (SOBP) depth dose profiles as used for the irradiation at HIMAC by LEM/TRiP98 and a recalculation of the resulting RBE-weighted dose distribution. We present data according to the clinical studies conducted at GSI in the past decade (LEM I), as well as data used in current studies (refined LEM version: LEM IV).

Results: We found conversion factors (RBE-weighted dose LEM/RBE-weighted dose HIMAC) reaching from 0.4 to 2.0 for prescribed carbon ion doses from 1 to 60 Gy (RBE) for SOBP extensions ranging from 20 to 120 mm according to the HIMAC approach. A conversion factor of 1.0 was found for approximately 5 Gy (RBE). The conversion factor decreases with increasing prescribed dose. Slightly smaller values for the LEM IV–based data set compared with LEM I were found. A significant dependence of the conversion factor from the SOBP width could be observed in particular for LEM IV, whereas the depth dependence was found to be small.

Conclusions: For the interpretation and comparison of clinical trials performed at HIMAC and GSI/HIT, it is of extreme importance to consider these conversion factors because according to the various methods to determine the RBE-weighted dose, similar dose values might not necessarily be related to similar clinical outcomes.

Keywords: Carbon ion radiotherapy, Treatment planning, RBE, HIMAC, LEM

Reprint requests to: Olaf Steinsträter, Ph.D., Abteilung Biophysik, GSI Helmholtzzentrum für Schwerionenforschung, Planckstraße 1, 64291 Darmstadt, Germany. Tel: (+49) 6159-71-1650; Fax: (+49) 6159-71-2106; E-mail: o.steinstraeter@gsi.de

This work was supported by Siemens Healthcare, Particle Therapy, Erlangen, Germany.

Conflicts of interest: none.

Int J Radiation Oncol Biol Phys, Vol. 84, No. 3, pp. 854–860, 2012
0360-3016/$ - see front matter
doi:10.1016/j.ijrobp.2012.01.038

Introduction

Starting in 1994 and 1997, respectively, extensive clinical studies on carbon ion radiotherapy have been conducted at the National Institute of Radiological Science (NIRS), Chiba, Japan (1) and at the GSI Helmholtzzentrum für Schwerionenforschung, Darmstadt, Germany (2). To draw maximal benefit from these studies, a common basis for the mapping between center-related beam parameters and clinical outcomes should be established.

Although at both centers the treatment plans were based on the concept of RBE (Relative Biological Effectiveness)-weighted doses, the approaches to estimate these doses are quite different, strongly influenced by the different beam delivery systems. At HIMAC, the RBE-weighted dose is derived from an empirically established equivalence between carbon and neutron beams exploiting experiences with neutron radiation therapy at NIRS (3). For the pilot project at GSI, a radiobiological model, the Local Effect Model (LEM) (4–7) has been developed that derives RBE values from experimental data available for photons.

Because of the different methods to relate RBE-weighted and physically absorbed dose, the same clinically prescribed RBE-weighted dose will typically not result in the same depth dose distribution at the two centers. Clinical outcomes are therefore not necessarily comparable if the given RBE-weighted doses are identical.

In this study, we provide a method to convert between a prescribed RBE-weighted dose as realized at NIRS and the dose specification based on the LEM used for treatment planning at GSI and other centers (*e.g.*, Heidelberg Ion-Beam Therapy Center [HIT], Particle Therapy Marburg, NRoCK Kiel, CNAO Pavia, Shanghai Heavy Ion Therapy Center).

Methods and Materials

Methods to determine the RBE-weighted dose at NIRS and GSI

The HIMAC irradiation system uses passive beam shaping (3): starting with a fixed beam energy, shape and depth of the spread-out Bragg peak (SOBP) are adjusted by a ridge filter designed to reach a uniform survival fraction of 10% for human salivary gland tumor (HSG) cells inside its nominal SOBP width. If $D(z;10\%HSG)$ is the physical depth dose distribution of the filter design (z the water equivalent depth), the physical dose $D(z;d_{presc}^{HIMAC})$ used at HIMAC for irradiation according to the clinically prescribed RBE-weighted dose, d_{presc}^{HIMAC}, is given by

$$D\left(z;d_{presc}^{HIMAC}\right)=\lambda_{presc}^{HIMAC}D(z;10\%HSG), \quad (1)$$

with a factor λ_{presc}^{HIMAC} depending on the prescribed dose d_{presc}^{HIMAC}. The calculation of λ_{presc}^{HIMAC} is based on the neutron-equivalent depth $z_{neutron}$ inside the SOBP, where the carbon beam is biologically equivalent to the NIRS neutron beam (30 MeV deuteron projectiles on beryllium target) (3). For HSG cells at 10% survival level, $z_{neutron}$ can be identified by an RBE of 2.0 (3):

$$D(z_{neutron};10\%HSG)=\frac{D^{RBE}(10\%HSG)}{2.0}. \quad (2)$$

Here, $D^{RBE}(10\%HSG)$ = 4.0359 Gy (RBE) (according to Kanai *et al.* (8): $\alpha=0.3312$ Gy^{-1}, $\beta_{photon}=0.0593$ Gy^{-2}) is the constant RBE-weighted dose within the SOBP.

The clinically determined RBE for the therapeutic neutron beam at NIRS was determined to 3.0 (3), and for a given prescribed dose d_{presc}^{HIMAC}, this results in

$$D\left(z_{neutron};d_{presc}^{HIMAC}\right)=d_{presc}^{HIMAC}/3.0 \quad (3)$$

at the neutron-equivalent position. Combining Eqs. 1, 2, and 3 leads to

$$\lambda_{presc}^{HIMAC}=2/3\frac{d_{presc}^{HIMAC}}{D^{RBE}(10\%HSG)}. \quad (4)$$

In contrast to the passive HIMAC irradiation system, at GSI a magnetic scanning system together with active energy variation is used (9). Starting with a clinically prescribed RBE-weighted dose, d_{presc}^{LEM}, for the tumor volume, the treatment planning system TRiP98 (TReatment planning for Particles) is used to derive an individually optimized physical depth dose profile (9–11). A detailed description of the radiobiological response of the irradiated tissue is needed for this optimization and provided to TRiP98 by an externally calculated data set (we use the term "RBE table" in this article) containing RBE information for each relevant ion type (carbon and possible fragments) and energy. An RBE table is individually derived from photon response data of the irradiated tissue by means of the Local Effect Model (LEM); the TRiP98 optimization results thus strongly depend on the particular choice of this input data set. This study is mainly based on the extended LEM version recently proposed by Elsässer *et al.* (7), here termed LEM IV. In addition, because the clinical data collected at GSI in the past decade was based on a previous version (4), LEM I, we also show results based on this version.

The biological basis of LEM-based RBE tables can be characterized by three parameters: α_{photon} and β_{photon} describing the linear and quadratic part of the Linear Quadratic (LQ) model, respectively, and D_t marking the high-dose transition from linear-quadratic to purely linear dose response, in accordance with (12). A LEM calculation additionally needs the effective radius of the cell nucleus, but for all RBE tables discussed in this article, a fixed radius of 5 μm was assumed.

Conversion between RBE-weighted dose specifications used at NIRS and GSI

We based our conversion method on a reconstruction of the physical dose distributions used at NIRS by the GSI treatment planning system. Because of the different beam delivery systems, the physical composition of the beams may be different even though the physical dose is identical; however, it was shown that for comparable depth-dose profiles, the biological effects are also comparable (13).

Following the requirements used to design the ridge filters at NIRS, TRiP98 was used to optimize SOBPs from 20 mm to 120 mm (step size 20 mm) and for the three depths reported by Kanai *et al.* (3) for a survival level of 10% for HSG cells (photon parameters (7): $\alpha_{photon}=0.3130$ Gy^{-1}, $\beta_{photon}=0.0615$ Gy^{-2}, $D_t=7.5$). Although the relative shapes of the calculated depth dose profiles were found to be in good agreement with the results reported in Kanai *et al.* (3), the absolute dose values were slightly higher than the measured values. Therefore, an additional scaling factor $\mu = 0.88$, determined by a least square fit, was applied. The need for a scaling factor might be attributed to long-term variation of cellular sensitivity of the HSG cells, as also discussed by Inaniwa *et al.* (14), and the corresponding change in the photon parameters α and β. However, because the main aspect of the work

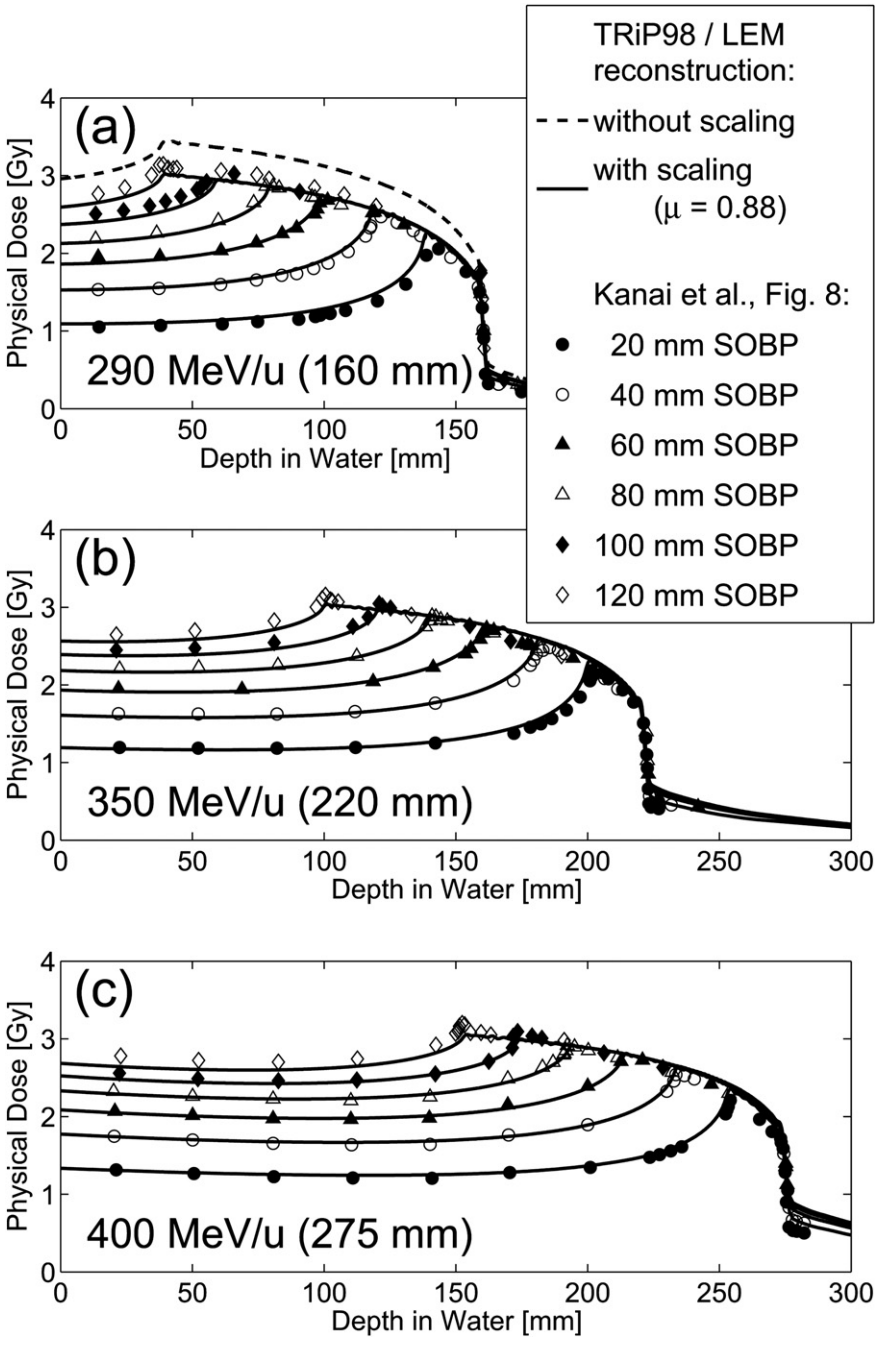

Fig. 1. Comparison of LEM IV/TRiP98 reconstructed SOBPs (solid and dashed curves) for carbon ion irradiation to experimental results for HIMAC (symbols) published by Kanai *et al.* (3) (their fig. 8a−8c). HIMAC data were available for six SOBP widths (20−120 mm) and three depths expressed as primary beam energies (according to the HIMAC system): 290 MeV/u (160 mm) in panel a, 350 MeV/u (220 mm) in panel b, and 400 MeV/u (275 mm) in panel c. The preoptimized LEM IV/TRiP98 results (panel a shows an example as dashed curve) were scaled by a common factor of $\mu = 0.88$ (solid curves) to fit the HIMAC requirements (symbols) in a least square sense. The curves shown are used as models for the SOBPs realized at HIMAC in our conversion method. HIMAC = Heavy-Ion Medical Accelerator facility, National Institute of Radiological Science, Japan; LEM = Local Effect Model; SOBP = spread-out Bragg peak; TRiP98 = TReatment planning for Particles.

presented here is to accurately reproduce the absorbed depth dose profile, we preferred to use biological input parameters consistent with our previous work and to optimally adapt the depth dose profile by the scaling procedure. The solid curves in Fig. 1 compare the reconstructed dose distributions (including the scaling factor μ) with the measurement results (symbols). For the 120 mm SOBP in Fig. 1a also the unscaled result is displayed as a dashed curve. The beam energies reported in Fig. 1 are taken from Kanai *et al.* (3) and are connected to the HIMAC irradiation system. At GSI, discrete numbers of pencil beams with different energies are superimposed to form the SOBP. The reconstructed SOBPs are therefore parameterized by the according SOBP depth (position of the distal end) also reported in the figure: 160 mm for panel a, 220 mm for panel b, and 275 mm for panel c.

For a given SOBP width w and depth h (distal end of the SOBP), the reconstructed physical dose distribution $D_{w,h}(z;10\%HSG)$ can now be used to convert between HIMAC- and LEM-based prescribed RBE-weighted doses, $d^{HIMAC}_{presc} \rightarrow d^{LEM}_{presc}$, by using TRiP98 and LEM to estimate the RBE-weighted dose distribution $D^{RBE}_{w,h}(z;d^{HIMAC}_{presc})$ connected with the physical dose distribution $D_{w,h}(z;d^{HIMAC}_{presc}) = \lambda^{HIMAC}_{presc} D_{w,h}(z;10\%HSG)$ (see Eqs. 1 and 4). The TRiP98 calculation and therefore also the actual mapping between d^{HIMAC}_{presc} and d^{LEM}_{presc} depends on the RBE table provided by LEM, *i.e.*, on the selected LEM version and more fundamentally on the underlying tissue type and biological endpoint.

$D^{RBE}_{w,h}(z;d^{HIMAC}_{presc})$ is not necessarily flat within the SOBP. In this study, we therefore calculated the median d^{LEM}_{median} of $D^{RBE}_{w,h}(z;d^{HIMAC}_{presc})$ across the SOBP as representative for d^{LEM}_{presc}. At GSI, an actual treatment plan parameterized by d^{LEM}_{presc} tries to realize a flat profile of the RBE-weighted dose inside the tumor. The clinical comparability of the treatment plans connected with d^{HIMAC}_{presc} and d^{LEM}_{presc} therefore depends on the homogeneity of $D^{RBE}_{w,h}(z;d^{HIMAC}_{presc})$. In addition to d^{LEM}_{presc}, we will therefore also report $D^{RBE}_{w,h}(z;d^{HIMAC}_{presc})$ at the proximal and distal end of the SOBP: d^{LEM}_{prox}, d^{LEM}_{dist}. To avoid instabilities due to slight oscillations at the proximal part of the dose distributions resulting from the optimization procedure, instead of the actual d^{LEM}_{prox}, in the Results section, we report the value found for a linear approximation of $D^{RBE}_{w,h}(z;d^{HIMAC}_{presc})$ restricted to the first third of the SOBP.

Impact of tissue characteristics

The actual mapping depends on the RBE tables derived from the measured photon responses by means of the LEM. We present results based on two RBE tables, both representing tissues with $\alpha/\beta = 2$ Gy as characteristic for late effects in the central nervous system. The first table was actually used during the clinical trials at GSI and was based on LEM I and $\alpha_{photon} = 0.1$ Gy^{-1}, $\beta_{photon} = 0.05$ Gy^{-2}, and $D_t = 30$ Gy. The second RBE table was derived according to LEM IV with $\alpha_{photon} = 0.0030$ Gy^{-1}, $\beta_{photon} = 0.0015$ Gy^{-2}, and $D_t = 22$ Gy. In addition to the LEM version here, the photon based tissue parameters were also updated to better reflect the differences in the order of magnitude of the LQ parameters between *in vitro* and clinical endpoints as discussed, for example, by Tai *et al.* (15).

Results

Shape of the RBE-weighted dose distributions

In Fig. 2, RBE-weighted dose profiles calculated by TRiP98 for three prescribed doses and both LEM versions are shown. For an improved visualization, only 120-mm SOBPs are displayed. In Fig. 2a results for LEM I are shown. Around 6 Gy (RBE), where the scaling factor λ^{HIMAC}_{presc} is approximately 1, the profile is nevertheless not flat but shows a slight depression at the distal end of the SOBP. This depression increases with increasing d^{HIMAC}_{presc}, but even for 10 Gy (RBE), the deviation from the intended flat profile can be considered moderate and the median should be a representative quantity to relate prescribed doses between NIRS and GSI: $d^{LEM}_{presc} \approx d^{LEM}_{median}$.

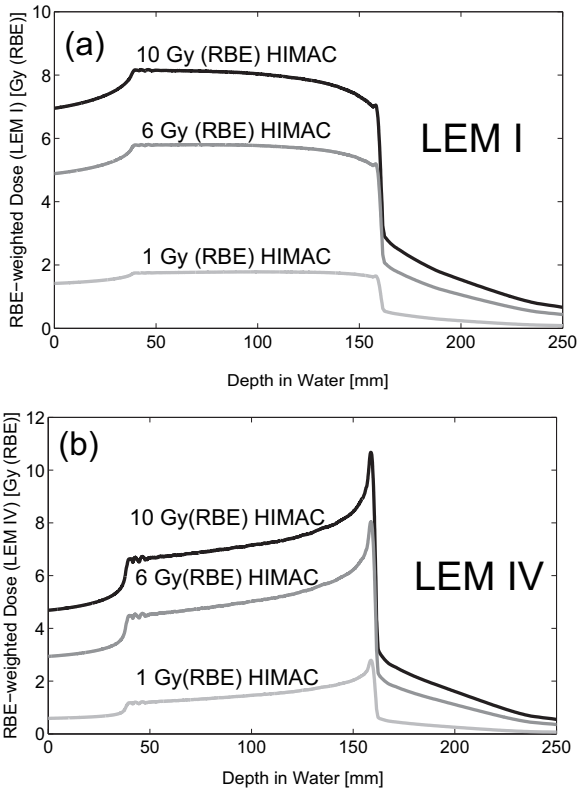

Fig. 2. RBE-weighted dose profiles for carbon ion irradiation calculated by TRiP98/LEM for three scalings $\lambda^{HIMAC}_{presc}(d^{HIMAC}_{presc})$ of the physical dose distribution of the 120-mm SOBP shown in Fig. 1b: $d^{HIMAC}_{presc} = 1$ Gy (RBE), 6 Gy (RBE), and 10 Gy (RBE). The conversion to LEM−based RBE-weighted doses depends on the underlying RBE tables: in panel a, the calculations are based on LEM I, and in panel b results for the same calculations based on LEM IV are shown. HIMAC = Heavy-Ion Medical Accelerator facility, National Institute of Radiological Science, Japan; LEM = Local Effect Model (versions I and IV); RBE = Relative Biological Effectiveness; SOBP = spread-out Bragg peak; TRiP98 = TReatment planning for Particles.

Figure 2b shows results based on LEM IV. The peak at the distal end of the SOBP can be explained by the use of the refined Local Effect Model, resulting in a more pronounced increase of the RBE-weighted dose with depth compared with LEM I. This was desirable because it was known that LEM I underestimates this gradient (5, 16).

Although the deviation from the flat distribution in the target is larger in Fig. 2b than in Fig. 2a, the median is still a reliable quantity for the description of the clinical effect of the irradiation. This has also been analyzed by calculating the corresponding equivalent uniform dose (EUD) (17). The deviation between EUD and median were typically found to be <5%. Only for very high dose levels and for LEM I, larger difference were observed (see Table 1). We therefore again assume $d^{LEM}_{presc} \approx d^{LEM}_{median}$.

Conversion factors

The conversion factors $d^{LEM}_{presc}/d^{HIMAC}_{presc}$ are shown as solid black curves in Fig. 3a and 3b for LEM I and LEM IV, respectively. They are close to 1 around $d^{HIMAC}_{presc} = 5$ Gy (RBE) and can be significantly higher at low doses and significantly lower at high doses. For both

Table 1 Comparison of median and EUD calculated for LEM estimated RBE-weighted dose distributions in dependence of prescribed HIMAC RBE-weighted doses, d_{presc}^{HIMAC}, for 60-mm SOBPs (depth according to Fig. 1b) and both RBE tables (LEM I/LEM IV)

Prescribed RBE-weighted dose HIMAC, Gy (RBE)	RBE-weighted dose LEM, Gy (RBE)			
	LEM IV		LEM I	
	Median	EUD	Median	EUD
1	1.65	1.73	1.76	1.74
2	2.65	2.76	2.80	2.78
3	3.46	3.59	3.64	3.61
4	4.17	4.31	4.37	4.33
5	4.81	4.97	5.03	4.98
6	5.41	5.58	5.64	5.58
7	5.98	6.15	6.22	6.15
8	6.52	6.70	6.77	6.69
9	7.04	7.23	7.30	7.20
10	7.54	7.73	7.81	7.70
20	12.08	12.26	12.32	11.92
30	16.14	16.31	16.33	15.30
40	20.07	20.15	20.14	18.18
50	23.95	23.95	23.82	20.81
60	28.06	27.97	27.44	23.30

Abbreviations: EUD = equivalent uniform dose; HIMAC = Heavy-Ion Medical Accelerator facility, National Institute of Radiological Science, Japan; LEM = Local Effect Model (versions I and IV); RBE = Relative Biological Effectiveness; SOBP = spread-out Bragg peak.

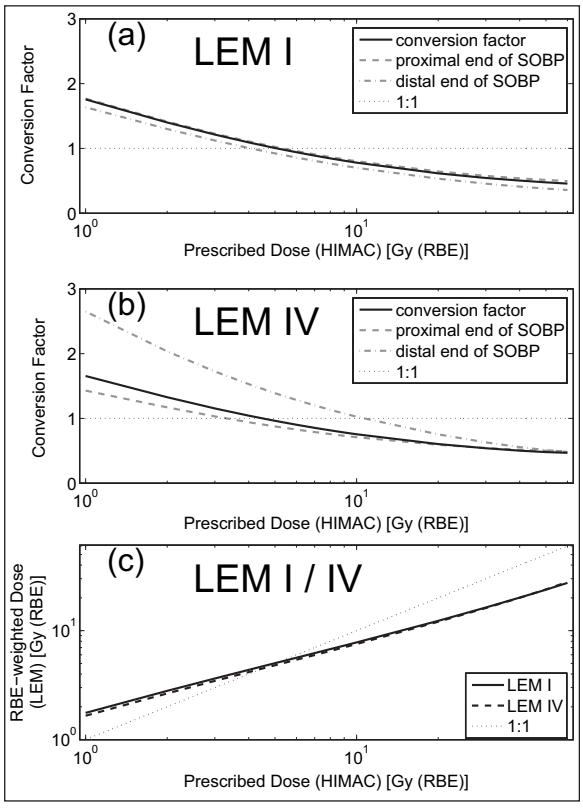

Fig. 3. Course of the mapping $d_{presc}^{HIMAC} \rightarrow d_{presc}^{LEM}$ for an SOBP width of 60 mm and a SOBP depth as in Fig. 1b for carbon ion irradiation. In panels a and b, conversion factors ($d_{presc}^{LEM}/d_{presc}^{HIMAC}$) for LEM I and LEM IV, respectively, are shown as solid curves. Absolute values (d_{presc}^{LEM}) for LEM I and LEM IV are compared in panel c. In addition to the abscissa, the ordinate is here logarithmic as well. The nearly linear course of the curves therefore shows that $d_{presc}^{HIMAC} \rightarrow d_{presc}^{LEM}$ can be approximated by a power law. In all figures, the $d_{presc}^{LEM} = d_{presc}^{HIMAC}$ relation is marked as dotted line. To visualize the deviation from the demanded flatness of the RBE-weighted dose distribution, the RBE-weighted doses found at the proximal (dashed curve) and distal end (dashed-dotted curve) of the SOBP are also shown (as relative values $d_{prox}^{LEM}/d_{presc}^{HIMAC}$ and $d_{dist}^{LEM}/d_{presc}^{HIMAC}$) in panels a and b. HIMAC = Heavy-Ion Medical Accelerator facility, National Institute of Radiological Science, Japan; LEM = Local Effect Model (versions I and IV); RBE = Relative Biological Effectiveness; SOBP = spread-out Bragg peak.

LEM versions, the conversion factor was monotonically decreasing with increasing d_{presc}^{HIMAC}. In Fig. 3c, LEM I and LEM IV are directly compared, but in contrast to panels a and b, absolute values, d_{presc}^{LEM}, are shown here. For LEM I, slightly larger d_{presc}^{LEM} were observed, but in general, the differences were found to be small. In addition, both curves appear as straight lines in the double-logarithmic plot. Therefore, at least for the presented RBE tables, $d_{presc}^{HIMAC} \rightarrow d_{presc}^{LEM}$ can be approximated by a power law, $d_{presc}^{LEM} \approx A \cdot (d_{presc}^{HIMAC})^{B}$, with only two needed parameters, A and B.

Homogeneity of the RBE-weighted dose distributions

Figures 3a and 3b additionally include the values found at the proximal and distal ends of the SOBPs as relative values ($d_{prox}^{LEM}/d_{presc}^{HIMAC}$, $d_{dist}^{LEM}/d_{presc}^{HIMAC}$). Absolute values for these quantities and numerical values for $d_{presc}^{LEM}/d_{presc}^{HIMAC}$ and d_{presc}^{LEM} are shown in Table 2. Consistent with Fig. 2a and 2b, the values for the proximal ends were found close to the median, whereas the deviations to the distal ends were significantly larger. Figure 3b shows even larger deviations from a homogeneous dose profile at the distal end than Fig. 3a. Consistent with Fig. 2b, this indicates relative high distal peaks found for lower d_{presc}^{HIMAC}. Differences between LEM I and LEM IV are also found toward very high doses, where the LEM IV curves converge, whereas LEM I curves run parallel. However, the values at high doses must be taken with some caution, because the LEM/TRiP98 predictions are based on an approximation where the β values of the dose−response curve are estimated from the effects of single particle traversals (10). This approximation is expected to be sufficiently accurate at least in the dose range below 10 Gy. A more detailed analysis of the quality of this approximation at high doses is currently under investigation (18). The courses of the LEM based RBE-weighted dose for $d_{presc}^{HIMAC} > 10$ Gy (RBE) may therefore be less exact than for the clinically more relevant lower doses.

Influence of the width of the SOBP

Figure 4 shows the conversion factor for different SOBP widths from 20 to 120 mm. At least for small dose levels, d_{presc}^{HIMAC}, the dependence on the SOBP width is significantly larger for LEM IV compared with LEM I. Whereas in Fig. 4a the dependence on the SOBP width slightly increases with increasing d_{presc}^{HIMAC}, we

Table 2 Numerical values according to Fig. 3

Prescribed RBE-weighted dose HIMAC, Gy (RBE)	RBE-weighted dose LEM, Gy (RBE)							
	LEM IV				LEM I			
	Proximal end of SOBP	Distal end of SOBP	Median across SOPB	Conversion factor	Proximal end of SOBP	Distal end of SOBP	Median across SOP	Conversion factor
1	1.4	2.7	1.7	1.65	1.8	1.6	1.8	1.76
2	2.3	4.1	2.7	1.33	2.8	2.6	2.8	1.40
3	3.1	5.2	3.5	1.15	3.7	3.4	3.6	1.21
4	3.8	6.1	4.2	1.04	4.4	4.0	4.4	1.09
5	4.4	6.9	4.8	0.96	5.1	4.6	5.0	1.01
6	5.0	7.7	5.4	0.90	5.8	5.2	5.6	0.94
7	5.5	8.4	6.0	0.85	6.4	5.7	6.2	0.89
8	6.1	9.1	6.5	0.81	6.9	6.1	6.8	0.85
9	6.6	9.7	7.0	0.78	7.5	6.6	7.3	0.81
10	7.1	10.3	7.5	0.75	8.0	7.0	7.8	0.78
20	11.8	15.1	12.1	0.60	12.9	10.6	12.3	0.62
30	16.3	18.9	16.1	0.54	17.3	13.7	16.3	0.54
40	20.6	22.2	20.1	0.50	21.5	16.4	20.1	0.50
50	25.0	25.5	23.9	0.48	25.7	19.0	23.8	0.48
60	29.6	28.9	28.1	0.47	29.7	21.5	27.4	0.46

Abbreviations: HIMAC = Heavy-Ion Medical Accelerator facility, National Institute of Radiological Science, Japan; LEM = Local Effect Model (versions I and IV); RBE = Relative Biological Effectiveness; SOBP = spread-out Bragg peak.

observed a significant decrease of the dependence on the SOBP width in Fig. 4b. Similar to the findings in Fig. 3b, in the latter case, we found a minimum for the deviation between the curves at a higher d_{presc}^{HIMAC}, here around 30 Gy (RBE), followed by a slow increase. The dependence of the conversion factor from the SOBP width can be explained by the inhomogeneity of the RBE-weighted dose within the SOBP. Because the inhomogeneity is mainly caused by the distal end of the SOBP and this part is shared by all SOBP widths, the mainly inhomogeneous fraction of the SOBP is included in each of the different SOBPs, but the contribution of the more homogeneous fraction (found upstream) increases with increasing width.

Influence of the depth of the SOBP

In Figs. 2–4, the depths of the SOBPs were selected according to Fig. 1b. For the depths shown in Figs. 1a and c, the results are only slightly different. For d_{presc}^{HIMAC} from 1 Gy (RBE) to 60 Gy (RBE) and an SOBP width of 60 mm, we found a maximum difference between the conversion factors with respect to the SOBP depths of 0.015 for LEM I and 0.075 for LEM IV, which is 6–8 times smaller compared with the maximal deviations found in Fig. 4a and 4b, respectively.

Discussion

In this article, we presented a method to convert clinically prescribed RBE-weighted doses from the HIMAC/NIRS approach to the LEM-based TRiP98 approach, which is in use in the pilot project at GSI and at HIT, as well as in upcoming facilities in Marburg, Kiel, Pavia, and Shanghai. For the interpretation and comparison of clinical trials performed at HIMAC and GSI/HIT, it turned out to be of extreme importance to consider the presented conversion factors because, given the different methods to determine the RBE-weighted dose, similar dose values might not necessarily result in similar clinical outcomes.

We presented data according to the clinical studies conducted at GSI in the past decade (LEM I) as well as data currently in validation for clinical studies (LEM IV). Because fixed depth-dose profiles are used, the resulting RBE-weighted dose profiles in the target region can deviate from the ideally flat profile (up to 60% deviation between peak at distal end and median dose for low dose levels and LEM IV), and details of the deviation depend on the dose level and the biological/clinical effect under consideration. Furthermore, the predicted deviation depends on the model version; because in general the depth-dependent gradient of RBE was underestimated with LEM I, the deviations from the ideally flat RBE-weighted dose profile are also less pronounced for this model version. Nevertheless, in the scope of the EUD description, the inhomogeneities of the RBE-weighted dose profiles were found to have no significant impact on the resulting biological effects. Moreover, we could show that the effect of the remaining inhomogeneities is mapped to the dependence of the conversion factor on the width of the underlying SOBPs.

The conversion factor reaches from 0.4 to 2.0 for prescribed RBE-weighted doses (HIMAC) ranging from 1 to 60 Gy (RBE). For both, LEM I and LEM IV, the conversion factor decreases monotonically with increasing prescribed dose, but slightly smaller values for the data set based on the LEM IV compared with LEM I were observed. $d_{presc}^{LEM} \approx d_{presc}^{HIMAC}$ could be found around 5 Gy (RBE). For lower doses, a conversion factor above, and for higher doses below, 1.0 was found. In the pilot project, an RBE-weighted dose of 3 Gy (RBE) per fraction (20 fractions) was used, corresponding to a conversion factor of approximately 1.2. However, because there is a clear trend toward lower fraction numbers in the clinical trials at HIMAC, the conversion factors will be considerably lower for hypofractionation studies using, *e.g.*, four fractions or even only a single fraction. For these cases, conversions factors might be as low as 0.5.

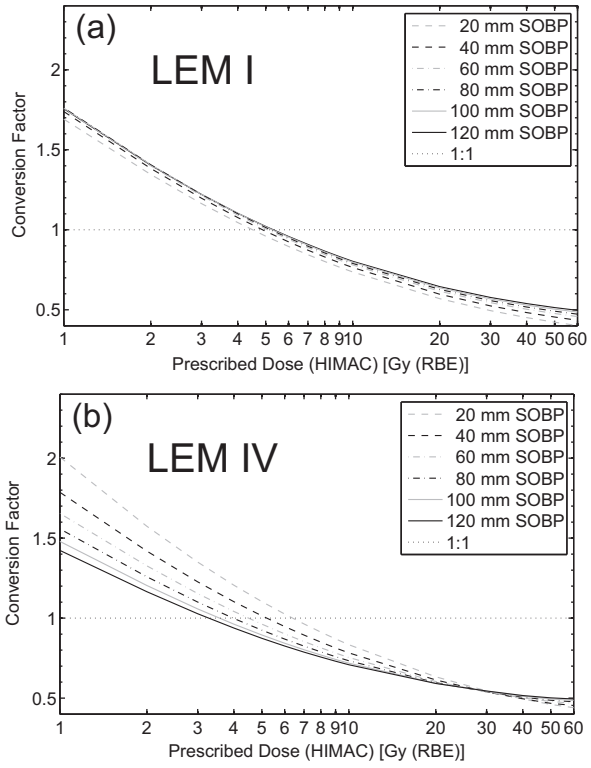

Fig. 4. Conversion factors, $d_{presc}^{LEM}/d_{presc}^{HIMAC}$, in dependence of d_{presc}^{HIMAC} for SOBPs from 20 to 120 mm (depth as in Fig. 1b) for carbon ions. a, results for LEM I; b, results for LEM IV. The $d_{presc}^{LEM} = d_{presc}^{HIMAC}$ relation is marked as dotted line. LEM = Local Effect Model (versions I and IV); SOBP = spread-out Bragg peak.

The conversion factor depends on tissue and endpoint. The results shown here must therefore be considered specific to the tissue parameters and corresponding RBE tables discussed in this article. Similar analyses will thus be carried out for other LEM-based RBE tables as soon as they are considered for clinical implementation. It is expected that the curves shown in Figs. 3 and 4 shift to the left for tissues with α/β ratios <2, because according to the general trend, the corresponding RBE predicted by the LEM will be lower. However, the main trend that the conversion factors are >1 at low doses per fraction and <1 at very high doses per fraction will be unaffected.

It will then also be of interest in how far a simple power-law representation, as given for the results in Fig. 4, will be applicable for other endpoints. If this is found to be feasible, it will allow easy implementation of this type of conversion factor and serve as a guideline for comparability in treatment planning procedures without the need to run elaborate alternative treatment planning programs. Furthermore, the method can easily be extended to other models, allowing calculating clinically applicable RBE distributions in SOBPs such as, *e.g.*, the MKM (Microdosimetric Kinetic Model), which is currently being investigated for implementation in treatment planning (14). On this basis, a lookup table-based system can be established to easily convert RBE-weighted doses from one system to another and thus support clinicians in comparison of clinical data obtained at different institutions with different approaches for treatment planning. In the same way, the impact of possible additional improvements of the LEM can be assessed.

References

1. Tsujii H, Mizoe J, Kamada T, *et al*. Clinical results of carbon ion radiotherapy at NIRS. *J Radiat Res* 2007;48(Suppl. A):A1−A13.
2. Schulz-Ertner D, Karger CP, Feuerhake A, *et al*. Effectiveness of carbon ion radiotherapy in the treatment of skull-base chordomas. *Int J Radiat Oncol Biol Phys* 2007;68:449−457.
3. Kanai T, Endo M, Minohara S, *et al*. Biophysical characteristics of HIMAC clinical irradiation system for heavy-ion radiation therapy. *Int J Radiat Oncol Biol Phys* 1999;44:201−210.
4. Scholz M, Kellerer AM, Kraft-Weyrather W, *et al*. Computation of cell survival in heavy ion beams for therapy. The model and its approximation. *Radiat Environ Biophys* 1997;36:59−66.
5. Elsässer T, Scholz M. Cluster effects within the local effect model. *Radiat Res* 2007;167:319−329.
6. Elsässer T, Krämer M, Scholz M. Accuracy of the local effect model for the prediction of biologic effects of carbon ion beams in vitro and in vivo. *Int J Radiat Oncol Biol Phys* 2008;71:866−872.
7. Elsässer T, Weyrather WK, Friedrich T, *et al*. Quantification of the relative biological effectiveness for ion beam radiotherapy: Direct experimental comparison of proton and carbon ion beams and a novel approach for treatment planning. *Int J Radiat Oncol Biol Phys* 2010; 78:1177−1183.
8. Kanai T, Matsufuji N, Miyamoto T, *et al*. Examination of GyE system for HIMAC carbon therapy. *Int J Radiat Oncol Biol Phys* 2006;64: 650−656.
9. Krämer M, Jäkel O, Haberer T, *et al*. Treatment planning for heavy-ion radiotherapy: Physical beam model and dose optimization. *Phys Med Biol* 2000;45:3299−3317.
10. Krämer M, Scholz M. Treatment planning for heavy-ion radiotherapy: Calculation and optimization of biologically effective dose. *Phys Med Biol* 2000;45:3319−3330.
11. Krämer M, Scholz M. Rapid calculation of biological effects in ion radiotherapy. *Phys Med Biol* 2006;51:1959−1970.
12. Astrahan M. Some implications of linear-quadratic-linear radiation dose-response with regard to hypofractionation. *Med Phys* 2008;35: 4161−4172.
13. Uzawa A, Ando K, Koike S, *et al*. Comparison of biological effectiveness of carbon-ion beams in Japan and Germany. *Int J Radiat Oncol Biol Phys* 2009;73:1545−1551.
14. Inaniwa T, Furukawa T, Kase Y, *et al*. Treatment planning for a scanned carbon beam with a modified microdosimetric kinetic model. *Phys Med Biol* 2010;55:6721−6737.
15. Tai A, Erickson B, Khater KA, *et al*. Estimate of radiobiologic parameters from clinical data for biologically based treatment planning for liver irradiation. *Int J Radiat Oncol Biol Phys* 2008;70:900−907.
16. Wilkens JJ, Oelfke U. Direct comparison of biologically optimized spread-out Bragg peaks for protons and carbon ions. *Int J Radiat Oncol Biol Phys* 2008;70:262−266.
17. Niemierko A. Reporting and analyzing dose distributions: A concept of equivalent uniform dose. *Med Phys* 1997;24:103−110.
18. Friedrich T, Scholz U, Elsässer T, *et al*. Calculation of the biological effects of ion beams based on the microscopic spatial damage distribution pattern. *Int J Radiat Biol* 2012;88:103−107.

IOP Publishing Physics in Medicine and Biology

Phys. Med. Biol. **58** (2013) 6827–6849 doi:10.1088/0031-9155/58/19/6827

Sensitivity analysis of the relative biological effectiveness predicted by the local effect model

T Friedrich[1], **R Grün**[1,2,3], **U Scholz**[1,4], **T Elsässer**[1,5], **M Durante**[1,4] **and M Scholz**[1]

[1] GSI Helmholtzzentrum für Schwerionenforschung, Darmstadt, Germany
[2] Medizinische Fakultät, Philipps-Universität Marburg, Marburg, Germany
[3] Institut für Medizinische Physik und Strahlenschutz, TH Mittelhessen, Gießen, Germany
[4] Institut für Festkörperphysik, TU Darmstadt, Darmstadt, Germany

E-mail: t.friedrich@gsi.de

Received 26 April 2013, in final form 5 July 2013
Published 11 September 2013
Online at stacks.iop.org/PMB/58/6827

Abstract

The relative biological effectiveness (RBE) is a central quantity in particle radiobiology and depends on many physical and biological factors. The local effect model (LEM) allows one to predict the RBE for radiobiologic experiments and particle therapy. In this work the sensitivity of the RBE on its determining factors is elucidated based on monitoring the RBE dependence on the input parameters of the LEM. The relevance and meaning of all parameters are discussed within the formalism of the LEM. While most of the parameters are fixed by experimental constraints, one parameter, the threshold dose D_t, may remain free and is then regarded as a fit parameter to the high LET dose response curve. The influence of each parameter on the RBE is understood in terms of theoretic considerations. The sensitivity analysis has been systematically carried out for fictitious *in vitro* cell lines or tissues with $\alpha/\beta = 2\,\mathrm{Gy}$ and 10 Gy, either irradiated under track segment conditions with a monoenergetic beam or within a spread out Bragg peak. For both irradiation conditions, a change of each of the parameters typically causes an approximately equal or smaller relative change of the predicted RBE values. These results may be used for the assessment of treatment plans and for general uncertainty estimations of the RBE.

(Some figures may appear in colour only in the online journal)

[5] Now working at Siemens Healthcare.

1. Introduction

The RBE is used to quantify the enhanced effect of ion beams in comparison to low LET radiation such as x-rays or gamma rays. For applications in radiobiologic research as well as in ion radiotherapy the precise characterization of RBE is of importance. Many experimental and clinical studies have been carried out to reveal the RBE under various conditions (Ando and Kase 2009, Gerweck and Kozin 1999, Friedrich *et al* 2013). However, as the RBE depends on several factors whose versatile combinations cannot be investigated solely by experiments, models for predicting the RBE have been developed. The LEM in its original version (LEM I) (Scholz *et al* 1997) and the microdosimetric kinetic model (MKM) (Hawkins 1994, 1996) are currently the only ones used for clinical treatment planning. Within the recent years, the LEM has been gradually improved (Elsässer and Scholz 2007, Elsässer *et al* 2008). The latest version LEM IV (Elsässer *et al* 2010, Friedrich *et al* 2012b) comprises a mechanistic interpretation on the level of double strand break (DSB) induction. This allowed one to significantly improve the accuracy to model the RBE for all therapy relevant ions and energies with *one unique* set of necessary parameters which have been fixed once for all model calculations. As their values, as well as other experimental parameters (e.g. those specifying the tissue considered), are associated with uncertainties the question arises how these translate into uncertainties of the predicted RBE. Hence, for applications in radiobiology and in the clinics it is of interest to quantify the consequence of a change of each input parameter for the RBE. The rates of RBE change will reflect themselves in the robustness of treatment plans for ion beam therapy.

This paper is dedicated to the sensitivity analysis of RBE, obtained by a systematic variation of parameters used within the LEM IV. The strategy is to carry out the analysis in a very systematic way, where at first all parameters are inspected and classified, then their relevance is quantitatively investigated for monoenergetic beams as well as for extended irradiated volumes[6]. This strategy finally allows one to understand the parameter sensitivity based on the physical or biological meaning of the parameter under consideration and to compare the expectations for RBE uncertainty for the different ways of beam delivery. Our approach is complementary to a recent publication (Böhlen *et al* 2012), where the authors investigated the parameter influence on RBE for extended targets and in detail discuss possible implications for ion beam therapy.

The parameters needed for calculating RBE values with LEM may be subdivided according to the model parts they are used in:

- specification of the physical aspects of track structure
- specification of the initial DNA damage distribution
- characterization of the cell and DNA conformation geometry
- characterization of the photon dose response curve.

In section 2 the basic principles of the LEM are revisited and the parameters needed for RBE calculations are introduced. The relevant parameters for LEM calculations are classified and discussed in section 3. The parameter sensitivity of the RBE values for monoenergetic beams is presented in section 4. Section 5 is dedicated to the same analysis for a clinical situation, where a SOBP is optimized in such a way that a homogenous distribution of the RBE-weighted dose covers the target volume. Finally, the results are discussed and conclusions are drawn in section 6.

[6] Throughout the paper with monoenergetic beams we understand that the samples are irradiated under track segment conditions, i.e. that energy and LET do not change along an ion track through a cell nucleus.

2. Conceptual basis of the LEM

The LEM bases on the assumptions that the nuclear DNA is the unique sensitive part of the cell to radiation, that DSB are the most relevant lesions, and that the radiation damage on a molecular level is predominantly mediated by secondary electrons and hence only depends on the local distribution of these secondaries. This includes the implicit assumption that for all radiation qualities the spectra of the slowing down secondary electrons are similar. The main idea is then to trace back the effect of ions to the effect of photons inducing locally a similar pattern of initial damage.

In a first step, ions are assumed to pass through the cell nucleus, in which the DNA is assumed to be distributed homogenously. Practically, for most applications we restrict here to one single ion passing right through the centre of the cell nucleus. This allows one to assess the effect of exactly one ion, from which the effect of a distribution of ions can be derived as outlined in (Scholz *et al* 1997). A Monte Carlo simulation of the full spatial dose distribution of a distribution of ions has also been implemented in LEM (Friedrich *et al* 2012b), but is not used for this study for the sake of computation time. We checked that this so called single particle approximation is valid up to several Gy and hence can be used for normal fractionated radiotherapy. Furthermore track segment conditions are required, i.e. the particles show no significant change of kinetic energy or LET along their way through the nucleus. According to their track structure a local dose deposition is converted into a damage pattern of DSB distributed within the nucleus. The local rate for the induction of initial DSB is proportional to the local dose in each location within the track. The proportionality factor is the DSB yield as measured in experiments with low LET radiation. In addition to these DSB, further DSB arise due to neighbouring single strand breaks (SSB) on opposite DNA strands combining to a full break of the DNA double strand (Elsässer and Scholz 2007), resulting in an overall RBE for DSB induction greater than one. In the implementation the simulation of the damage patterns is performed by means of a Monte Carlo routine simulating many cells, each being affected by one spatial DSB distribution. The procedure is stopped when the number of Monte Carlo runs is sufficient to finally determine the effect of ions within a requested accuracy.

In a second step the initial damage distribution is converted into a distribution of isolated or clustered DSBs, where the classification is defined based on the picture of a hierarchical compartmented organization of chromatin into DNA giant loops (Yokota *et al* 1995) of some Mbp size, corresponding to the micrometer length scale. The relevance of such a length scale is known since a long time in radiobiology (Neary *et al* 1959, Rossi and Zaider 1996, Goodhead 2006) and thus supportive for this conception, though its interpretation in terms of DNA conformation is under continuous debate. It is suggestive to assume that lesions can interact if they were induced in the same DNA loop, while lesions in different chromatin domains are processed independently. Consequently, the model distinguishes between domains without any DSB, with exactly one DSB (called isolated DSB), or with more than one DSB (called clustered DSB). Note that this term is not uniquely defined and used for different constellations of lesions by different authors. All definitions, however, have in common that the term means an accumulation of lesions (at least one of which is a DSB) in close neighbourhood. Indeed it is known that isolated DSB can be repaired quite efficiently by the repair mechanism of a cell, while complex damage is believed to have a higher impact on cell killing, supporting the assumption used in LEM, that the fraction of complex damage is a determining factor for the RBE.

In the third step a photon dose causing the same proportion of isolated to clustered DSBs is evaluated. The effect corresponding to that photon equivalent dose is obtained from the photon dose response curve. As for this case the local damage pattern of ion and photon irradiation

Table 1. Overview over the parameters of the LEM, classified in groups corresponding to different stages of a LEM model calculation. One can distinguish specific parameters which specify the situation to be modelled, and general parameters which have been obtained by measurements, fitted to reference data or estimated by theoretic considerations. For general parameters, the values used are given, and their origin is indicated.

Parameter class	Parameter	Type	Value	Origin
Track structure	γ	General	0.062	Measured[a]
	δ	General	1.7	Measured[a]
	r_c	General	6.5 nm	Fit + theoretic arguments[b]
	σ	General	4 nm	Theoretic arguments[a]
	E	Specific		
	LET	Specific		
Initial DNA damage	α_{DSB}	General	$30\,\mathrm{Gy}^{-1}$	Measured[a]
	α_{SSB}	General	$1250\,\mathrm{Gy}^{-1}$	Measured[a]
	h	General	25 bp	Measured[a]
	L_{Gen}	Specific		
Cell nuclear geometry	V_n	Specific		
	r_n	Specific		
	l_{DSB}	General	540 nm	Fit[b]
Photon dose response curve	α	Specific		
	β	Specific		
	D_t	Specific		

[a] See (Elsässer and Scholz 2007) and references therein.
[b] See (Elsässer *et al* 2010) and references therein.

is comparable, the effect of ions can be calculated by a proper normalization from the photon effect, and all related quantities such as the RBE are obtained easily. For a mathematical precise formulation of the LEM we refer to (Friedrich *et al* 2012b).

Note that in this general formulation up to this point no specific endpoint is considered. The LEM is appropriate for any endpoint as long as the effect is mediated primarily by the induction of DSB to DNA loops or correlating strongly with it. The difference in RBE between different endpoints originates from different associated photon dose response curves. The most prominent endpoints to which the LEM was applied up to now are cell survival for cell culture experiments and tumour control as well as normal tissue complication in carbon ion cancer therapy or *in vivo* experiments (Elsässer *et al* 2010, Scholz and Elsässer 2007, Grün *et al* 2012).

3. Parameters of the LEM

Calculating the effect of an ion impact from a photon equivalent situation requires knowledge or modelling of (i) physical properties of the ions, (ii) factors determining the DNA damage induction rates, (iii) geometric properties of the cellular nucleus and the chromatin, and (iv) the photon dose response for the endpoint under consideration. The relevant parameters are summarized in table 1 according to this classification, and their meaning will be discussed below.

Some of the parameters have been fixed once, because there is no evidence for any dependence on e.g. cell type or ion species. Their values are used for all simulations and have been either extracted from experimental results, derived by theoretic arguments, or fixed by fitting the LEM predictions to a reference set of experimentally obtained RBE data (Furusawa *et al* 2000, Suzuki *et al* 2000). They are marked with *general* in table 1 and listed along with their attributed values. All other parameters, marked as *specific* parameters, specify the experiment or clinical situation to be modelled, i.e. they characterize the cell- or tissue type

and their radiation response, define the particle species used and the energy. The distinction of general and specific input parameters of the LEM is used throughout this publication.

Note that both general and specific parameters are associated with uncertainties. For some parameters these are quite large (some ten per cents), e.g. for the radical diffusion length σ or the yield parameters α_{DSB} and α_{SSB}. However, as two general parameters, the giant loop domain size for DSB interaction l_{DSB} and the maximum inner core radius r_c, have been fixed by a fit to RBE reference data sets, the fitted parameters calibrate the model and compensate for uncertainties in the others, and therefore the uncertainties of the general parameters do not propagate to the uncertainty of the RBE. This compensation is not mathematically strict, and there might be combinations of all parameters where this procedure of calibrating the LEM model might fail, leading to systematic errors in RBEs. However, some systematic errors in the RBE predictions are only detected at low LET values, while mostly RBE predictions are reasonably correct. This strongly suggests that the model set-up and the chosen parameters are sufficiently accurate, which implies that the compensation of parameter errors works good enough to predict RBEs correctly. Moreover this is supported by the values of the two fitted parameters which are in agreement with theoretical expectations (nm range for r_c and μm range for l_{DSB}). As a consequence of the compensation of parameters, for an uncertainty analysis of RBE primarily the specific parameters characterizing an experiment or a clinical case are of relevance.

Using the set of parameters as listed in table 1 in LEM IV allows one to simulate RBE for a wide range of LET and for all therapy relevant ion species from protons to carbon in reasonable agreement with experimentally or clinically evaluated RBE values (Grün *et al* 2012). The different groups of relevant parameters needed for a LEM calculation are addressed in the following point by point.

3.1. Physical parameters of beam and track structure

The incident particle is characterized by a kinetic energy per nucleon, E, and a corresponding LET for a given particle species. Here energy and LET are determined within the cellular nucleus. The LEM assumes that the LET does not change considerably along a passage of an ion through the nucleus. If track segment conditions are violated, deviations between LEM and experimental data may occur.

Microscopically the energy is transferred from the ion to the surrounding matter in point-like ionization events. For many purposes it is sufficient to use the average dose distribution pattern around the central axis of a passing ion. This parametrization of the energy loss of particles in matter is commonly referred to as amorphous track structure (Cucinotta *et al* 1999). Note that the concept of dose used here is a local dose, being proportional to a probability density function for finding an ionization. In our implementation we follow the amorphous track structure model according to (Elsässer *et al* 2008), where the track structure consists of an inner core with a constant dose up to an energy dependent radius which is parameterized by $r_{\mathrm{min}} = \beta_{\mathrm{ion}} r_c$ with $\beta_{\mathrm{ion}} = v/c$, particle velocity v and velocity of light c. Its maximum value, $r_c = 6.5$ nm was adequately chosen in (Elsässer *et al* 2010) to fit experimental data and matches the order of magnitude expected from theoretic considerations perfectly (Mozumder 2007).

Beyond r_{min} the local dose falls off quadratically up to a maximum radius $r_{\mathrm{max}} = \gamma E^{\delta}$, where r_{max} is given in microns and E in MeV per nucleon. The parameters γ and δ have been derived by a fit to experimental data obtained in experiments using tissue equivalent proportional counters (Kiefer and Straaten 1986). In this work there is no analysis of involved uncertainties given, but it is evident that the uncertainties of γ and δ are smaller than their values, but larger than on the per cent level. Below an energy of 2 MeV u^{-1} this parametrization

does not resemble the measured doses with sufficient accuracy. Here, values different from those in table 1 are used ($\gamma = 0.124$ and $\delta = 0.7$). As the remaining range of particles of such small energy is very limited and track segment conditions might be violated, the accuracy of RBE predictions might be questionable, but for the same reason their importance within a SOBP is low.

It is known that an essential fraction of lesions is induced by an indirect effect, i.e. by free radicals which have been produced by secondary electrons. To account for this, the initial dose distribution according to the parametrization discussed previously is convoluted with a radial Gaussian of width $\sigma = 4$ nm, modelling an effective diffusion of free radicals. The value of σ was fixed in (Elsässer *et al* 2008) and is in agreement with diffusion lengths calculated by Monte Carlo codes (Nikjoo *et al* 1997, Moiseenko *et al* 2001). Here it is important to note that LEM follows an effective approach: as different radical species have different mean free path lengths, its uncertainty on the nm scale is given by the corresponding wide spread of different radical diffusion lengths.

3.2. Parameters for damage induction to the DNA

The crucial initial lesions of interest in the LEM are DSBs. Several experiments show that for photons the initial DSB yield is $\alpha_{\mathrm{DSB}} \approx 30\,\mathrm{Gy}^{-1}$ per cell for a DNA content $L_{\mathrm{Gen}} = 5.4 \times 10^9$ bp as typical for rodents (Prise *et al* 2001, Stenerlöw *et al* 2003). This DSB yield refers to the initial induction of DSB and is observed experimentally with low LET radiation. Likewise, experiments showed that the yield SSB is $\alpha_{\mathrm{SSB}} \approx 1250\,\mathrm{Gy}^{-1}$.

It is well accepted that SSB can be repaired effectively. However, for high LET radiation two SSB in close vicinity on opposite strands may combine and form an additional DSB. Hence the number of initial DSB calculated from α_{DSB} is enhanced. This amplification is explicitly modelled within the LEM. A fixed threshold of $h = 25$ bp for the maximum interaction length of SSB is used in our implementation, in agreement with experimental results using plasmids (Shao *et al* 1999), see (Elsässer and Scholz 2007) for a more detailed discussion. While it is negligible for photon irradiation, for high LET radiation qualities this effect can enhance the DSB yield up to one order of magnitude, depending on particle species, LET and genomic length (Elsässer and Scholz 2007). Concerning the uncertainties of the parameters for damage induction, in the literature typically values of 20–40 DSB and 1000–1500 SSB per cell and Gy are discussed in the literature. For the distance threshold h a huge span of 3–60 bp is reported in the literature. This motivates a reasonable fixation to 25 bp.

3.3. Parameters of the cell nucleus geometry

We assume that the DNA content of the cell is uniformly distributed in a cylindrical cell nucleus, specified by parameters for the volume of the nucleus, V_n and its radius, r_n. The impinging particles are assumed to hit the nucleus in direction of the symmetry axis of the nucleus. Note that the height of the nucleus is uniquely fixed by the two geometry parameters. Distributions of nuclear sizes are discarded up to now.

To model chromatin loop domains a three-dimensional rectangular grid is superimposed on the cell nucleus. The boxes of the grid resemble the domains in which DSBs are counted. They have equal side lengths of $l_{\mathrm{DSB}} = 540$ nm. This length was determined by a fit to survival data of Furusawa and coworkers (Furusawa *et al* 2000), and is in agreement with the typical interaction length scale derived from microdosimetric considerations (Goodhead 2006). The parameter l_{DSB} thus determines the interaction lengths of distant DSB and fixes the proportion of isolated and clustered DSB for a given dose and radiation quality.

3.4. Photon dose response parameters

Within the LEM usually the linear-quadratic (LQ) model is used, in which the effect is given by $\alpha D + \beta D^2$ with photon dose D and linear and quadratic coefficient parameters α and β. The choice of the LQ model is somewhat arbitrary but convenient, as for almost all *in vitro* and *in vivo* data as well as for most clinical reports on radiation effects are characterized in terms of this model (Friedrich *et al* 2013, Ando and Kase 2009, Steel and Peacock 1989, Fertil and Malaise 1985).

At high doses, however, it becomes more and more evident that the LQ model loses validity, as the dose response tends towards a pure linear component. This is suggested by theoretic considerations of the repair dynamics of the cell (Curtis 1986, Tobias 1985) as well as by experimental findings from both *in vitro* (Astrahan 2008, Garcia *et al* 2007, Fertil *et al* 1994) and *in vivo* experiments (Guerrero and Li 2004, Carlone *et al* 2005). In the LEM we model the different properties of the dose response curves at low and high doses by a instantaneous transition from an LQ to a linear dose response at the transition dose D_t. Then the main principle of the LEM is the mapping of the damage pattern caused by ions to a damage pattern as induced by photons. For regions of high local doses, photon irradiation will induce comparable damage patterns at doses above D_t, and hence D_t is an important parameter for RBE calculations. There are three distinct ways of asserting a numerical value to it: One can extract it from measurements, if the photon dose response curve is available to sufficient high doses. Alternatively an empirical linear relationship between D_t and α/β exists, which can serve to estimate D_t (Friedrich *et al* 2013). If one proceeds (and only if) along these ways, the LEM is free of any specific fit parameters. However, if both of these procedures are not applicable or affected with unacceptable accuracy (e.g. when the photon dose response parameters are only known within a limited low dose range), the parameter must be fitted individually to experimental high LET data from the cells or tissues under investigation.

4. Sensitivity analysis for irradiation with monoenergetic ion beams under track segment conditions

In this section the change of RBE-LET relationships for cells or tissues irradiated with a monoenergetic ion beam due to parameter variation is investigated. The results can be used to estimate the influence of parameter uncertainties on the RBE for radiobiological experiments mimicking aspects of carbon radiotherapy in the different situations with monoenergetic beams in track segment conditions. They might also be useful to understand differences in RBE values if calculated for or measured with different cell lines under comparable conditions.

Both the RBE at full survival (RBE_α) and at 10% survival level (RBE_{10}) are considered as a function of the LET. The simulations have been performed for carbon ions and two hypothetic cell- or tissue types, characterized by $\alpha/\beta = 2\,\mathrm{Gy}$ and $\alpha/\beta = 10\,\mathrm{Gy}$. The general strategy of the sensitivity analysis is to calculate for each parameter listed in table 1 (except energy and LET) three RBE-LET relationships, one for a designed value of that parameter and the other two obtained by increasing or decreasing this parameter by 25% of its initial value[7].

In particular we chose $\alpha = 0.1\,\mathrm{Gy}^{-1}$, $\beta = 0.05\,\mathrm{Gy}^{-2}$ and $D_t = 8\,\mathrm{Gy}$ as design parameters for $\alpha/\beta = 2\,\mathrm{Gy}$ and $\alpha = 0.5\,\mathrm{Gy}^{-1}$, $\beta = 0.05\,\mathrm{Gy}^{-2}$ and $D_t = 14\,\mathrm{Gy}$ for $\alpha/\beta = 10\,\mathrm{Gy}$.

[7] We chose here the reference change of 25% for all parameters to allow for an inter-comparison of the sensitivity on the RBE determining parameters. Moreover, 25% resemble the order of magnitude of the uncertainties of the input parameters, as none of the parameters is known to per cent accuracy, but also the uncertainties typically do not exceed some ten per cents. A mathematical, more rigorous treatment would require one to consider the differential expressions $\mathrm{dRBE}/\mathrm{d}x$ for any parameter x.

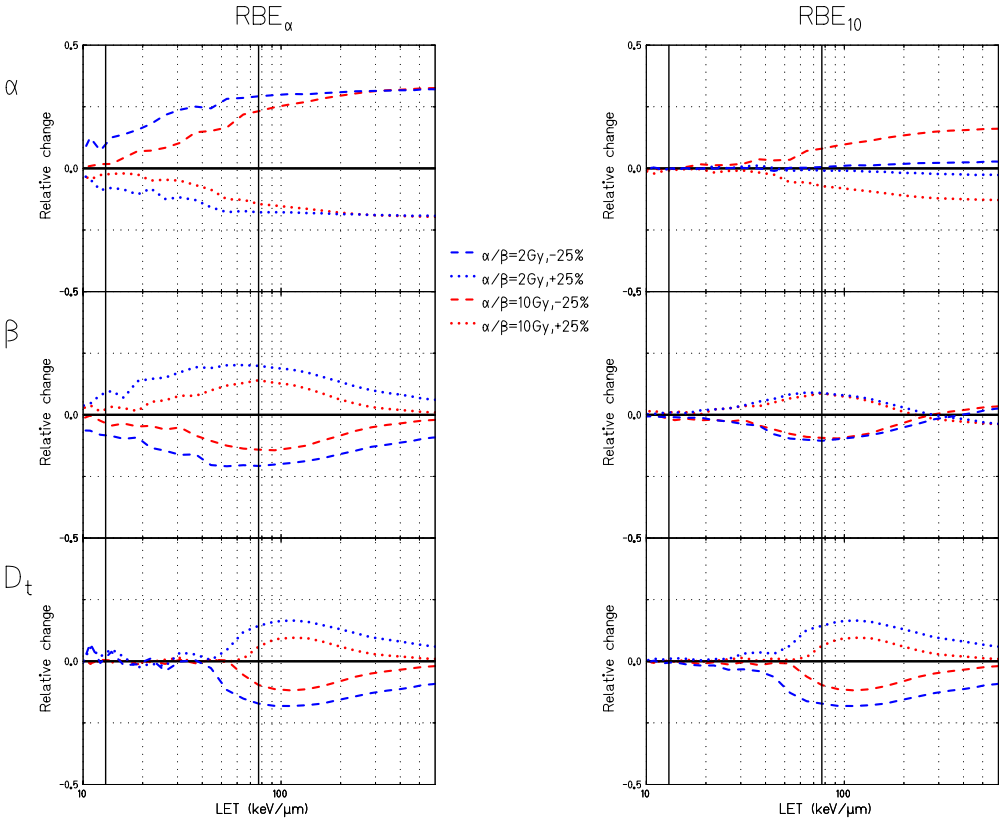

Figure 1. Relative change of RBE_α (left) and RBE_{10} (right) over LET for carbon ions and cells or tissues on the photon parameters for $\alpha/\beta = 2\,\mathrm{Gy}$ (blue) and $\alpha/\beta = 10\,\mathrm{Gy}$ (red). The horizontal axis corresponds to the RBE at the design parameters (see text), and the dashed and dotted curve emerge by decreasing or increasing the specific parameter about 25%, respectively. The vertical lines indicate the LET values of 13 and 77 keV $\mu\mathrm{m}^{-1}$ used in table 2.

These parameter settings are typical for *in vitro* cell survival assays (Friedrich *et al* 2013). The parameter D_t was adapted according to an empirical relation between α/β and D_t. This linear relation was found when using the LEM over a huge set of experimental cell survival data (Friedrich *et al* 2013), and is in agreement with experimental findings (Astrahan 2008). The geometric specific parameters for both cases were chosen $V_n = 500\,\mu\mathrm{m}^3$ and $r_n = 5\,\mu\mathrm{m}$. Again, these parameters approach typical values for mammalian cell lines.

For all combinations of effect levels for which the RBE is evaluated (RBE_α or RBE_{10}) and for both α/β ratios (2 Gy or 10 Gy), we obtained for each parameter a band in the RBE-LET characteristics which describes the variability of RBE under variation of $\pm 25\,\%$ of this parameter[8]. In all cases but one, sensitivity was investigated by varying one single parameter. As an exception, for a change of the parameter V_n we also changed l_{DSB} as a second parameter in order to keep the number of chromatin loops within the cell nuclei constant. Figure 1 shows the dependence of the RBE variation on the photon LQ parameters α, β and D_t. In figure 2 the influence of the nuclear volume V_n, nuclear radius r_n, the DNA loop domain size l_{DSB} and the DSB yield α_{DSB} on RBE is presented.

[8] Note that a change of one of the LQ parameters α or β immediately implies a modification of their ratio α/β. Here the assumed α/β ratios of 2 and 10 Gy refer to the designed (unchanged) parameter values.

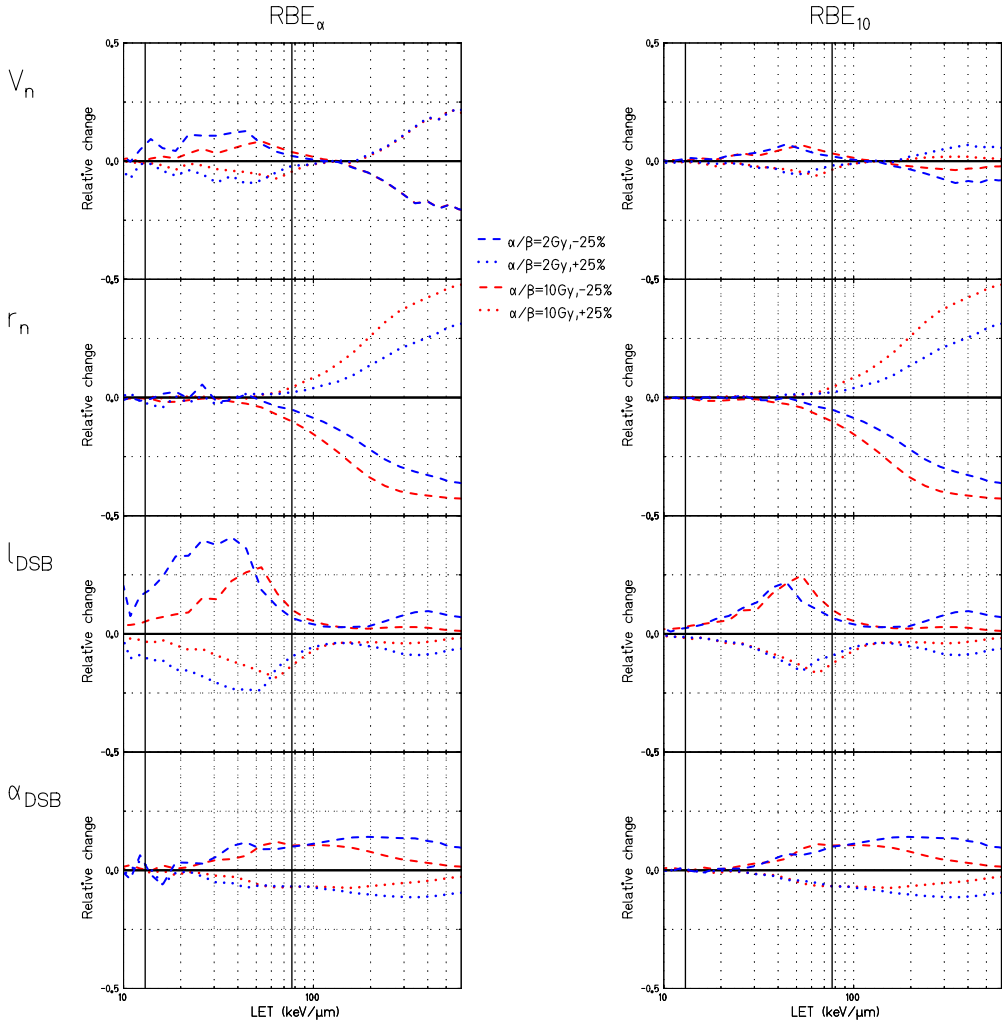

Figure 2. Relative change of RBE as presented in figure 1 for the nuclear volume, the nuclear radius, the DNA loop domain size and the DSB yield.

Generally from the figures it can be seen that in most cases there is less or at most equal sensitivity on parameter variations for $\alpha/\beta = 10$ Gy compared to $\alpha/\beta = 2$ Gy. Similarly, the RBE at 10% survival is typically less sensitive to parameter variations compared to RBE$_\alpha$. Moreover it becomes evident that the increase of some parameters leads to either a decrease or an increase of RBE. Based on some simple mechanistic interpretations within the framework of the LEM the different sensitivity patterns can be interpreted, as shall be demonstrated at some examples in the following.

To β, D_t, and α_{DSB} the RBE is primarily sensitive for intermediate LET values. These parameters show a bulb-like pattern in the plots. For very low LET they are of minor importance (as all parameters), as the nature of the radiation field converges to that of photons, and hence RBE will get close to one. At high LET the overkill effect will take place, i.e. in the limit of high LET a cell will only survive if it is not hit, and will be inactivated as consequence of any hit. Due to this simplistic picture these biologic parameters lack of importance in the high LET regime.

The parameters α and r_n in contrast show pronounced importance for high LET, which can be explained by the same argument: The probability for a cell to be hit and with that the effect increases with the nuclear radius and thus with the geometrical cross section r_n. The photon parameter α has, in contrast to β and D_t, for high LET almost no influence on the ion dose response curve within LEM. Nevertheless there is a prominent dependence of RBE on α because it directly affects the dose at which the reference effect level is reached on the photon dose response curve.

The parameter l_{DSB} shows two pronounced sensitivity regions, while there is almost no sensitivity between 100 and 200 keV $\mu\mathrm{m}^{-1}$. The reason is an interference of the length scales involved: Generally an increase of l_{DSB} allows for more DSB clustering within the photon radiation field, while this effect is not so prominent for ions, which results in a decrease of RBE. But in the intermediate LET regime the track diameter is of the order of the loop domain size. In this case an increase of the domain size will lead to an effective increase of clustering almost as much as for photons, because for increased loop domains all DSB caused in the whole track structure may contribute to DSB clusters. As there is not much differential effect between photons and ions in this case, the RBE sensitivity to changes of l_{DSB} is low. For very high LET finally a further increase of l_{DSB} will not lead to more clustered lesions caused by the ion track, hence the sensitivity recovers.

In a similar way the direction of RBE change with respect to the direction of change of the input parameter can be interpreted: An increase of the photon parameter α, e.g. implies a steeper photon dose response curve and consequently a lower dose needed to reach a desired effect level. A higher α will also correlate to a steeper ion dose response curve. But as the enhanced effect of the ion dose response is primarily caused by the inhomogeneity of the local dose deposition pattern in combination with the nonlinear response to local doses, which is parameterized by β and D_t, the steepening due to an increase in α is less pronounced than for photons. As a result the RBE will decrease, if α is increased. All parameters show a unique directional RBE change except V_n for which at low LET a parameter decrease and at high LET a parameter increase leads to RBE increase.

The analysis presented here has also been performed for other particle species (protons, helium and neon). However, the results generally follow a similar systematics, and thus no detailed discussion is presented here. The most relevant difference is that as the whole RBE-LET characteristics is shifted towards higher LET for heavier ions, they provide a lower sensitivity on the parameters for low LET, while lighter particles are more sensitive there.

To project out the findings of this sensitivity analysis with monoenergetic beams for particle therapy, the most important results of the sensitivity analysis for carbon ions are summarized for therapy relevant LET values in tables 2 and 3 for $\alpha/\beta = 2$ Gy and 10 Gy, respectively. In a treatment like situation a good conformity to a tumour in the target region is desirable and the therapy benefits from the high RBE of carbon ions just before stopping as it allows one to keep the doses applied to normal tissue low. Hence in the target region typically a high average LET and a high dose are expected, leading to low survival of tumour cells, while in the entrance channel doses should remain low, and the LET of the high energetic carbon ions is small. In the tables these situations are represented by results for RBE_{10} at a high LET and for RBE_{α} at a rather small LET, respectively. But also the complementary cases occur: At the margins of the spread out Bragg peak (SOBP), depending on the field geometry and the irradiation angles, some parts of the tissues might be covered by radiation with rather high doses of rather low LET radiation or vice versa. These interfaces between peak and plateau regions are of particular interest in therapy as all tumour cells must be inactivated, while in the same way normal tissue shall be spared as much as possible. As tumour and healthy tissue

Table 2. Parameter dependence of RBE for monoenergetic carbon ions in therapy comparable situations for $\alpha/\beta = 2$ Gy. The header part of the table contains the RBE_α and RBE_{10} for LET values typically found in the entrance channel and the Bragg peak region in carbon ion therapy, respectively. Here the design parameter settings were used. Below the header part the relative changes in RBE in per cent after change of one parameter about −25% or +25% (bottom or top numbers) are given. The second column contains the correlation direction, labelled as 0, + or − if RBE does not change, goes typically up or down with increasing parameter, respectively. Note that this information is valid below the overkill regime—for high LET the correlation might change (see text).

		Entrance (13 keV μm^{-1})		Bragg peak (77 keV μm^{-1})	
		RBE_α 1.44	RBE_{10} 1.04	RBE_α 9.08	RBE_{10} 2.31
	corr.	$\frac{\Delta RBE_\alpha}{RBE_\alpha}$ (%)	$\frac{\Delta RBE_{10}}{RBE_{10}}$ (%)	$\frac{\Delta RBE_\alpha}{RBE_\alpha}$ (%)	$\frac{\Delta RBE_{10}}{RBE_{10}}$ (%)
V_n	−/+	−4.97 7.66	−0.77 1.06	−1.98 1.98	−2.16 1.73
r_n	+	+0.46 +0.64	+0.12 −0.04	+2.23 −5.44	+2.24 −5.44
l_{DSB}	−	−9.44 +19.41	−1.29 +2.76	−9.13 +7.27	−8.84 +7.27
α	−	−6.19 +10.30	+0.04 −0.05	−17.56 +29.25	−0.63 +0.55
β	+	+7.68 −7.68	+0.74 −0.83	+19.74 −20.41	+8.77 −10.15
D_t	0/+	±0	+0.48 −0.80	+14.47 −17.05	+14.47 −17.05
γ	−	−2.39 +2.92	−0.33 +0.40	−1.78 +2.42	−1.78 +2.43
δ	−	−8.79 +13.79	−1.20 +1.95	−10.42 +12.46	−9.90 +12.46
r_c	−	−0.51 +3.26	−0.07 +0.45	−4.78 +6.14	−4.77 +6.14
σ	−	+1.96 +0.46	+0.27 +0.06	−6.16 +8.39	−6.15 +8.39
α_{DSB}	−	−0.74 +1.71	−0.10 +0.23	−6.44 +10.01	−6.44 +10.01
α_{SSB}	+	+2.27 −0.77	+0.31 −0.11	+14.86 −12.62	+14.86 −11.69
h	+	+0.03 −0.22	+0.00 −0.03	+6.46 −6.85	+6.46 −6.86
L_{Gen}	−	+0.43 +1.31	+0.06 +0.18	−5.59 +8.53	−5.59 +8.53

show often different radiosensitivities, beneath dose and LET also the α/β ratio plays a role here, which reflects the complexity of RBE.

In the tables the design RBE values as well as the RBE values after parameter change are given for typical situations in the entrance channel (LET = 13 keV μm^{-1}) as well as in the SOBP (LET = 77 keV μm^{-1}). The representative values for the LETs have been adopted from (Suzuki *et al* 2000). In the tables, also the direction of change of the RBE is given: when a parameter is increased, the RBE may either typically go up as well (as marked with a '+' sign to indicate that positive correlation) or down (as marked with a '−' sign). In the case of D_t there is for small LET no dependence for RBE_α, which is labelled by '0'. Exceptions of a unique correlation occur only for the parameter V_n where the direction of RBE change gets reverted at an LET of 150 keV μm^{-1} (thus labelled with '+/−' and for very small parameter sensitivities where an increase and a decrease may hardly change RBE, while nevertheless small changes are seen in the simulations in the same direction due to fluctuations in the Monte Carlo calculation. The dependence on energy or LET is not listed in the tables, as LET is the dependent variable in the figures presented, and for a given particle species energy is uniquely defined for a given LET in the Bethe–Bloch regime.

Note that the RBE depends on each of the quantities typically less than proportional, i.e. when a parameter is changed about 25% the RBE usually changes less than 25%. Up to few

Table 3. As table 2, for $\alpha/\beta = 10$ Gy.

		Entrance (13 keV μm^{-1})		Bragg peak (77 keV μm^{-1})	
		RBE_α 1.09	RBE_{10} 1.04	RBE_α 3.27	RBE_{10} 2.44
	corr.	$\frac{\Delta RBE_\alpha}{RBE_\alpha}$ (%)	$\frac{\Delta RBE_{10}}{RBE_{10}}$ (%)	$\frac{\Delta RBE_\alpha}{RBE_\alpha}$ (%)	$\frac{\Delta RBE_{10}}{RBE_{10}}$ (%)
V_n	+/−	−0.74 1.10	−0.48 0.58	−3.06 3.36	−3.28 3.28
r_n	+	+0.42 −0.54	+0.34 −0.55	+4.58 −9.94	+4.61 −9.96
l_{DSB}	−	−2.49 +5.12	−1.39 +2.89	−13.52 +10.49	−12.71 +10.46
α	−	−1.80 +2.90	−0.42 +0.37	−14.21 +23.44	−6.96 +8.18
β	+	+2.03 −2.02	+0.73 −0.81	+13.80 −14.49	+8.55 −9.71
D_t	0/+	±0	+0.13 −0.22	+6.08 −9.50	+6.44 −9.52
γ	−	−0.96 +0.37	−0.53 +0.21	−2.12 +2.87	−2.01 +2.85
δ	−	−2.76 +3.77	−1.54 +2.12	−12.96 +14.30	−12.19 +14.28
r_c	−	−0.21 +0.77	−0.12 +0.43	−5.33 +6.73	−5.04 +6.70
σ	−	+0.27 +0.33	+0.15 +0.18	−6.66 +8.89	−6.30 +8.87
α_{DSB}	−	−0.75 +0.47	−0.42 +0.27	−7.09 +10.78	−6.70 +10.75
α_{SSB}	+	+0.74 −0.61	+0.42 −0.34	+15.60 −13.85	+15.57 −13.02
h	+	+0.38 −0.06	+0.21 −0.03	+6.92 −7.40	+6.90 −6.99
L_{Gen}	−	+0.10 +0.64	+0.06 +0.36	−6.06 +9.06	−5.73 +9.04

exceptions RBE does not change by more than 25%. From figures 1 and 2 it is evident that for a 10% survival level only the nuclear radii r_n exceed the 25% level for RBE changes. At 77 keV μm^{-1} as representative for the target region the RBE is very sensitive on the photon dose response parameters, the track structure parameter δ and the yield of SSB.

5. Sensitivity analysis for a clinical situation

The application of carbon ions for cancer treatment in the clinics requires treatment planning which accounts for the RBE in such a way, that the target volume is covered uniformly by a described RBE-weighted dose, while the doses in the normal tissues and in particular in organs at risk remain low. This strategy is followed in the particle treatment facilities in Japan (Tsujii and Kamada 2012) as well as in Europe (Combs *et al* 2010, Schulz-Ertner *et al* 2007), although their beam characteristics and the methods in accounting for RBE differ.

The RBE in a voxel based treatment plan corresponds to a mixed radiation field, because several particle species, each having an individual energy distribution, may contribute to the overall dose deposited due to fragmentation, straggling and scattering. Because of this mixing the large sensitivities detected in the last section are balanced out, and hence the irradiation of extended targets will show a damped sensitivity of RBE to its input parameters.

In this section the same sensitivity analysis is presented for SOBPs, as before for monoenergetic beams and cells or tissues under track segment conditions. Thus, each of the specific parameters of the LEM listed in table 1 was again modified by ±25% and the induced change in RBE was monitored. To facilitate the analysis a sphere as idealized target geometry with 60 mm depth extension placed in a depth of 150 mm (isocentre) was regarded[9].

[9] Note that this choice corresponds to rather large, deep seated tumours.

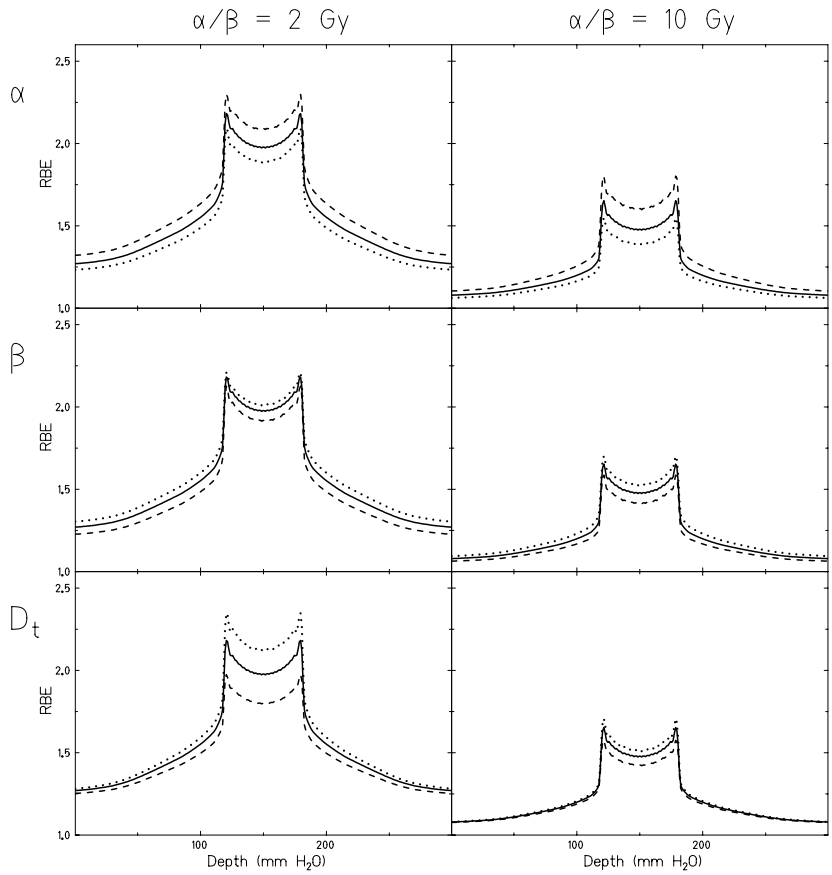

Figure 3. Dependence of RBE over water equivalent depth for carbon ions and cells or tissues with $\alpha/\beta = 2$ Gy and $\alpha/\beta = 10$ Gy on the LQ parameters. The corresponding RBE-weighted dose distributions were all optimized to 3 Gy in the target region. The solid curve corresponds to design parameters (see text), and the dashed and dotted curves emerge by decreasing or increasing the specific parameters about 25%, respectively.

The treatment planning software TRiP98 (Krämer *et al* 2000, Krämer and Scholz 2000) was used to optimize a physical dose leading to a homogeneous RBE-weighted dose throughout the SOBP. In general the RBE varies with the depth in tissue because the LET distribution changes. For this reason we here discuss depth distributions of the RBE, instead of its LET dependencies.

The strategy closest to the clinical routine is an optimization of two directly opposing fields to give a flat RBE-weighted dose of 3 Gy within the target, in line with the fraction dose used in the GSI clinical trial (Schulz-Ertner *et al* 2007). Note that for each parameter setting of the sensitivity analysis an individual optimization must be performed. As before, all calculations were performed for tissues with $\alpha/\beta = 2\,\mathrm{Gy}$ and $\alpha/\beta = 10\,\mathrm{Gy}$ with the same absolute values as in the previous section. The results are visualized in figures 3 and 4 where the depth distributions of the RBE values along an axis right through the isocentre (beam's eye view) are presented. We chose here to present the absolute RBEs instead of relative changes after parameter variation as in the previous figures, because for a SOBP the RBE profile is very instructive. Note that the mixed radiation field provides a variation of the average LET

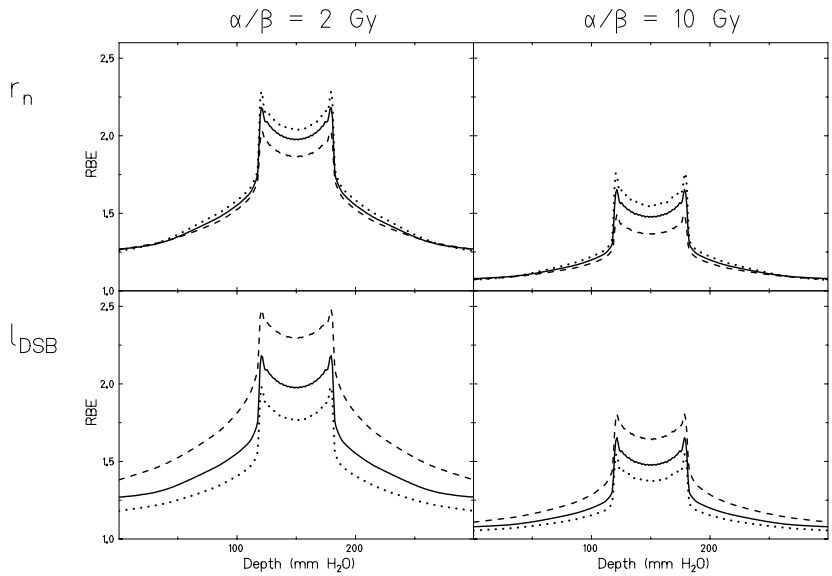

Figure 4. As figure 3, for the nuclear radius and the size of the chromatin loops.

with depth. Hence here the depth is the appropriate quantity to replace the dependence on LET, which was discussed in the last section.

At this point it is important to note that often for *in vivo* systems and clinical endpoints the LQ parameters happen to be much smaller (Brenner 1993). In order to establish comparability to the results in the previous section, here the absolute values were kept the same. However, it is known that RBE values for small and large absolute values are comparable for the same α/β ratios, with the only difference that overkill effects appear more pronounced for higher absolute values. Hence for small absolute values less sensitivity on parameters which affect overkill is expected, and we checked that conjecture at some examples (data not shown).

Generally, the curves in figures 3 and 4 show a low RBE in the entrance channels and a considerably higher RBE in the target, where particles are stopping and have a higher LET consequently. This is one of the superiorities of carbon ions compared to protons in radiotherapy. For a single field treatment plan the RBE distribution across the SOBP shows pronounced maxima towards the distal boundary of the target volume. There exclusively stopping particles (except some fragments) are present, causing a high LET, while at the proximal regions and within the SOBP broader mixtures of LETs exists. In a treatment plan consisting of two or more fields the statement holds in general, i.e. at the whole boundary of the target region. There the fraction of stopping particles is higher compared to within the target. Consequently the high LET components, causing a high RBE, are most prominent at the boundary. A relative uncertainty will therefore translate into a higher uncertainty of RBE-weighted dose at the margins of a SOBP. In contrast, in the figures the RBE distributions appear to be almost parallel for different parameter adjustments, leading to a reduced sensitivity at the margins of the target volume. This is due to the usage of two opposing fields, where at the margins high LET and comparably low LET components are mixed. Strategies for optimizing treatment plans such that the high LET components in the radiation field are more uniform distributed across the SOBP are currently discussed (Bassler *et al* 2010) and might help to diminish uncertainties of RBE (Böhlen *et al* 2012).

When varying one of the input parameters, the RBE values are shifted into the same direction as was detected in the previous section. That means that the direction of the correlation

between RBE and any specific parameter remains the same for both monoenergetic beams and SOBPs.

Regarding the quantity of the deviations a damping is observed compared to the maximum variations detected in the previous section. This is due to the mixture of LETs which is caused by the spread of pristine Bragg peaks forming the SOBP and due to fragments, which have to be taken into account properly (Lühr *et al* 2012, Gunzert-Marx *et al* 2008). The mixed radiation quality also implies a smaller overall RBE, also giving rise to smaller sensitivities. The feature of damping is of interest for the robustness of treatment plans. Furthermore, as before, the deviations typically do not exceed 25% and are therefore less than direct proportional to the change of the specific parameters.

A RBE-weighted dose of 3 Gy approximately corresponds to about 50% and 15% cell survival for the original set of specific parameters for $\alpha/\beta = 2$ Gy and 10 Gy, respectively. But in contrast to the last section, where the survival levels were fixed in advance by considering RBE_α or RBE_{10}, here the dose remains fixed at 3 Gy, when parameters are varied. Thus an optimization to 3 Gy when one of the LQ parameters is changed leads to slightly different survival levels for each parameter adjustment.

Figure 4 presents the results of the sensitivity analysis of the geometric parameters r_n and l_{DSB}. When changing the nuclear radius a variation in RBE is primarily visible in the target region and suppressed in the entrance channel. This behaviour can be again understood by looking at the case of monoenergetic ions, where there is only a marginal dependence on r_n in the low LET region. The difference in RBE after a change of the chromatin loop size l_{DSB} is, in particular for $\alpha/\beta = 2$ Gy, comparably large and in contrast to all other parameters also very prominent in the entrance channels. Again, the reason can be understood by looking at figure 2 and tables 2 and 3: while the Bragg peak typically covers LETs between 50 and 100 keV $\mu\mathrm{m}^{-1}$, in the entrance channels lower LET values occur. For RBE_α a quite high sensitivity to l_{DSB} has been found with monoenergetic beams at low LET values. Remnants of this finding cause the sensitivity in an extended treatment plan.

6. Discussion

6.1. Justification of the approach

The sensitivity analysis presented in this work is based on an approach using single parameter variations. The question arises if such a 'factorized' approach is appropriate and overall RBE changes could be calculated by a linear superposition of the RBE changes of each individual parameter. Instead, one also could expect that shifts in any two parameters act on RBE dependent on each other in a correlated way. We will argue in the following that these correlations between parameters with respect to RBE change play only a second order role.

Formally, the RBE can be regarded as a mathematical function dependent on a set of parameters $\{p_i\}$, i.e. $\mathrm{RBE} = \mathrm{RBE}(\{p_i\})$. If parameters are changed from $\{p_i\}$ to $\{p_i + \delta p_i\}$, the RBE can be expanded in a Taylor series, where the first order term contains a sum of terms $\frac{\mathrm{dRBE}}{\mathrm{d}p_i}\delta p_i$, and the second order term of type $\frac{\mathrm{d}^2\mathrm{RBE}}{\mathrm{d}p_i \mathrm{d}p_j}\delta p_i \delta p_j$. Hence the 'factorization' approach is resembled by first order terms, and correlated RBE change by second and higher order terms. So, if the values of changes are not too large, the second order contributions will be smaller than the first order contributions and thus can be neglected. For a proper uncertainty analysis this has to be fulfilled anyway: only if the uncertainties associated with the parameters are smaller than the parameter values (which is typically the case), the principles of error calculus will apply, and under this conditions the argument given is valid. We also checked that numerically for

some examples by calculating the RBE after a coexisting parameter detuning and comparing it with the RBE calculated with a linear superposition of RBE changes.

6.2. Importance of parameters for RBE uncertainty

The sensitivity analysis presented in the two previous sections reflects how RBE changes, when one of the input parameters is varied. This allows one to assess the variability of RBE based on the variability of one of the input parameters. While some of the general parameters such as δ are obtained with a quite good accuracy from experimental results, others have relatively large error bars. In this case we followed the strategy to use average values from the literature. For instance, values in the typical range between 20 and 40 DSB per Gy are reported for α_{DSB}. Recent works also indicate that the yield could be much higher, but is underestimated due to systematic experimental errors (Neumaier *et al* 2012). So, according to the state of research these parameters may be subject to change in future. However, it is important to note that the sensitivity on input parameters does not directly provide information about RBE uncertainty, as shall be explained in the following.

Despite remarkable uncertainties in the input parameters, in combination all general parameters form a consistent input parameter set, as two of them, l_{DSB} and r_c (cf table 1), were fitted once to experimental data (Furusawa *et al* 2000, Suzuki *et al* 2000) to calibrate the model. By this procedure they compensate for possible misadjustments of the measured general parameters and minimize the model inherent systematic uncertainties of RBE. Indeed, a large contribution of the general parameters to the overall uncertainty of RBE values has not been observed, which indicates that the systematic errors of the LEM are small. For *in vitro* cell survival experiments (Elsässer *et al* 2010) and clinical cases (Grün *et al* 2012) we showed in several publications that the LEM predicts RBEs with reasonable accuracy for different LET values or depths, dose levels and cell types.

The specific parameters characterize the experiment or clinical situation and have to be evaluated in order to use the LEM. Among them, the genomic length and the geometric parameters are usually known or can be obtained without too much effort. Thus the interesting consequence is that the predominant source of uncertainty of RBE, which is a quantity for *high* LET radiation is due to the uncertainty of the photon parameters α, β, and D_t, i.e. the response parameters of the *low* LET radiation. Thus in the following we focus on these parameters only.

Moreover for RBE simulations it is usually sufficient to fix the ratio α/β, because the RBE does only marginally depend on a common scaling factor of the absolute values of α and β, for small and intermediate LET. A plausible reasoning for this is, that the nonlinear dose response curve leads to a high RBE foremost by means of high local doses. A measure for the excess effect due to the nonlinearity, normalized to the linear component is just the inverse of the α/β ratio. Indeed, RBE seems to scale linearly with $(\alpha/\beta)^{-1}$ (Friedrich *et al* 2013). The α/β ratio can also be used to find an estimate for D_t by means of an empirical relationship. Another strategy could be to replace the linear quadratic linear model used within the current LEM implementation by a different photon dose response model which provides the saturation of effect increments without an explicit threshold parameter. Investigations towards this direction are on the way, and one possible option is to use the GLOBLE model (Friedrich *et al* 2012a) which fulfills these requirements.

6.3. RBE uncertainty for monoenergetic beams and SOBPs

In this section we want to make use of the presented sensitivity analysis and provide examples for an uncertainty analysis. To understand the influence of the composition of a radiation field

Table 4. Parameter dependence of RBE for monoenergetic carbon ions in therapy comparable situations at 3 Gy and for a SOBP composed of two opposing fields and optimized to 3 Gy (RBE) formed by carbon ions for $\alpha/\beta = 2$ and 10 Gy. The upper part contains the LET or dose averaged LET and the reference RBE values. In the middle section of the table the relative changes in RBE after change of one parameter about −25% or +25% (bottom or top numbers) are given in per cent. In the bottom line the overall uncertainty of the RBE value is given, provided the uncertainties of α, β and D_t are 10%, 20% and 30%, respectively.

	$\alpha/\beta = 2$ Gy		$\alpha/\beta = 10$ Gy	
	Monoenergetic	SOBP	Monoenergetic	SOBP
LET or LET_D	77 keV μm^{-1}	54 keV μm^{-1}	77 keV μm^{-1}	52 keV μm^{-1}
RBE	3.63	1.98	2.52	1.48
	$\frac{\Delta\text{RBE}}{\text{RBE}}$(%)	$\frac{\Delta\text{RBE}}{\text{RBE}}$(%)	$\frac{\Delta\text{RBE}}{\text{RBE}}$(%)	$\frac{\Delta\text{RBE}}{\text{RBE}}$(%)
α	−6.3 +7.7	−4.5 +5.7	−10.1 +32.8	−5.9 +8.5
β	+4.1 −6.4	+1.9 −3.0	+7.7 −9.3	+3.4 −4.3
D_t	+14.5 −17.1	+7.6 −9.0	+6.4 −9.5	+2.5 −3.7
Δ(%)	20.2	10.7	18.1	7.0

on the parameter sensitivity of RBE in more detail, the centre of a carbon SOBP composed from two opposing beams and representing a mixed radiation field, was compared with a monoenergetic beam of high LET, mimicking the distal end of a one-sided SOBP. While in the former case the radiation field is composed of an overlay of low and high LET components, in the latter only one high LET component is contributing. Table 4 contains the relative change of the RBE after an initial change of one of the specific parameters α, β and D_t of $\pm 25\%$ for both cases, where the restriction to the photon parameters is justified by arguments given in the last subsection. The SOBP has been chosen as in section 5 with two opposing fields optimized to a RBE-weighted dose of 3 Gy and extended to 60 mm in a depth of 150 mm in the isocentre. There, the dose averaged LET is 54 keV μm^{-1} and 52 keV μm^{-1} for $\alpha/\beta = 2$ Gy and $\alpha/\beta =$ 10 Gy, respectively, where there is a small difference as the dose optimization respects the α/β ratio and hence results in different LET compositions of the fields. For the monoenergetic beam an LET of 77 keV μm^{-1} was chosen as in section 4, but to allow comparison on the same dose level the RBE was here evaluated at 3 Gy RBE-weighted dose instead of considering RBE_α or RBE_{10} as before.

For any varied parameter, the relative change of the RBE in the SOBP is damped compared to the change detected for the monoenergetic beam. The damping can still be observed for a comparison of the SOBP with a monoenergetic beam of comparable LET (about 50 keV μm^{-1}, data not shown). Thus it is obviously a consequence of the broader LET distribution within a SOBP. But the damping of RBE sensitivity goes along with a smaller RBE. Hence for clinical applications a compromise between the RBE and its uncertainties has to be found. If the RBE is large, so will be its relative uncertainty, and vice versa.

When a photon dose response curve is known, often one of the parameters α and β can be determined quite well, while the other has a higher uncertainty. The most crucial part, however, is to determine an appropriate value for D_t, which is hardly accessible in experiments or clinical data. As a good estimate one can apply an empirical relationship between D_t and the α/β ratio, or determine D_t by a fit to high LET data, if available. Exemplarily we here assume that α, β and D_t are known with uncertainties of 10%, 20% and 30%, respectively, which seem to be typical estimates. We calculated the corresponding partial uncertainties of RBE by scaling the numbers given in table 4 from a 25% variation to these uncertainty levels. By calculating the propagation of the errors one can now evaluate an overall uncertainty in the following way:

bearing in mind that there is an anti-correlation between α and β induced by the common LQ fit procedures we simply added their relative errors, which is a rather pessimistic way of propagating errors, as it does not allow for mutual uncertainty compensation. From this sum and the uncertainty of D_t then a total uncertainty was calculated by means of Gaussian error propagation, allowing for such partial compensation of uncertainties. As a result, the overall relative uncertainties Δ given in the bottom line of table 4 are obtained.

These numbers are on the one hand typical and indicate the order of magnitude of uncertainty which is usually expected for RBE simulations with the LEM. They clearly demonstrate the damping of RBE uncertainties within a SOBP compared to monoenergetic irradiations. In particular the detected deviations for the irradiation within a SOBP is about 10%, which is in the order of magnitude acceptable for clinical applications. But this calculation is an example and specific for the choice of the parameters and uncertainty levels of the specific parameters as well as on the irradiation geometry. The numbers given should hence not be understood as a general uncertainty analysis. They rather indicate the order of magnitude of RBE uncertainty to be expected, while for any particular case such an analysis should be considered individually.

6.4. Sensitivity on photon and ion dose response

As RBE is a relative quantity comparing the doses needed with photons and ions for the same effect, the question arises if the RBE sensitivity on an input parameter is caused by the sensitivity of either the ion or the photon dose response curve. This was approached by monitoring the relative change of doses for ion and photon radiation at the same effect under parameter variation.

Generally, a change of α will result in larger dose changes for photons as compared to ions. Hence the RBE sensitivity on α is not due to the high LET dose response, but rather reflects the uncertainty of the photon dose response itself. In contrast, a change of β term will, for moderate effects, change the ion dose response curve more severely than the photon dose response curve. This is because the initial slope of ion survival curves strongly depends on the photon β parameter which quantifies the nonlinear dose response and hence scales the enhanced effects of high local doses as delivered to the tissues by individual charged particles along their tracks.

Thus, concerning α, there is a smaller level of uncertainty in ion therapy as compared to conventional photon therapies, while for β it is just the opposite. Hence a good fraction (cf table 4) of the overall uncertainty calculated in the last subsection, corresponding to α will also be present in a treatment with photon radiation.

6.5. Sensitivity for fixed α/β ratio

From clinical studies there are several ways of obtaining information of the photon dose response parameters. Quite often the α/β ratio can be fixed quite well (e.g. when found from fractionation studies) while the derived absolute parameter values α and β can be challenged. Hence it is also of interest to investigate the RBE dependence on photon parameter change when the α/β ratio stays fixed, i.e. when α and β are changed jointly by the same factor of 25%. This was checked, and we found for the therapeutic relevant LET range that there is almost no dependence of RBE_α on parameter change, and that there is about 10% or 5% maximum change of RBE_{10} for $\alpha/\beta = 2$ and 10 Gy, respectively. This can be interpreted by the principles of LEM: The action of individual ions is expressed by the linear coefficient α_I of ion dose response curves, which directly determines RBE_α. In LEM, it is obtained as an

extrapolation from photon effects, which are linear in both α and β. If they both are scaled by a common factor, so will α_I, and hence RBE_α remains constant. As for the quadratic component β_I nonlinear terms arise, describing the interaction of lesions from different ions, this argument does not hold and thus a sensitivity of RBE_{10} on parameter change is detected.

In clinical practice, however, as both α and β are affected by uncertainties (e.g. due to a limited patient number but also due to inter-individual differences), the α/β will also show an uncertainty. Thus always a sensitivity analysis for different α/β ratios should be carried out in prospective treatment planning.

6.6. Sensitivity on distributions of input parameters

In a population of cells the input parameters for estimating the RBE might not assume a single value but rather be subject to a distribution. For instance the geometrical cross section of cell nuclei shows a broad distribution for most cell lines. Then in a first approach the strategy is to rely on the mean of the parameter values, resulting in a RBE which approximates the mean RBE to first order. Associated uncertainties can be estimated using the sensitivity analysis presented here.

A full consideration of distribution effects would require to determine the contribution of each subpopulation of the distribution to the corresponding RBE distribution. However, for a more pragmatic handling the parameter distribution is replaced by an effective parameter, reproducing the mean RBE. For the nuclear geometrical cross sections at high LET where the RBE is sensitive on the nuclear cross section due to overkill, for a given distribution of cross sections an effective cross section of typically less than the mean (about 80%) will reproduce the mean RBE (Elsässer *et al* 2008).

Another example where uncertainties due to parameter distributions play a role is the variability in dose response within a patient population in therapy. It is common procedure to apply non-individualized regimens, where recommended doses are found by dose escalation studies over sufficient large patient numbers. The distribution of radiosensitivity parameters leads to a flattening of the dose response curve of tumour control (Dasu *et al* 2003). This phenomenon can be quite crucial and eventually has to be taken into account for analysis of clinical outcomes (Kanai *et al* 2006). However, as seen for the α term in this study the population heterogeneity has higher impact on dose response to photon than to ion radiation (Scholz *et al* 2006). A more personalized determination of input parameters, e.g. by means of biomarkers, could help to further reduce uncertainties.

6.7. Strategies for sensitivity minimization

The general goal of any kind of radiation therapy modality is to deliver dose in the target region and to avoid dose delivery as good as possible within the surrounding healthy tissue. Further constraints as sparing out organs at risk may apply. But regarding charged particle therapy recent work (Bassler *et al* 2010, Grassberger *et al* 2011) questions if a homogeneous dose distribution across the target should be the only objective in treatment planning. Additionally, LET homogeneity could be another promising objective. In addition to dose homogeneity, LET homogeneity promises to reduce RBE uncertainties. Other studies investigated practical applicability, e.g. by ramp fields (Krämer and Jäkel 2005) or by modifying the LET distribution by active scanning (Grassberger *et al* 2011) and quantified implications for the RBE uncertainty (Böhlen *et al* 2012). In a previous work (Grün *et al* 2012) we demonstrated that the delivery of dose in two opposing fields, both contributing equally to the overall dose, reduces the

uncertainties very effectively. Table 4 gives evidence for the reduced RBE uncertainty (damping), but also demonstrates the reduction of RBE going along.

Unavoidably, an uncertainty-free RBE model cannot exist, as the biological determinants of RBE, i.e. the radiosensitivity parameters, are subject to variability. Hence a reduction of RBE uncertainty as much as possible as a consequence of a more homogeneous LET distribution might be desirable, and could be realized by combining different fields irradiated in different angles in the target volume, or even inhomogeneous dose fields adding up to a homogeneous dose across the target volume. Finally, depending on particular aspects of the treatment plans, a compromise between a high RBE in the target (without caring about LET distribution) and a lower, but less uncertain RBE (applying a rather homogeneous LET distribution) has to be found.

6.8. Relation to other RBE models and to experimental RBE data

Throughout this paper, many aspects of RBE uncertainty have been discussed at hand of the LEM. But most of the implications of this study are also revealed by other high LET models. In the MKM, which is the only model apart from LEM used in clinical practice in recent versions (Inaniwa *et al* 2010, Sato and Furusawa 2012), the prediction of the RBE is based on the dose response to photon radiation, too, and hence their uncertainties are propagated to RBE in a similar way. The model of Carabe and Jones (Carabe-Fernandez *et al* 2007, Jones *et al* 2012) is a reformulation of the LQ model and thus input data of both radiation qualities are needed for which the RBE is to be predicted. It uses only few assumptions and also demonstrates the direct dependence of RBE on photon dose response parameters.

Finally, by investigating experimental RBE data (Friedrich *et al* 2013, Paganetti *et al* 2002), a scatter of measured RBE values of *in vitro* cell survival experiments reflects the order of magnitude of RBE uncertainty corresponding to the model predictions (calculated from typical uncertainties of the photon parameters as in table 4), except for low LET where some remaining systematic deviations of LEM predictions in comparison to experimental RBE values are present. To give an order of magnitude, for monoenergetic carbon ions with an LET of 77 keV μm^{-1} at 3 Gy the typical RBE uncertainty is 20% and almost independent on the α/β ratio. As outlined before, this number will be damped within an SOBP.

This agreement between RBE uncertainties observed in experiments and the uncertainties predicted by RBE modelling is a further strong support that LEM is able to predict essential characteristics of RBE. This also implies that the results presented in this study are not model specific, but are rather general properties of RBE.

7. Conclusions

This work provides a detailed and systematic discussion of the sensitivity of RBE to its determining parameters. It demonstrates that radiobiologic models such as LEM are suitable to predict RBE along with the RBE uncertainty for applications in radiobiologic experiments and particle therapy. In particular two findings which have been presented in the previous sections are important for the discussion of simulated RBE values. First, the RBE values depend typically less than proportional on the determining parameters, with few exceptions only. Second, going over from cells or tissues irradiated with monoenergetic beams to extended volumes irradiated with a SOBP, the influence of uncertainties on RBE values are damped due to the mix of radiation qualities at each position in the SOBP. The results and methods presented may thus be helpful for optimizing the precision of RBE predictions.

Acknowledgments

This work was partly supported by Siemens Healthcare. Work is part of HGS-HIRe.

References

Ando K and Kase Y 2009 Biological characteristics of carbon-ion therapy *Int. J. Radiat. Biol.* **85** 715–28

Astrahan M 2008 Some implications of linear-quadratic-linear radiation dose-response with regard to hypofractionation *Med. Phys.* **35** 4161–72

Bassler N, Jäkel O, Søndergaard C S and Petersen J B 2010 Dose- and LET-painting with particle therapy *Acta Oncol.* **49** 1170–6

Böhlen T T *et al* 2012 Investigating the robustness of ion beam therapy treatment plans to uncertainties in biological treatment parameters *Phys. Med. Biol.* **57** 7983–8004

Brenner D J 1993 Dose, volume, and tumor-control predictions in radiotherapy *Int. J. Radiat. Oncol. Biol. Phys.* **26** 171–9

Carabe-Fernandez A, Dale R G and Jones B 2007 The incorporation of the concept of minimum RBE (RBEmin) into the linear-quadratic model and the potential for improved radiobiological analysis of high-LET treatments *Int. J. Radiat. Biol.* **83** 27–39

Carlone M, Wilkins D and Raaphorst P 2005 The modified linear-quadratic model of Guerrero and Li can be derived from a mechanistic basis and exhibits linear-quadratic-linear behaviour *Phys. Med. Biol.* **50** L9–15

Combs S E *et al* 2010 Heidelberg ion therapy center (HIT): initial clinical experience in the first 80 patients *Acta Oncol.* **49** 1132–40

Cucinotta F A, Nikjoo H and Goodhead D T 1999 Applications of amorphous track models in radiation biology *Radiat. Environ. Biophys.* **38** 81–92

Curtis S B 1986 Lethal and potentially lethal lesions induced by radiation—a unified repair model *Radiat. Res.* **106** 252–70

Dasu A, Toma-Dasu I and Fowler J F 2003 Should single or distributed parameters be used to explain the steepness of tumour control probability curves? *Phys. Med. Biol.* **48** 387–97

Elsässer T, Cunrath R, Krämer M and Scholz M 2008 Impact of track structure calculations on biological treatment planning in ion radiotherapy *New J. Phys.* **10** 075005

Elsässer T, Krämer M and Scholz M 2008 Accuracy of the local effect model for the prediction of biologic effects of carbon ion beams *in vitro* and *in vivo* *Int. J. Radiat. Oncol. Biol. Phys.* **71** 866–72

Elsässer T and Scholz M 2007 Cluster effects within the local effect model *Radiat. Res.* **167** 319–29

Elsässer T *et al* 2010 Quantification of the relative biological effectiveness for ion beam radiotherapy: direct experimental comparison of proton and carbon ion beams and a novel approach for treatment planning *Int. J. Radiat. Oncol. Biol. Phys.* **78** 1177–83

Fertil B and Malaise E P 1985 Intrinsic radiosensitivity of human cell lines is correlated with radioresponsiveness of human tumors: analysis of 101 published survival curves *Int. J. Radiat. Oncol. Biol. Phys.* **11** 1699–707

Fertil B, Reydellet I and Deschavanne P J 1994 A benchmark of cell survival models using survival curves for human cells after completion of repair of potentially lethal damage *Radiat. Res.* **138** 61–9

Friedrich T, Durante M and Scholz M 2012a Modeling cell survival after photon irradiation based on double-strand break clustering in megabase pair chromatin loops *Radiat. Res.* **178** 385–94

Friedrich T, Scholz U, Elsässer T, Durante M and Scholz M 2013 Systematic analysis of RBE and related quantities using a database of cell survival experiments with ion beam irradiation *J. Radiat. Res.* **54** 494–514

Friedrich T, Scholz U, Elsässer T, Durante M and Scholz M 2012b Calculation of the biological effects of ion beams based on the microscopic spatial damage distribution pattern *Int. J. Radiat. Biol.* **88** 103–7

Furusawa Y *et al* 2000 Inactivation of aerobic and hypoxic cells from three different cell lines by accelerated 3He-, 12C- and 20Ne-Ion beams *Radiat. Res.* **154** 485–96

Garcia L M, Wilkins D E and Raaphorst G P 2007 Alpha/beta ratio: a dose range dependence study *Int. J. Radiat. Oncol. Biol. Phys.* **67** 587–93

Gerweck L E and Kozin S V 1999 Relative biological effectiveness of proton beams in clinical therapy *Radiother. Oncol.* **50** 135–42

Goodhead D T 2006 Energy deposition stochastics and track structure: what about the target? *Radiat. Prot. Dosim.* **122** 3–15

Grassberger C, Trofimov A, Lomax A and Paganetti H 2011 Variations in linear energy transfer within clinical proton therapy fields and the potential for biological treatment planning *Int. J. Radiat. Oncol. Biol. Phys.* **80** 1559–66

Grün R *et al* 2012 Impact of enhancements in the local effect model (LEM) on the predicted RBE-weighted target dose distribution in carbon ion therapy *Phys. Med. Biol.* **57** 7261–74

Guerrero M and Li A X 2004 Extending the linear-quadratic model for large fraction doses pertinent to stereotactic radiotherapy *Phys. Med. Biol.* **49** 4825–35

Gunzert-Marx K, Iwase H, Schardt D and Simon R S 2008 Secondary beam fragments produced by 200 MeVu^{-1} ^{12}C ions in water and their dose contributions in carbon ion radiotherapy *New J. Phys.* **10** 075003

Hawkins R B 1994 A statistical theory of cell killing by radiation of varying linear energy transfer *Radiat. Res.* **140** 366–74

Hawkins R B 1996 A microdosimetric-kinetic model of cell death from exposure to ionizing radiation of any LET, with experimental and clinical applications *Int. J. Radiat. Biol.* **69** 739–55

Inaniwa T *et al* 2010 Treatment planning for a scanned carbon beam with a modified microdosimetric kinetic model *Phys. Med. Biol.* **55** 6721–37

Jones B, Wilson P, Nagano A, Fenwick J and McKenna G 2012 Dilemmas concerning dose distribution and the influence of relative biological effect in proton beam therapy of medulloblastoma *Br. J. Radiol.* **85** e912–8

Kanai T *et al* 2006 Examination of GyE system for HIMAC carbon therapy *Int. J. Radiat. Oncol. Biol. Phys.* **64** 650–6

Kiefer J and Straaten H 1986 A model of ion track structure based on classical collision dynamics *Phys. Med. Biol.* **31** 1201–9

Krämer M and Jäkel O 2005 Biological dose optimization using ramp-like dose gradients in ion irradiation fields *Phys. Medica* **21** 107–11

Krämer M, Jäkel O, Haberer H, Kraft G, Schardt D and Weber U 2000 Treatment planning for heavy-ion radiotherapy: physical beam model and dose optimization *Phys. Med. Biol.* **45** 3299–317

Krämer M and Scholz M 2000 Treatment planning for heavy-ion radiotherapy: calculation and optimization of biologically effective dose *Phys. Med. Biol.* **45** 3319–30

Lühr A, Hansen D C, Teiwes R, Sobolevsky N, Jäkel O and Bassler N 2012 The impact of modeling nuclear fragmentation on delivered dose and radiobiology in ion therapy *Phys. Med. Biol.* **57** 5169–85

Moiseenko V V, Hamm R N, Waker A J and Prestwich W V 2001 Calculation of radiation-induced DNA damage from photons and tritium beta-particles: part II. Tritium RBE and damage complexity *Radiat. Environ. Biophys.* **40** 23–31

Mozumder A 2007 Track-core radius of charged particles at relativistic speed in condensed media *J. Chem. Phys.* **60** 1145–48

Neary G J, Evans H J, Tonkinson S M and Williamson F S 1959 The relative biological efficiency of single doses of fast neutrons and gamma-rays on Vicia faba roots and the effect of oxygen: part III. Mitotic delay *Int. J. Radiat. Biol.* **1** 230–40

Neumaier T *et al* 2012 Evidence for formation of DNA repair centers and dose-response nonlinearity in human cells *Proc. Natl Acad. Sci. USA* **109** 443–8

Nikjoo H, O'Neill P, Goodhead D T and Terrissol M 1997 Computational modelling of low-energy electron-induced DNA damage by early physical and chemical events *Int. J. Radiat. Biol.* **71** 467–83

Paganetti H, Niemierko A, Ancukiewicz M, Gerweck L E, Goitein M, Loeffler J S and Suit H D 2002 Relative biological effectiveness (RBE) values for proton beam therapy *Int. J. Radiat. Oncol. Biol. Phys.* **53** 407–21

Prise K M, Pinto M, Newman H C and Michael B D 2001 A review of studies of ionizing radiation-induced double-strand break clustering *Radiat. Res.* **156** 572–76

Rossi H H and Zaider M 1996 *Microdosimetry and its Application* (Berlin: Springer)

Sato T and Furusawa Y 2012 Cell survival fraction estimation based on the probability densities of domain and cell nucleus specific energies using improved microdosimetric kinetic models *Radiat. Res.* **178** 341–56

Scholz M and Elsässer T 2007 Biophysical models in ion beam radiotherapy *Adv. Space Res.* **40** 1381–91

Scholz M, Kellerer A M, Kraft-Weyrather W and Kraft G 1997 Computation of cell survival in heavy ion beams for therapy: the model and its approximation *Radiat. Environ. Biophys.* **36** 59–66

Scholz M, Matsufuji N and Kanai T 2006 Test of the local effect model using clinical data: tumour control probability for lung tumours after treatment with carbon ion beams *Radiat. Prot. Dosim.* **122** 478–9

Schulz-Ertner D *et al* 2007 Effectiveness of carbon ion radiotherapy in the treatment of skull-base chordoma *Int. J. Radiat. Oncol. Biol. Phys.* **68** 449–57

Shao C, Saito M and Yu Z 1999 Formation of single- and double-strand breaks of pBR322 plasmid irradiated in the presence of scavengers *Radiat. Environ. Biophys.* **38** 105–9

Steel G G and Peacock J H 1989 Why are some human tumours more radiosensitive than others? *Radiother. Oncol.* **15** 63–72

Stenerlöw B, Karlsson K H, Cooper B and Rydberg B 2003 Measurement of prompt DNA double-strand breaks in mammalian cells without including heat-labile sites: results for cells deficient in nonhomologous end joining *Radiat. Res.* **159** 502–10

Suzuki M, Kase Y, Yamaguchi H, Kanai T and Ando K 2000 Relative biological effectiveness for cell-killing effect on various human cell lines irradiated with heavy-ion medical accelerator in Chiba (HIMAC) carbon-ion beams *Int. J. Radiat. Oncol. Biol. Phys.* **48** 241–50

Tobias CA 1985 The repair–misrepair model in radiobiology: comparison to other models *Radiat. Res. Suppl.* **8** S77–95

Tsujii H and Kamada T 2012 A review of update clinical results of carbon ion radiotherapy *Japan J. Clin. Oncol.* **42** 670–85

Yokota H *et al* 1995 Evidence for the organization of chromatin in megabase pair-sized loops arranged along a random walk path in the human G0/G1 interphase nucleus *J. Cell. Biol.* **130** 1239–49

Physical and biological factors determining the effective proton range

Rebecca Grün
Department of Biophysics, GSI Helmholtzzentrum für Schwerionenforschung, Darmstadt 64291, Germany; Institute of Medical Physics and Radiation Protection, University of Applied Sciences Gießen, Gießen 35390, Germany; and Medical Faculty of Philipps-University Marburg, Marburg 35032, Germany

Thomas Friedrich and Michael Krämer
Department of Biophysics, GSI Helmholtzzentrum für Schwerionenforschung, Darmstadt 64291, Germany

Klemens Zink
Institute of Medical Physics and Radiation Protection, University of Applied Sciences Gießen, Gießen 35390, Germany and Department of Radiotherapy and Radiation Oncology, University Medical Center Giessen and Marburg, Marburg 35043, Germany

Marco Durante
Department of Biophysics, GSI Helmholtzzentrum für Schwerionenforschung, Darmstadt 64291, Germany and Department of Condensed Matter Physics, Darmstadt University of Technology, Darmstadt 64289, Germany

Rita Engenhart-Cabillic
Medical Faculty of Philipps-University Marburg, Marburg 35032, Germany and Department of Radiotherapy and Radiation Oncology, University Medical Center Giessen and Marburg, Marburg 35043, Germany

Michael Scholz[a)]
Department of Biophysics, GSI Helmholtzzentrum für Schwerionenforschung, Darmstadt 64291, Germany

(Received 27 June 2013; revised 19 September 2013; accepted for publication 20 September 2013; published 11 October 2013)

Purpose: Proton radiotherapy is rapidly becoming a standard treatment option for cancer. However, even though experimental data show an increase of the relative biological effectiveness (RBE) with depth, particularly at the distal end of the treatment field, a generic RBE of 1.1 is currently used in proton radiotherapy. This discrepancy might affect the effective penetration depth of the proton beam and thus the dose to the surrounding tissue and organs at risk. The purpose of this study was thus to analyze the impact of a tissue and dose dependent RBE of protons on the effective range of the proton beam in comparison to the range based on a generic RBE of 1.1.
Methods: Factors influencing the biologically effective proton range were systematically analyzed by means of treatment planning studies using the Local Effect Model (LEM IV) and the treatment planning software TRiP98. Special emphasis was put on the comparison of passive and active range modulation techniques.
Results: Beam energy, tissue type, and dose level significantly affected the biological extension of the treatment field at the distal edge. Up to 4 mm increased penetration depth as compared to the depth based on a constant RBE of 1.1. The extension of the biologically effective range strongly depends on the initial proton energy used for the most distal layer of the field and correlates with the width of the distal penumbra. Thus, the range extension, in general, was more pronounced for passive as compared to active range modulation systems, whereas the maximum RBE was higher for active systems.
Conclusions: The analysis showed that the physical characteristics of the proton beam in terms of the width of the distal penumbra have a great impact on the RBE gradient and thus also the biologically effective penetration depth of the beam. [http://dx.doi.org/10.1118/1.4824321]

Key words: proton radiotherapy, biologically effective range, RBE, LEM, treatment planning, distal penumbra

1. INTRODUCTION

Proton beam therapy is becoming a clinical standard treatment procedure in radiotherapy for specific types of cancer which are difficult to treat with surgery or conventional radiotherapy with photons. Protons are known for their superior depth dose profile compared to x-rays, and their tissue sparing effects make them particularly suitable for tumors located close to critical structures. The biological effectiveness of protons in tissue has been shown to be on average very similar to that of x-rays for *in vivo* endpoints[1] and most of their path which is why a constant relative biological effectiveness (RBE) of 1.1 is used in clinical practice.[2]

Nevertheless, *in vitro* studies show that even protons have an increased RBE at the end of their range, which significantly exceeds 1.1 depending on the tissue type.[3] There are only

few experiments which determined a RBE at the distal end of the extended Bragg peak, but nearly all showed an increase, which clearly exceeds 1.1.[4–10] This increase of the RBE can be explained by the sharply increasing linear energy transfer (LET) at the distal edge of the spread-out Bragg peak (SOBP), which consequently leads to an extension of the effective proton range as described, e.g., by Larsson and Kihlman,[11] Sweet *et al.*,[12] and Robertson *et al.*[4] The major deviation from a constant RBE of 1.1 thus occurs at the distal field end and strongest in the distal edge of the Bragg peak. The resulting biological extension can be of special concern for organs at risk (OAR) located close to treated tumors, especially if the beam is directed toward the critical structure. Moreover, as in general for high-LET radiation, the tissue type and dose level are expected to have significant impact on the RBE and thus also on the extension of the effective range as also shown by Carabe *et al.*[13]

The Local Effect Model (LEM) in its recently published version (LEM IV) (Refs. 14 and 15) has shown to be suitable to predict tissue and energy dependent RBE values not only for carbon ions but also for protons and other clinically relevant ions. In the present work, we thus use the LEM IV for a systematic analysis of the factors influencing the biological range extension. We first analyze the impact of the biological characteristic of a given tissue and physical parameters such as dose, dimension, and depth of the SOBP on the extension of the effective range. Special attention is then turned to the influence of the physical beam characteristics on the biological extension and the subsequent systematics by comparing different beam delivery methods, i.e., active and passive beam delivery. We finally discuss the potential impact of these factors in clinical cases, where the range extension might be of concern for the dose delivered to the surrounding tissue.

2. MATERIALS AND METHODS

2.A. Treatment planning

To investigate the biologically effective range of protons, idealized target geometries (cubes) placed in a simulated water phantom were used to facilitate the systematic analysis. The cubic volume has a fixed lateral dimension of 50×50 mm^2 but varies in its dimension along the beam axis. Treatment plans consisted of only one field to most clearly illustrate the range extension. The treatment planning system TRiP98 was used to optimize the physical dose distribution.[16–18]

As proton treatments can utilize active or passive range modulation, both modalities were simulated. For active range modulation,[19] the primary beam energy was varied in order to shift the Bragg peaks in depth, for example, used at the Heidelberg Ion-Beam Therapy Center (HIT). For passive range modulation, a range shifter was simulated. With the range shifter modality, only single primary proton energies are used and polymethyl methacrylate (PMMA) plates are positioned in between the beam exit window and target area to degrade the beam energy and shift the Bragg peak in depth.[20] Note that with active range modulation the energies used depend on the location and dimension of the target volume whereas the passive range modulation uses one fixed energy. We thus simulated typical energies used in proton beam therapy with the passive modality, i.e., 160 and 235 MeV as well as monoenergetic beams from 71 to 220 MeV. However, the details of the beam characteristic at different institutions are expected to be accelerator and beam line dependent, and thus the analysis presented here mainly focuses on the general aspects of the range modulation technique rather than a detailed facility-dependent beam description.

Note that within this paper the terms "active" and "passive" only refer to the range modulation technique. Concerning the lateral extension of the treatment field for both range modulation modalities, a spot scanning technique via horizontal and vertical deflection of the beam was simulated. The dose levels were chosen from 1 to 10 Gy absorbed dose to cover the whole clinically relevant range of dose prescriptions including hypofractionation.

2.B. RBE data

Biological optimization with TRiP98 requests RBE input data, which are calculated with the LEM. The basic principle of the LEM is to derive the biological effectiveness of ion beam radiation from a combination of the known dose response curve for photon radiation with the description of the microscopic dose deposition pattern of individual particle tracks.[14,21–23] For the prediction of the RBE, the latest version of the LEM (LEM IV) was used, which has been shown in a previous publication[14] to predict the RBE over a wide range of particles from protons to carbon ions with sufficient accuracy. The LEM can be used to precalculate RBE values for all projectiles from protons to neon in the energy range from 0.1 to 1000 MeV/u, which characterize the RBE for the initial slope of the dose response curves and are stored in a so-called "RBE-table". These precalculated values are used as input for the TRiP98 treatment planning system, which determines actual RBE values based on the mixed composition of the radiation field and the dose in each voxel of the treatment volume.[17,24]

The biological input parameters of the LEM are the parameters α_γ, β_γ, and D_t describing the photon dose-response curves according to a modified linear-quadratic model. This modification is characterized by a transition to a linear shape for doses larger than D_t,[21] which is consistent with the linear-quadratic-linear model as proposed by Astrahan[25] with

$$S(D) = \begin{cases} e^{-(\alpha_\gamma D + \beta_\gamma D^2)} & \text{for } D < D_t \\ e^{-(\alpha_\gamma D_t + \beta_\gamma D_t^2 + s_{\max}(D - D_t))} & \text{for } D \geq D_t \end{cases}, \quad (1)$$

where $s_{\max} = \alpha_\gamma + 2\beta_\gamma D_t$ is the maximum slope of the photon dose response curve for doses larger than D_t. All other parameters of the LEM are kept constant and were chosen as described in Elsässer *et al.*[14]

In a first step, it was demonstrated that the combination of LEM and TRiP98 actually allows to accurately predict the variation of RBE along the SOBP for proton beams. Therefore, the model predictions were validated by comparison

TABLE I. Input parameters for the RBE tables.

RBE table	α_γ (Gy^{-1})	β_γ (Gy^{-2})	$\alpha_\gamma/\beta_\gamma$ (Gy)	D_t (Gy)
AB6.5[a]	0.16	0.0246	6.5	13
AB47.5	0.57	0.012	47.5	15
AB2	0.1	0.05	2	8
AB10	0.5	0.05	10	14

[a]AB is the abbreviation for the photon $\alpha_\gamma/\beta_\gamma$-ratio with the number representing its value.

with two sets of experimental RBE data obtained for different cell lines with significantly different sensitivities. Tang *et al.*[7] measured the RBE for survival of Chinese hamster ovary (CHO) cells exposed to doses of 1, 2, 4, 6, and 8 Gy and at different depth positions of 2, 10, 18, and 23 mm, using a 65 MeV proton beam to produce a SOBP with about 17.5 mm extension located between approximately 10 and 27.5 mm depth. As input parameters for the model calculations, the photon parameters obtained with Cs-137 gamma rays given in Tang *et al.*[7] together with a D_t of 13 Gy for the RBE table AB6.5 (Table I) were used.

Bettega *et al.*[8] determined the RBE for the survival of SCC25 cells derived from human squamous cell carcinoma of the tongue in a 65 MeV modulated proton beam of 15 mm extension. The corresponding photon input parameters, as given in Bettega *et al.*[8] for Co-60 gamma rays, together with a D_t of 15 Gy, were used for the RBE table AB47.5 (Table I). For the two simulated SOBP, a bolus of 5.9 mm was used to adapt the position of the Bragg peak in depth; this accounts for facility- and beam line specific details not taken into account in this simulation study.

For the systematic studies regarding the biological range extension, two different RBE tables were used (Table I). The RBE tables describe two hypothetical cell or tissue types with an $\alpha_\gamma/\beta_\gamma$-ratio of 2 Gy (AB2), characteristic for rather radioresistant late responding cell or tissue types, and with an $\alpha_\gamma/\beta_\gamma$-ratio of 10 Gy (AB10), characteristic for rather radiosensitive early responding cell or tissue types.[26] The parameter settings are typical for *in vitro* cell survival assays, where a change of the $\alpha_\gamma/\beta_\gamma$-ratio usually goes along with a change of α_γ rather than of β_γ. The parameter D_t was adapted according to an empirical approximated linear relation between $\alpha_\gamma/\beta_\gamma$-ratio and D_t. This relation was found empirically when using the LEM over a huge set of experimental cell survival data.[27]

2.C. Determination of the biologically effective range

The biological range extension was quantified by taking into account the RBE predicted by the LEM IV for different dose-levels and biological endpoints described by the $\alpha_\gamma/\beta_\gamma$-ratio. As a reference dose distribution, we optimized a physical absorbed dose and calculated the corresponding RBE-weighted dose with constant RBE of 1.1; the depth where the RBE-weighted dose decreased to 80% of the prescribed RBE-weighted dose, i.e., $d_{80}^{\mathrm{cRBE}} = 0.8 \cdot d_{\mathrm{prescr}}^{\mathrm{cRBE}}$ was used to determine the corresponding biologically effective

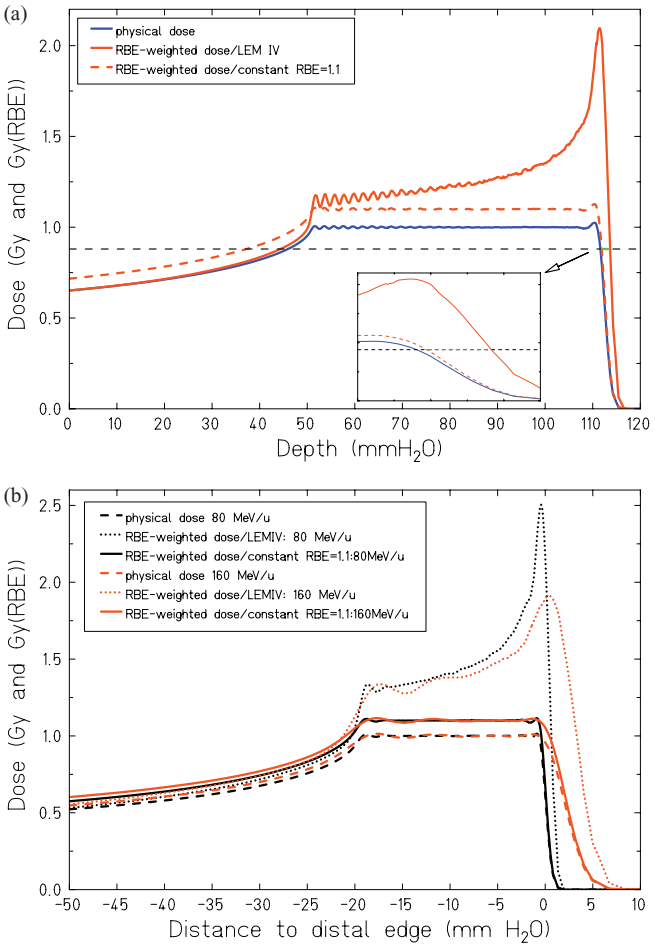

FIG. 1. (a) Schematic example for the difference R_{80}^{diff} between biological range for constant RBE = 1.1 and variable RBE. The black dashed line corresponds to the d_{80}^{cRBE}. (b) Schematic comparison of the range extension for two initial proton energies of 80 and 160 MeV. For 160 MeV, a water equivalent absorber was simulated in order to shift the distal end of the SOBP to the same position as for 80 MeV.

range R_{80}^{cRBE}. The 80% isodose d_{80} was chosen according to considerations of Gottschalk[28] where it was stated that the distal d_{80} is a well suited value to describe the range of the proton beam since it is independent of the energy spread of a certain beam and reflects the mean projected range of the protons.[28,13] Figure 1(a) schematically shows the biological range extension due to a variable RBE with depth indicated by the green line segment.

In analogy to the reference value, the biologically effective range in the case of a variable RBE, R_{80}^{varRBE}, was also determined from the position where the RBE-weighted dose decreases to the reference value of $d^{\mathrm{varRBE}} = d_{80}^{\mathrm{cRBE}} = 0.8 \cdot d_{\mathrm{prescr}}^{\mathrm{cRBE}}$ as defined above for the case of constant RBE. The biological extension, i.e., the difference in biological range predicted by the LEM IV as compared to the case of a constant RBE is then calculated as $R_{80}^{\mathrm{diff}} = R_{80}^{\mathrm{varRBE}} - R_{80}^{\mathrm{cRBE}}$.

The biological extensions were determined for the RBE tables AB2 and AB10 (Table I) together with all the previously described settings and field arrangements. Moreover, the biological extension was determined for monoenergetic

Bragg peaks ranging from 71 to 220 MeV optimized to different dose levels and covering penetration depths from approximately 50 to 300 mm. For the monoenergetic Bragg peaks, the peak defines the dose level and the R_{80}^{diff} is determined as described above.

Furthermore, the influence of the width of the 80/20 distal penumbra of the Bragg peak on the biological extension was investigated. The width is defined as the difference in penetration depth from the 80% isodose (percentage of the prescribed dose) to the 20% isodose.[2] Note that the symbols in Figs. 3–6 correspond to simulated data points and the corresponding lines are empirical best fit-curves to the data points with the aim to guide the eye. Figure 1(b) demonstrates the difference in the width of the distal edge of the Bragg peak using different energies to modulate the SOBP. Due to momentum spread and range straggling effects (scattering and range modulation components in the nozzle), which are more prominent for higher energies, the 80/20 distal penumbra increases with increasing energy.[29]

Finally, the RBE at the position of the maximum RBE-weighted dose was evaluated to investigate the correlation with the width of the 80/20 distal penumbra. The RBE at maximum RBE-weighted dose was chosen because it is a measure for the highest effect in the tissue. To choose the maximum RBE would be not suitable since the RBE further increases throughout the distal penumbra and is highest for infinitesimal doses which go along with high uncertainties. The ranges R_{80}^{cRBE} and R_{80}^{varRBE} were determined along the central axis of the beam using TRiP98.

3. RESULTS

3.A. Comparison with experimental RBE measurements along depth

Figure 2(a) shows the RBE measurements reported by Tang *et al.*[7] with CHO cells in different depths for 1, 2, 4, 6, and 8 Gy, respectively. The model predictions based on the RBE table AB6.5 are in accordance with the experimentally observed RBE within the SOBP; the RBE is slightly underestimated by the model in the entrance region.

Figure 2(b) shows the RBE measurements reported by Bettega *et al.*[8] with the SCC25 cell line in different depth positions including the declining edge for 2, 5, and 7 Gy, respectively. The RBE prediction is based on the RBE-table AB47.5 for a 65 MeV modulated proton beam. Only a minor dose dependence, but still a strong increase of RBE at the declining edge, is observed.

Since in both cases a good agreement of the model predictions and experimental data was observed, the accuracy of the model was considered to be sufficient for the systematic analysis described in Secs. 3.B and 3.C.

3.B. The biologically effective range

We systematically analyzed the impact of the increased RBE of low energetic protons on the extension of the effective range considering various physical and biological parameters:

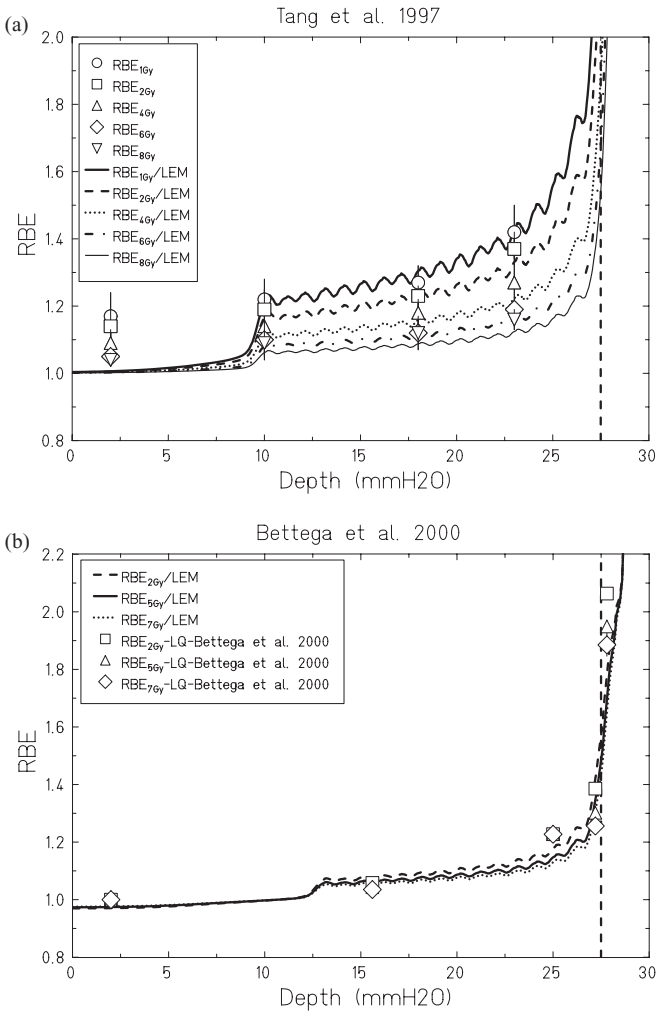

FIG. 2. (a) RBE predicted by the LEM for CHO cells based on RBE table AB6.5 (Table I) (lines). The symbols correspond to the RBE values measured by Tang *et al.* (Ref. 7) for CHO cells at different positions of a passively modulated 17.5 mm SOBP with a pristine energy of 65 MeV for different physical dose levels in the SOBP of 1, 2, 4, 6, and 8 Gy. (b) RBE predictions by the LEM for SCC25 cells based on RBE table AB47.5 (lines). The symbols correspond to the RBE values measured by Bettega *et al.* (Ref. 8) at different positions of a passively modulated 15 mm SOBP with a pristine energy of 65 MeV for different physical dose levels of 2, 5, and 7 Gy in the SOBP. The vertical dashed line in both plots indicates the depth at which the dose drops to d_{80}^{cRBE} in the case of a constant RBE.

- The dose level
- The extension and position in depth of the target volume
- The range modulation technique (active and passive)
- The tissue type as characterized by the $\alpha_\gamma/\beta_\gamma$-ratio for photon irradiation.

Figure 3 shows the biological range extension dependent on the dose for target volumes all having the same proximal end (a) and target volumes all having the same distal end but differing in their depth dimension (b). The calculation was performed using the active range modulation method with different energies to cover the target volume. Independent from the dimension of the SOBP, only minor differences are observed when the distal end of the spread out Bragg peak is positioned at the same depth. In contrast, target geometries of

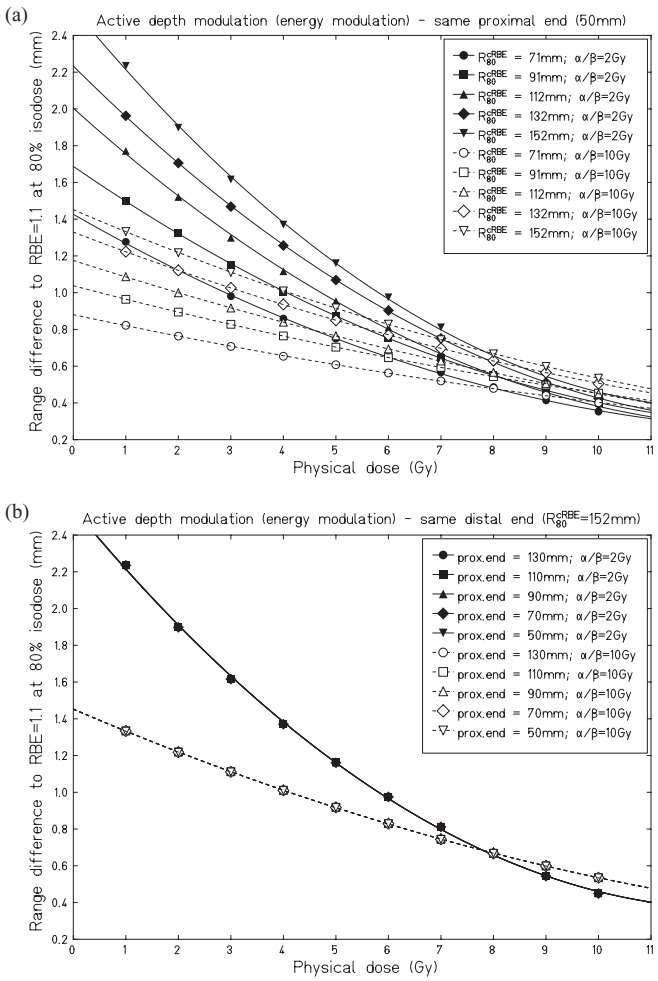

FIG. 3. Dose dependent biological range difference R_{80}^{diff} for different target depth dimensions from 20 to 100 mm for active beam modulation with same proximal end at 50 mm but different R_{80}^{cRBE} (a) and same R_{80}^{cRBE} at 152 mm but different proximal end (b). The solid symbols correspond to an $\alpha_\gamma/\beta_\gamma$-ratio of 2 Gy and the open symbols to an $\alpha_\gamma/\beta_\gamma$-ratio of 10 Gy, in (b) the curves lie on top of each other. Note that here and in subsequent figures the symbols represent the simulated data points and the lines are empirical best fit-curves to the data points with the aim to guide the eye.

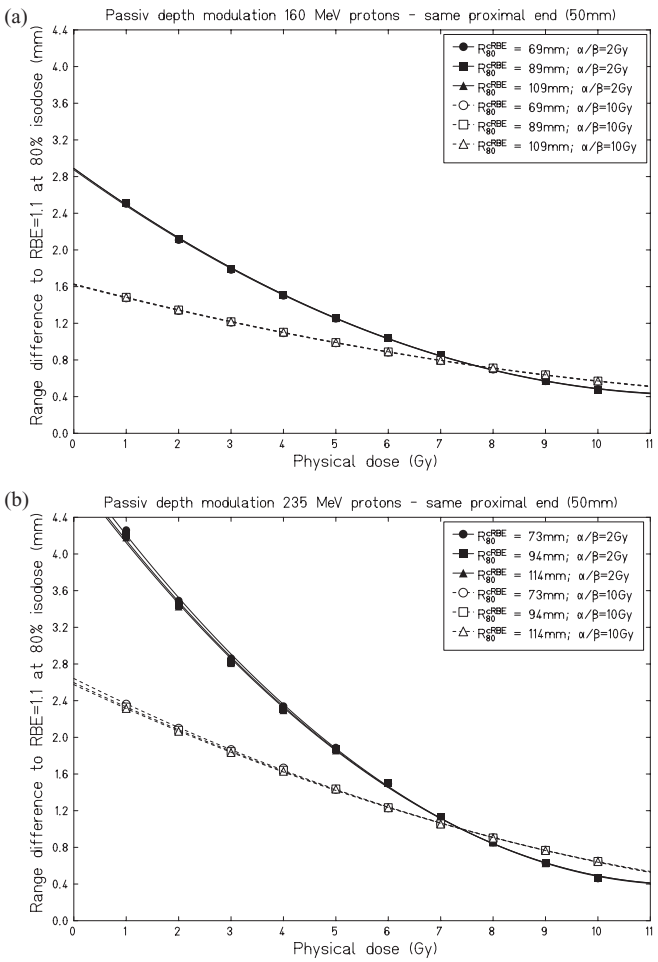

FIG. 4. Dose dependent biological range difference for different target depth dimensions in depth from 20 to 60 mm using the passive range modulation with the same proximal end at 50 mm but different distal ends R_{80}^{cRBE} for initial energies of 160 (a) and 235 MeV (b). The solid symbols correspond to an $\alpha_\gamma/\beta_\gamma$-ratio of 2 Gy and the open symbols to an $\alpha_\gamma/\beta_\gamma$-ratio of 10 Gy. Note that the curves for the different dimensions lie on top of each other.

the same dimension with the distal end positioned in different depth (same proximal end) show large variations in the biologically effective range extension.

For passive range modulation, a bolus was simulated to shift the proximal end of the SOBP to the same position in depth when using different energies. As shown in Fig. 4, the biological extension is largely different when comparing the different initial energies of 160 and 235 MeV, respectively. This demonstrates that the biological extension is not explicitly depth dependent, but the primary energy determines the effect. The difference between the active and the passive modulation results from the difference to vary the penetration depth of the primary beam. In the first case, the penetration depth of the primary beam is varied using different initial energies (Fig. 3) whereas in the second case the penetration depth is varied placing material behind the beam exit window (Fig. 4), leading to more pronounced range straggling.

The fact that the biological extension of the beam does not depend on the extension of the target volume, but seems to primarily depend on the initial energy indicates that the biological range extension is mainly determined by the width of the 80/20 distal penumbra. We thus analyzed the correlation of the biological extension with the width of the 80/20 distal penumbra using monoenergetic Bragg peaks with different initial energies ranging from 71 to 220 MeV.

Figure 5(a) illustrates the biological range extension dependent on the 80/20 distal penumbra. Variation of the distal penumbra is achieved by variation of the energy from 71 to 220 MeV, and with increasing energy an increase of the distal penumbra is observed due to a more pronounced range straggling. The increasing distal penumbra is connected to an increased extension of the biologically effective range, which is most pronounced for low doses, low $\alpha_\gamma/\beta_\gamma$-ratios, and high energies as used for deep seated tumors, i.e., 235 MeV, where range differences exceeding 4 mm are observed [Fig. 4(b)]. The extension of the biologically effective range emerges due to a competition between the decreasing dose and increasing

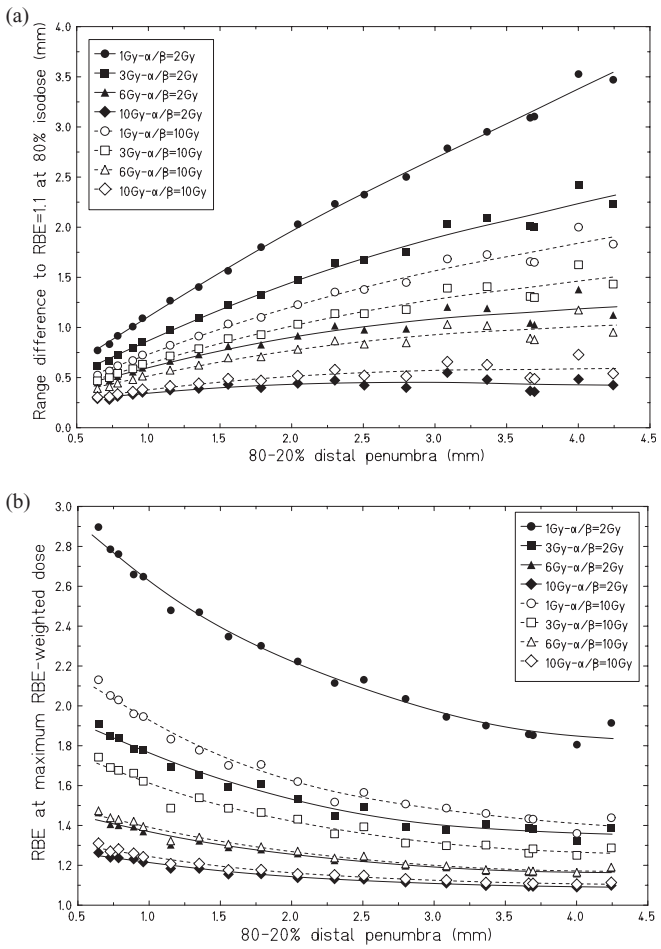

FIG. 5. Biological range difference (a) and RBE at maximum RBE weighted dose (b) vs the distal penumbra for different physical dose levels of 1, 3, 6, and 10 Gy. The data points represent the distal penumbra for energies from 71 to 220 MeV. The solid symbols correspond to an $\alpha_\gamma/\beta_\gamma$-ratio of 2 Gy and the open symbols to an $\alpha_\gamma/\beta_\gamma$-ratio of 10 Gy.

RBE. Decreasing initial energy accompanies a steeper dose penumbra and leads to a higher LET and thus maximum RBE at the distal part of the SOBP [Fig. 5(b)]. Simultaneously, the LET gradient in the distal penumbra of the dose distribution becomes steeper and covers a smaller region in depth, and correspondingly the biological range extension becomes less pronounced [Fig. 5(a)]. Figure 5 thus demonstrates that the RBE at maximum RBE-weighted dose is anticorrelated with the width of the 80/20 distal penumbra, whereas the biological range extension correlates with the 80/20 distal penumbra.

3.C. Influence of the reference isodose

The range of the proton beam is a matter of definition. In the clinical routine, the range of the proton beam in water is defined at the distal 90% isodose.[2,30] In this study, the 80% isodose is used as reference for the biological range extension. The 80% isodose is a good compromise to describe the biological spread of the beam since it reflects the extension of the high dose region at the distal end as well as for the physical properties.[28] Figure 6 shows the influence of the isodose

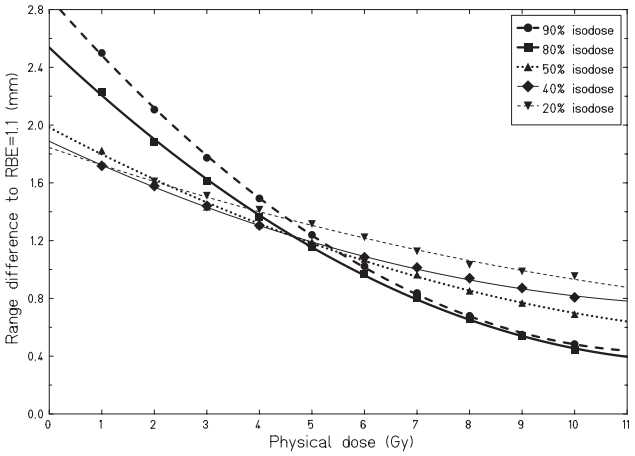

FIG. 6. Difference in biological range extension of the proton beam for range definitions based on various isodoses from 90% to 20%. The differences are shown for a target volume of 100 mm depth dimension with the R_{80}^{cRBE} at 152 mm which corresponds to an energy of ~150 MeV. The assumed $\alpha_\gamma/\beta_\gamma$-ratio is 2 Gy.

level used for the proton range definition on the biological range extension with different reference isodoses from 90% to 20%. The choice of the reference isodose matters mainly for small doses where the largest deviations are observed in the predicted biological range difference between the reference isodoses.

4. DISCUSSION

4.A. Relevance of a variable RBE

With the increasing interest in protons as a promising treatment modality for cancer radiotherapy, an accurate prediction of the increased biological effectiveness and assessment of the associated uncertainties becomes important. Two aspects especially have to be considered here:

- The increased RBE-weighted dose observed at the distal end of the SOBP
- The extension of the RBE-weighted depth-dose profile due to the rise of RBE in the distal penumbra.

Due to the competition between increasing RBE with depth and decreasing dose, the position of the maximum RBE-weighted dose and maximum RBE typically do not coincide; the maximum RBE-weighted dose is reached close to the end of the SOBP, whereas the maximum RBE is found beyond that position at low doses in the penumbra region of the dose distribution.[8,31]

Experiments which focus on the measurement of RBE along the proton SOBP typically aim at the determination of the maximum RBE-weighted dose, since this is of particular interest with respect to constraints concerning the tolerance of normal tissues located close to the distal end of the treatment field. Many *in vitro* experiments indicate a rise of RBE at the distal end significantly above the clinically used value of 1.1.[4–10] However, the experimentally determined RBE in the distal edge is associated with large uncertainties since the

measurement is very difficult due to the steep dose and LET gradient.

Because of uncertainties in the systematic description of this increased RBE, e.g., in terms of dose level and tissue characteristics, a detailed depth dependence is currently not taken into account in clinical practice.[3,1] Instead, situations are avoided where an increased RBE could lead to unacceptable high normal tissue doses, and consequently the potential advantages of proton beams cannot be fully exploited yet. Therefore, there is a clear need to make progress in the detailed analysis of the factors influencing the RBE in proton beams and to take them into account in treatment planning.[32–35] Biophysical models are valuable in that respect because they allow extrapolation to situations that are difficult to exploit experimentally. However, thorough validation of a model by means of available experimental data is of course required before it can be used for this extrapolation.

4.B. Validation of the LEM for proton irradiation

For the analysis presented here, we used the LEM IV that has been demonstrated to accurately predict the biological effectiveness of protons for a typical clinical treatment scenario.[14] However, a more detailed analysis is desirable to further validate the model with respect to the dependencies of RBE on the depth position in the SOBP, the dose level and the cell or tissue type under consideration. We have thus compared the model prediction along the SOBP to two data sets reported by Tang *et al.*[7] and Bettega *et al.*[8] for CHO and SCC25 cells, respectively.

For both cellular systems, in general a very good agreement between model prediction and experimental data has been achieved for different dose levels and different positions within the SOBP. In the entrance region, the LEM somewhat underestimates the RBE in the case of CHO cells. This might be traced back to the contribution of secondary recoil protons induced in the target material, which are not taken into account in the current version of the treatment planning system. Other studies[36,37] have shown that this contribution could lead to about 8% higher RBE values in the entrance region. In contrast to CHO cells, for SCC25 good agreement is also observed in the entrance region. However, because of the generally lower RBE values for SCC25 as compared to CHO cells, this cell system might not be sufficiently sensitive to detect this subtle difference. Anyhow, the observed underestimation of the RBE in the entrance channel has no influence on the agreement of the RBE prediction in the distal end and penumbra and thus is not of concern for the estimated biological range extension.

4.C. Impact of dose and tissue type on the biological range extension

Because of its good agreement with measured RBE values, the LEM is suitable to analyze in detail the extension of the biologically effective range that results from a variable RBE as compared to a constant RBE value of 1.1. In general, according to the LEM prediction the extension is expected to be more pronounced for tissues characterized by a low $\alpha_\gamma/\beta_\gamma$-ratio as compared to tissues with a high $\alpha_\gamma/\beta_\gamma$-ratio. The difference is most significant at low doses and gets smaller with increasing dose. We did not focus on the sensitivity of the threshold dose D_t since we adapted the parameter according to an empirical relation between the $\alpha_\gamma/\beta_\gamma$-ratio and D_t found by Friedrich *et al.*[27] Apparently, a variation of D_t accompanies a RBE variation which also influences the biological range extension. However, in the case of protons, the RBE is rather robust for a D_t variation and the main determinant for the RBE remains the $\alpha_\gamma/\beta_\gamma$-ratio.

These general trends are in line with the results recently published by Carabe *et al.*[13] They also analyzed the biological range extension, but used another empirical model for the calculation of RBE values[38] and a different evaluation method for the biological range difference based on the differences becoming apparent in the dose-volume histogram (DVH). However, this evaluation method is not too different from the central axis approach we used due to the fact that we as well as Carabe *et al.*[13] consider idealized target geometries (cubes) in our analysis. We thus expect no differences since deviations in the DVH are only due to the biological range extension at the distal end. Their results also indicate a dose dependence of the range extension, although this dose dependence seems significantly less pronounced as in our case. Similarly, Carabe *et al.*[13] also demonstrate a tissue dependence of the range extension, where for small $\alpha_\gamma/\beta_\gamma$-ratios the range extension is much more pronounced than for high $\alpha_\gamma/\beta_\gamma$-ratios. However, in this case, the results reported by Carabe *et al.*[13] differ not only quantitatively but also qualitatively from our results. Whereas in our analysis for all situations an increased extension as compared to the assumption of a constant RBE is found, in the analysis of Carabe *et al.*[13] in general negative extensions are found for higher $\alpha_\gamma/\beta_\gamma$-ratios, indicating that the corresponding RBE values in the distal penumbra are smaller than the reference value of 1.1. This is in contrast to our case, where RBE values always higher than 1.1 are predicted for all combinations of dose levels and $\alpha_\gamma/\beta_\gamma$-ratios that were analyzed.

Since the predicted extension obviously significantly depends on the model that is used for the RBE calculations, a detailed conceptual comparison of the different models and their underlying assumptions would be highly desirable. Although this detailed discussion would be beyond the scope of the present paper, we would like to address the main aspects that are likely to contribute most to the differences observed between the two models. For the LEM, according to the track structure properties, the minimum RBE value predicted for low LET protons is 1 [the slightly lower value of 0.97 observed in Fig. 2(b) for the very sensitive SCC25 cells is considered to be insignificant with respect to the magnitude and range of RBE values discussed here]. In contrast, the parameterization used by Carabe *et al.*[13] allows for RBE values substantially below 1 at low LET and in particular for higher $\alpha_\gamma/\beta_\gamma$-ratios; the limiting value for LET $\rightarrow$ 0 is reported to be 0.843. This difference is likely due to the fact that actually the RBE-LET relationship is not exactly linear in the LET range up to 20 keV/μm. The LEM predicts a vanishing

slope for the RBE-LET dependence in the limit of LET $\rightarrow$ 0, but then shows an overproportional increase toward the high LET values. A linear fit to such a bended curve would typically show an underestimation of the RBE at very low and high LET values, but an overestimation at intermediate LET values. A more thorough comparison to experimental data would however be required to analyze this aspect in detail. Furthermore, if for a given proton energy the LEM predicts RBE values greater than 1, the RBE values in general decrease with increasing dose. In contrast, although details depend on the LET and $\alpha_\gamma/\beta_\gamma$-ratios, according to the parameterization used by Carabe *et al.*[13] the maximum RBE values observed at low doses (RBE_{max}) can be smaller than the minimum RBE values (RBE_{min}) that represent the RBE values for D $\rightarrow \infty$. This corresponds to an inverted dose dependence of RBE as compared to the LEM prediction. Taken together, although the general trends like increase of RBE with increasing LET and decreasing $\alpha_\gamma/\beta_\gamma$-ratio are similarly predicted by both approaches, the RBE values along a SOBP might be systematically shifted in the model used by Carabe *et al.*[13] as a consequence of the above mentioned quantitative differences, and might show an inverted dose dependence of RBE for low LET values.

4.D. Impact of the dose gradient at the distal penumbra on the biological range extension

In our analysis, we showed that for different range modulation techniques significantly different range extensions are expected, and that these variations can be traced back to the gradient in the distal penumbra of the dose distribution. To our knowledge, this aspect has not been addressed in detail by other studies so far; they mainly focus on the maximum RBE-weighted dose in the distal edge and the consequential overdosage, which are of concern for the nearby OARs.[3,39] Nevertheless, the impact, e.g., of the full-width at half maximum (FWHM) of the proton peak on RBE effects in general has been recognized, but not been specifically analyzed in terms of the dose gradient at the distal penumbra. For example, Paganetti *et al.*[31] reported about the anticorrelation between the RBE_α (ratio of initial slopes, α_1/α_γ) at the maximum dose of pristine Bragg peaks for different beam energies and their corresponding FWHM. Surprisingly, although no supporting details are presented in this paper, the authors conclude that the biological extension "increases with decreasing initial proton energy," which is in contrast to our results. Furthermore, Paganetti and Schmitz[40] discuss the influence of beam modulation techniques on dose and RBE in proton radiation therapy. They show that the RBE gradient becomes less pronounced with increasing initial proton energy, but the aspect of range extension is not addressed in their paper.

In that respect, it might be important to emphasize that lower overall RBE values do not necessarily lead to a less pronounced biological extension of the SOBP. Instead, the range extension critically depends on the balance between increase of RBE and the dose gradient at the distal penumbra, as schematically illustrated in Fig. 7. If the dose gradient

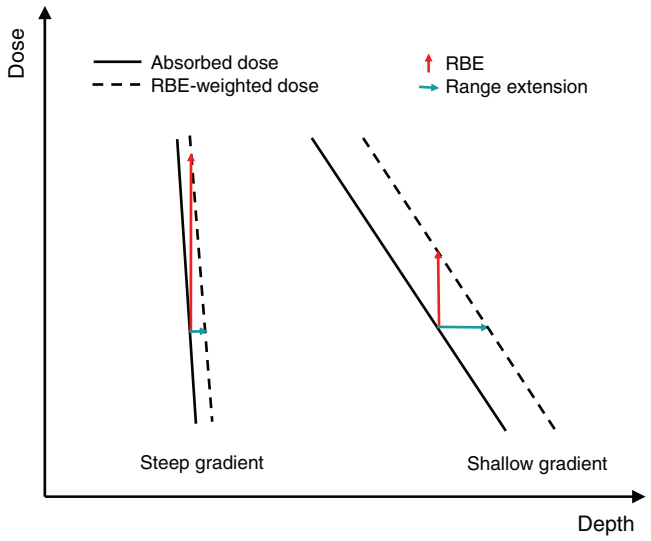

FIG. 7. Schematic example for the influence of the dose gradient at the distal penumbra on the biological range extension.

and with that the LET gradient is high, this results in comparably large RBE values. However, even a correspondingly large vertical shift of the depth-dose curve resulting from the high RBE values will not lead to a large longitudinal shift because of the high dose gradient. In contrast, for a shallower distal penumbra, the corresponding RBE values might be lower, but due to the inclination of the distal penumbra even a comparably small vertical shift can lead to a more pronounced longitudinal shift. This effect is, moreover, independent on the model used to predict the RBE.

Consequently, the biological range extension is also affected by the beam delivery method. In active range modulation techniques, in general, lower initial energies are used, leading to a higher gradient of the distal penumbra. This results in a high maximum RBE at the distal edge, but a smaller biological range extension. In contrast, passive range modulation techniques use higher initial energies, leading to a shallower gradient of the distal penumbra. In this case, smaller maximum RBE values but a more significant biological extension is expected. Nevertheless, it is primarily the resulting gradient that determines the biological extension, but not the exact technique that is used to generate the SOBP.

According to these considerations, the increased RBE of protons at the distal end shows up in any case, either as a comparably high RBE at the distal end of the SOBP or a large biological extension. Appropriate choice of the radiation modality allows shifting between these two options, but there seems to be no possibility to completely avoid the impact of RBE effects.

Moreover, the extension is expected to affect not only the distal penumbra, but also the lateral penumbra. However, it is expected that in the lateral direction the dose dependence of RBE is more important, whereas the contribution of the increase of LET is less pronounced, although the detailed

balance between these effects will also depend on the position in depth.

4.E. Clinical impact of the biological range extension

Range uncertainties represent a major reason to avoid field configurations that point in the direction of a critical organ behind the target volume, although particularly in this configuration the specific advantages of particle beams could be exploited.[41] In order to account for these uncertainties, at present in many proton facilities 3.5% of the proton range plus extra additional 1–3 mm is used as an extra margin.[42,43] In case of prostate treatments with proton ranges of approximately 15 cm, this corresponds to more than 5 mm extra range and for anterior-oriented fields would deliver high dose to the anterior rectal wall.[41] Up to now, mainly physical aspects are considered in the estimation of these range uncertainties. According to the analysis presented here, extensions of up to about 4 mm have to be taken into account resulting from the increased RBE at the distal part of the SOBP, depending on the dose level and tissue characteristic under consideration.

Johansson[44] showed for the irradiation of hypopharyngeal carcinoma where they positioned the distal penumbra just before the spinal cord that the effective dose to the spinal cord with a variable RBE increased by a factor of 1.5 compared to the case where a constant RBE of 1.1 was chosen or only the physical dose was regarded. Even though the critical dose level was not exceeded, one should be aware that not only a larger part of the surrounding tissue is affected but also the integral dose to this volume is much higher than expected as discussed also by Jones *et al.*[45,46] Special caution is thus needed for pediatric patients where the same dose affects an even larger relative fraction of the surrounding tissue compared to adult patients.[47,48]

The impact of range uncertainties and extensions has been also addressed by Gensheimer *et al.*;[49] using MRI measurements, they were able to directly determine the biologically effective range in patients treated with proton beams. They reported an average overshoot of the proton beam in the lumbar spine of 1.9 mm (0.8–3.1 mm). They attributed a small part of the overshoot to the increased RBE in the distal edge but assumed that the overshoot should be less than 1 mm based on the study of Paganetti *et al.*[50] "because the higher beam energy causes a more gradual dose falloff."

However, according to the discussion above, we come to the opposite conclusion, namely, that the overshoot should increase with increasing energy precisely because of the more gradual penumbra. The biological extension predicted by the LEM IV is dependent on the pristine energy used and would be between 1.6–3 mm for 235 MeV and 1.1–1.8 mm for 160 MeV and a RBE-weighted dose (RBE = 1.1) of 2 Gy (RBE) at the 50% isodose, depending on the radiosensitivity of the tissue type. These values are significantly larger than the maximum value of 1 mm as estimated by Gensheimer *et al.*;[49] they could thus explain the discrepancy between the overshoot that according to the authors could be attributed to misregistration of the MRI and CT images and the overshoot actually measured in the patients.

5. CONCLUSION

The RBE predictions of the LEM for protons together with the treatment planning software TRiP98 showed to be consistent with experimental data and thus represent a useful tool to describe the variable RBE along the treated volume. It was demonstrated in this study that the biologically effective range of proton beams is strongly dependent on physical properties of the beam as well as on dose and the biological properties of the tissue irradiated and can lead to up to 4 mm extension of the SOBP in extreme situations. In general, the extension is more pronounced for shallow as compared to steep gradients of the dose in the distal penumbra for a given dose level and tissue type.

ACKNOWLEDGMENTS

Work is part of HGS-HIRe. The authors are grateful to John Eley for careful reading and suggestions to the paper.

[a]Author to whom correspondence should be addressed. Electronic mail: M.Scholz@gsi.de

[1]ICRU, "Prescribing, recording and reporting proton-beam therapy," ICRU Report No. 78 (International Commission on Radiation Units and Measurements, Bethesda, MD, 2007).
[2]H. Paganetti, A. Niemierko, M. Ancukiewicz, L. E. Gerweck, M. Goitein, J. S. Loeffler, and H. D. Suit, "Relative biological effectiveness (RBE) values for proton beam therapy," Int. J. Radiat. Oncol., Biol., Phys. **53**, 407–421 (2002).
[3]L. E. Gerweck and S. V. Kozin, "Relative biological effectiveness of proton beams in clinical therapy," Radiother. Oncol. **50**, 135–142 (1999).
[4]J. B. Robertson, J. R. Williams, R. A. Schmidt, J. B. Little, D. F. Flynn, and H. D. Suit, "Radiobiological studies of a high-energy modulated proton beam utilizing cultured mammalian cells," Cancer **35**, 1664–1677 (1975).
[5]A. Courdi, N. Brassart, J. Hérault, and P. Chauvel, "The depth-dependent radiation response of human melanoma cells exposed to 65 MeV protons," Br. J. Radiol. **67**, 800–804 (1994).
[6]B. G. Wouters, G. K. Y. Lam, U. Oelfke, K. Gardey, R. E. Durand, and L. D. Skarsgard, "Measurements of relative biological effectiveness of the 70 MeV proton beam at TRIUMF using Chinese hamster V79 cells and the high-precision cell sorter assay," Radiat. Res. **146**, 159–170 (1996).
[7]J. T. Tang, T. Inoue, H. Yamazaki, S. Fukushima, N. Fournier-Bidoz, M. Koizumi, S. Ozeki, and K. Hatanaka, "Comparison of radiobiological effective depths in 65-MeV modulated proton beams," Br. J. Cancer **76**, 220–225 (1997).
[8]D. Bettega, P. Calzolari, P. Chauvel, A. Courdi, J. Herault, N. Iborra, R. Marchesini, P. Massariello, G. L. Poli, and L. Tallone, "Radiobiological studies on the 65 MeV therapeutic proton beam at Nice using human tumour cells," Int. J. Radiat. Biol. **76**, 1297–1303 (2000).
[9]I. Petrović, A. Ristić-Fira, D. Todorović, L. Korićanac, L. Valastro, P. Cirrone, and G. Cuttone, "Response of a radioresistant human melanoma cell line along the proton spread-out Bragg peak," Int. J. Radiat. Biol. **86**, 742–751 (2010).
[10]V. Calugaru, C. Nauraye, G. Noël, N. Giocanti, V. Favaudon, and F. Mégnin-Chanet, "Radiobiological characterization of two therapeutic proton beams with different initial energy spectra used at the Institut Curie Proton Therapy Center in Orsay," Int. J. Radiat. Oncol., Biol., Phys. **81**, 1136–1143 (2011).
[11]B. Larsson and B. A. Kihlman, "Chromosome aberrations following irradiation with high-energy protons and their secondary radiation: A study of dose distribution and biological efficiency using root-tips of Vicia faba and Allium cepa," Int. J. Radiat. Biol. **2**, 8–19 (1960).

[12]W. H. Sweet, R. N. Kjellberg, R. A. Field, A. M. Koehler, and W. M. Preston, "Time-intensity data in solar cosmic-ray events: Biological data relevant to their effects in man," Radiat. Res. Suppl. **7**, 369–383 (1967).
[13]A. Carabe, M. Moteabbed, N. Depauw, J. Schuemann, and H. Paganetti, "Range uncertainty in proton therapy due to variable biological effectiveness," Phys. Med. Biol. **57**, 1159–1172 (2012).
[14]T. Elsässer, W. Kraft-Weyrather, T. Friedrich, M. Durante, G. Iancu, M. Krämer, G. Kragl, S. Brons, M. Winter, K.-J. Weber, and M. Scholz, "Quantification of the relative biological effectiveness for ion beam radiotherapy: Direct experimental comparison of proton and carbon ion beams and a novel approach for treatment planning," Int. J. Radiat. Oncol., Biol., Phys. **78**, 1177–1183 (2010).
[15]T. Friedrich, U. Scholz, T. Elsässer, M. Durante, and M. Scholz, "Calculation of the biological effects of ion beams based on the microscopic spatial damage distribution pattern," Int. J. Radiat. Biol. **88**, 103–107 (2012).
[16]M. Krämer, O. Jäkel, T. Haberer, G. Kraft, D. Schardt, and U. Weber, "Treatment planning for heavy-ion radiotherapy: Physical beam model and dose optimization," Phys. Med. Biol. **45**, 3299–3317 (2000).
[17]M. Krämer and M. Scholz, "Treatment planning for heavy-ion radiotherapy: Calculation and optimization of biologically effective dose," Phys. Med. Biol. **45**, 3319–3330 (2000).
[18]M. Krämer and M. Durante, "Ion beam transport calculations and treatment plans in particle therapy," Eur. Phys. J. D **60**, 195–202 (2010).
[19]T. Haberer, W. Becher, D. Schardt, and G. Kraft, "Magnetic scanning system for heavy ion therapy," Nucl. Instrum. Methods Phys. Res. **A330**, 296–305 (1993).
[20]C. Brusasco, B. Voss, and D. Schardt, "A dosimetry system for fast measurement of 3D depth-dose profiles in charged-particle tumor therapy with scanning techniques," Nucl. Instrum. Methods Phys. Res. **B168**, 578–592 (2000).
[21]M. Scholz, A. M. Kellerer, W. Kraft-Weyrather, and G. Kraft, "Computation of cell survival in heavy ion beams for therapy: The model and its approximation," Radiat. Environ. Biophys. **36**, 59–66 (1997).
[22]T. Elsässer and M. Scholz, "Cluster effects within the local effect model," Radiat. Res. **167**, 319–329 (2007).
[23]T. Elsässer, M. Krämer, and M. Scholz, "Accuracy of the local effect model for the prediction of biologic effects of carbon ion beams *in vitro* and *in vivo*," Int. J. Radiat. Oncol., Biol., Phys. **71**, 866–872 (2008).
[24]M. Krämer and M. Scholz, "Rapid calculation of biological effects in ion radiotherapy," Phys. Med. Biol. **51**, 1959–1970 (2006).
[25]M. Astrahan, "Some implications of linear-quadratic-linear radiation dose-response with regard to hypofractionation," Med. Phys. **35**, 4161–4172 (2008).
[26]T. Friedrich, R. Grün, U. Scholz, T. Elsässer, M. Durante, and M. Scholz, "Sensitivity analysis of the relative biological effectiveness predicted by the local effect model," Phys. Med. Biol. **58**, 6827–6849 (2013).
[27]T. Friedrich, U. Scholz, T. Elsässer, M. Durante, and M. Scholz, "Systematic analysis of RBE and related quantities using a database of cell survival experiments with ion beam irradiation," J. Radiat. Res. **54**, 494–514 (2013).
[28]B. Gottschalk, "On the characterization of spread out Bragg peaks and the definition of 'depth' and 'modulation'," 2003, (available URL: http://physics.harvard.edu/~gottschalk/).
[29]E. Pedroni, S. Scheib, T. Böhringer, A. Coray, M. Grossmann, S. Lin, and A. Lomax, "Experimental characterization and physical modelling of the dose distribution of scanned proton pencil beams," Phys. Med. Biol. **50**, 541–561 (2005).
[30]K. Gall, L. Verhey, J. Alonso, J. Castro, J. M. Collier, W. Chu, I. Daftari, M. Goitein, H. Kubo, B. Ludewigt, J. Munzenrider, P. Petti, T. Renner, S. Rosenthal, A. Smith, J. Staples, H. Suit, and A. Thornton, "State of the art? New proton medical facilities for the Massachusetts General Hospital and the University of California Davis Medical Center," Nucl. Instrum. Methods Phys. Res. B **79**, 881–884 (1993).
[31]H. Paganetti, P. Olko, H. Kobus, R. Becker, T. Schmitz, M. P. R. Waligorski, D. Filges, and H. W. Müller-Gärtner, "Calculation of relative biological effectiveness for proton beams using biological weighting functions," Int. J. Radiat. Oncol., Biol., Phys. **37**, 719–729 (1997).
[32]H. Paganetti, "Significance and implementation of RBE variations in proton beam therapy," Technol. Cancer Res. Treat. **2**, 413–426 (2003).
[33]C. Grassberger, A. Trofimov, A. Lomax, and H. Paganetti, "Variations in linear energy transfer within clinical proton therapy fields and the potential for biological treatment planning," Int. J. Radiat. Oncol., Biol., Phys. **80**, 1559–1566 (2011).
[34]M. C. Frese, J. J. Wilkens, P. E. Huber, A. D. Jensen, U. Oelfke, and Z. Taheri-Kadkhoda, "Application of constant vs. variable relative biological effectiveness in treatment planning of intensity-modulated proton therapy," Int. J. Radiat. Oncol., Biol., Phys. **79**, 80–88 (2011).
[35]A. Dasu and I. Toma-Dasu, "Impact of variable RBE on proton fractionation," Med. Phys. **40**, 011705 (9pp.) (2013).
[36]F. A. Cucinotta, R. Katz, J. W. Wilson, L. W. Townsend, J. Shinn, and F. Hajnal, "Biological effectiveness of high-energy protons: Target fragmentation," Radiat. Res. **127**, 130–137 (1991).
[37]H. Paganetti, "Nuclear interactions in proton therapy: Dose and relative biological effect distributions originating from primary and secondary particles," Phys. Med. Biol. **47**, 747–764 (2002).
[38]A. Carabe-Fernandez, R. G. Dale, and B. Jones, "The incorporation of the concept of minimum RBE (RBE_{min}) into the linear-quadratic model and the potential for improved radiobiological analysis of high-LET treatments," Int. J. Radiat. Biol. **83**, 27–39 (2007).
[39]N. Tilly, J. Johansson, U. Isacsson, J. Medin, E. Blomquist, E. Grusell, and B. Glimelius, "The influence of RBE variations in a clinical proton treatment plan for a hypopharynx cancer," Phys. Med. Biol. **50**, 2765–2777 (2005).
[40]H. Paganetti and T. Schmitz, "The influence of the beam modulation technique on dose and RBE in proton radiation therapy," Phys. Med. Biol. **41**, 1649–1663 (1996).
[41]S. Tang, S. Both, H. Bentefour, J. J. Paly, Z. Tochner, J. Efstathiou, and H.-M. Lu, "Improvement of prostate treatment by anterior proton fields," Int. J. Radiat. Oncol., Biol., Phys. **83**, 408–418 (2012).
[42]M. Goitein, "Calculation of the uncertainty in the dose delivered during radiation therapy," Med. Phys. **12**, 608–612 (1985).
[43]H. Paganetti, "Range uncertainties in proton therapy and the role of Monte Carlo simulations," Phys. Med. Biol. **57**, R99–R117 (2012).
[44]J. Johansson, "Comparative treatment planning in radiotherapy and clinical impact of proton relative biological effectiveness," Ph.D. dissertation, Acta Universitatis Upsaliensis, Uppsala, 2006.
[45]B. Jones, T. S. A. Underwood, and R. G. Dale, "The potential impact of relative biological effectiveness uncertainty on charged particle treatment prescriptions," Br. J. Radiol. **84**, S61–S69 (2011) (Special issue).
[46]B. Jones, P. Wilson, A. Nagano, J. Fenwick, and G. Mckenna, "Dilemmas concerning dose distribution and the influence of relative biological effect in proton beam therapy of medulloblastoma," Br. J. Radiol. **85**, e912–e918 (2012).
[47]T. I. Yock and N. J. Tarbell, "Technology insight: Proton beam radiotherapy for treatment in pediatric brain tumors," Nat. Clin. Pract. Oncol. **1**, 97–103 (2004).
[48]S. E. Cotter, S. M. McBride, and T. I. Yock, "Proton radiotherapy for solid tumors of childhood," Technol. Cancer Res. Treat. **11**, 267–278 (2012).
[49]M. F. Gensheimer, T. I. Yock, N. J. Liebsch, G. C. Sharp, H. Paganetti, N. Madan, P. E. Grant, and T. Bortfeld, "*In vivo* proton beam range verification using spine MRI changes," Int. J. Radiat. Oncol., Biol., Phys. **78**, 268–275 (2010).
[50]H. Paganetti, "Calculation of the spatial variation of relative biological effectiveness in a therapeutic proton field for eye treatment," Phys. Med. Biol. **43**, 2147–2157 (1998).

VII. Appendix

VII.I. Verzeichnis der akademischen Lehrer

Meine akademischen Lehrer waren die Damen und Herren…

…in Gießen

Böckmann, Breckow, Cemic, Fiebich, Gokorsch, Kirschbaum, Kleinöder, Klös, Koch, Prehn, Seipp, Subke, Trampisch, Zink

...in Jordanstown, Northern Ireland

Clark, McAdams, McLaughlin, Owens, Rau

…in Marburg

Jacob, Lill, Lillig

…in Darmstadt

Durante

VII.II. Danksagung

An dieser Stelle möchte ich mich bei allen bedanken, die zum Entstehen dieser Arbeit beigetragen haben.

Als erstes möchte ich mich bei Prof. Dr. Rita Engenhart-Cabillic bedanken, für die fachliche Unterstützung und die Möglichkeit unter Ihrer Leitung meine Promotion antreten zu dürfen.

Weiterhin gilt ein besonderer Dank Prof. Dr. Klemens Zink, der mit seinem Engagement meine Promotion wohl erst ermöglichte und der mich während der gesamten Zeit unterstützt hat.

Mein Dank gilt außerdem Prof. Dr. Marco Durante, der mich in der Abteilung Biophysik an der GSI herzlich aufgenommen hat und bei wichtigen Fragen und Diskussionen immer zur Seite stand.

Wohl der größte Dankt geht an Dr. Michael Scholz und Dr. Thomas Friedrich, für ihre intensive, geduldige und motivierende Betreuung, für viele wertvolle Ratschläge, konstruktive Kritik, die sorgfältigen Korrekturen der Artikel sowie auch der gesamten Arbeit und die Aufmunterungen, wenn einmal nicht alles so lief wie geplant. Wissenschaftlich und menschlich hätte ich mir keine bessere Betreuung meiner Arbeit vorstellen können. Eure Leidenschaft hat großen Einfluss auf mich, dafür danke ich euch.

Weiterhin möchte ich mich auch bei der restlichen Modellierungs-Truppe für jegliche Unterstützung und Hilfestellung bedanken.

Danke auch an Christoph Schuy, Dr. Emanuele Scifoni und Dr. Olaf Steinsträter für die tolle Büro-Atmosphäre und die Bereicherung meines Arbeitsalltags durch unterhaltsame und konstruktive Gespräche.

Ich danke auch dem PUNKT-11:30-LUNCH-Team für die erheiternden und mit “interessanten“ Themen gespickten Mittagspausen.

Mein Dank gilt auch den Setzern von PMB, die dem Wort “isocenter“ eine ganz neue Bedeutung gegeben haben.

Zu guter Letzt möchte ich meiner Familie und meinen Freunden danken. Meinen Eltern, weil sie mir zwar oft mahnende Worte mitgeben, aber mich dennoch immer unterstützen. Meiner Schwester, die immer eine gute Ratgeberin ist. Meinen Freunden, die für mich da sind und auf die ich mich immer verlassen kann.